CENTERS FOR ETHIO-MINES DEVELOPMENT,

ADDIS ABABA INSTITUTE OF TECHNOLOGY

MULTISTAGE HYDRAULIC FRACTURING DESIGN FOR HORIZONTAL WELLS IN HILALA GAS FIELD, IN THE OGADEN BASIN, ETHIOPIA.

BY: MENGISTU H. MARIAM H. MICHAEL

Presented in partial fulfillment of the requirements for the degree of Master of Engineering in Petroleum Engineering.

OFFICE OF GRADUATE STUDIES

ADDIS ABABA UNIVERSITY

JUNE 2023

ADDISABABA, ETHIOPIA

MULTISTAGE HYDRAULIC FRACTURING DESIGN FOR HORIZONTAL WELLS IN HILALA GAS FIELD, IN THE OGADEN BASIN, ETHIOPIA.

BY: -MENGISTU H. MARIAM H. MICHAEL

ADVISORS

KETSELA TADESSE (PHD)

SHIFERAW REGASSA (PHD)

BISRAT KEBEDE (PHD)

A graduate project work submitted to the Centers for Ethio-Mines Development,

***Addis Ababa Institute of Technology*.**

Presented in partial fulfillment of the requirements for the degree of Master of Engineering in Petroleum Engineering.

OFFICE OF GRADUATE STUDIES

ADDIS ABABA UNIVERSITY

JUNE 2023

ADDIS ABABA, ETHIOPIA

DECLARATION

I hereby declare that this Graduate Project Work entitled "***Multistage Hydraulic Fracturing Design for Horizontal Wells in Hilala Gas Field, in the Ogaden Basin, Ethiopia*"** is my original work. That is, it has not been submitted for the award of any academic degree, diploma, or certificate at any other university. All sources of materials that were used for this thesis have been duly acknowledged through citation.

Mengistu H. Mariam _____ _____

Name of student Signature Date

Place: Addis Ababa University, School of Graduate Studies, Addis Ababa, Ethiopia.

RECOMMENDATION

I/we, the advisor(s) of this Graduate Project Work, hereby certify that I/we have read the revised version of the thesis entitled "***Multistage Hydraulic Fracturing Design for Horizontal Wells in Hilala Gas Field, in the Ogaden Basin, Ethiopia*****",** prepared under my/our guidance by Mengistu H. Mariam and submitted in partial fulfillment of the requirements for the degree of Master of Engineering in Petroleum Engineering. Therefore, I/we recommend the submission of a revised version of the Graduate project Work to the Center following the applicable procedures.

_____	_____	_____
Major Advisor	Signature	Date
_____	_____	_____
Co-advisor	Signature	Date

APPROVAL PAGE OF MSc. GRADUATE PROJECT

I/we, the advisors of the Graduate Project Work entitled "***Multistage Hydraulic Fracturing Design for Horizontal Wells in Hilala Gas Field, in the Ogaden Basin, Ethiopia*"** and developed by **Mengistu H. Mariam**, hereby certify that the recommendation and suggestions made by the board of examiners are appropriately incorporated into the final version of the Graduate Project Work.

Major Advisor	Signature	Date
Co-advisor	Signature	Date

We, the undersigned, members of the Board of Examiners of the Graduate Project work of Mengistu H. Mariam have read and evaluated the Graduate Project "***Multistage Hydraulic Fracturing Design for Horizontal Wells in Hilala Gas Field, in the Ogaden Basin, Ethiopia"***, and examined the candidate during open defense. This is, therefore, to certify that the Graduate Project is accepted for partial fulfillment of the requirement of the degree of Master of Engineering in Petroleum Engineering.

Chairperson	Signature	Date
Examiner	Signature	Date
Examiner	Signature	Date

Finally, approval and acceptance of the Graduate Project Work are contingent upon submission of its final copy to the Office of Postgraduate Studies (OPGS) through the Department Graduate Council (DGC) and School Graduate Committee (SGC).

Center Director	Signature	Date
School Dean	Signature	Date
Office of Postgraduate Studies, Dean	Signature	Date

ACKNOWLEDGEMENTS

I am honored when I thank and glorify the Almighty God, who is always protecting me and giving me the ability to do this work.

I wish to express my gratitude to my Advisors, Dr. Ketsela Tadesse, Dr. Shiferaw Regassa, and Dr. Bisrat Kebede, for their assistance, advice, and support throughout the entire course of the project. I would like to sincerely thank Dr. Solomon Kassa and Dr. Samuel Getnet for their valuable suggestions and feedback during the evaluation of this work.

My very special thanks and appreciation go to Dr. Viatcheslav Guk and Dr. Serdar Dogulu for their guidance and expert advice throughout all stages of the project work and for numerous helpful suggestions.

My warmest thanks to my colleagues, Mr. Abduselam Endris, Mr. Bereket Essayas, Mr. Abraha Tesfay, Mr. Tefera Alemu, and Mr. Assefa Woldu, who encouraged me, worked actively, and showed their willingness to help. Thank you so much for the wonderful collaborations and helpful suggestions.

I am Thankful to Dr. Berhanu Assefa and Dr. Shegaw Ahmed for their coordination and support during the academic years and the completion of this project work.

I would like to thank the Ministry of Mines and POLY-GCL Petroleum Investment Limited for the various datasets and input received for the realization of this work through the Ministry archives. I am grateful to the Center for Ethio-Mines Development and all my Professors and Lecturers at Addis Ababa University Institute of Technology for all the support and for making my time great and precious.

Thanks to all who, in one way or another, contributed to the completion of this project.

Finally, I would like to express my deepest gratitude to my Family for their love and support.

DEDICATION

To My Family and My Colleagues

NOMENCLATURE

Symbol	Description
α	*Biot's constant*
β	*Formation volume factor*
Xf	Fracture half length,m
xe	*Reservoir width,m*
ye	*Reservoir length, m*
Wf	Fracture width,mm
hf	*Fracture half-length,m/ft*
J_D	Dimensionless fracture conductivity, dimensionless
σv	Vertical stress
σh	Minimum horizontal stress, psi/Mpa
σH	*Maximum horizontal stress,s psi/Mpa*
E	*Young's Modulus, psi/Mpa*
υ	*Poisson's ratio dimensionless*
ρ	*Density ,g/cm^3,Kg/m^3*
B	*Brittleness index ,%*
$\sigma_{closure}$	*Clossure stress, psi/MPa*
qi	*Fluid Flow rate, bbl/min , mm^3/min*
μ	*viscosity,cp/ Pascal.second*

Table of Contents

List of Tables

List of Figures

Abstract

The economically viable production of oil and gas is a direct function of the geological properties of reservoir rocks. Among these formation properties, permeability is critical for an effective hydrocarbon flow. The flow of fluids from the reservoir to the wellbore can be restricted due to low permeability or damage around the wellbore. Hydraulic fracturing is applied to stimulate the low permeability formation and bypass damaged formation areas, connecting the reservoir to the wellbore. Recently, the most popular layouts for increased production from low permeability reservoirs have been horizontal wells with numerous transverse fractures. Under various studies conducted, it has been proven that there is a significant commercially recoverable gas reserve in the Ogaden basin of Ethiopia that has been identified for development. Hilala Field is located within this basin, and it is considered for gas development and production through domestic and international gas market arrangements outlined in the recent field development plan. This fracture design study is undertaken for the Adigrat sandstone reservoir in Hilala Gas Field, buried at a depth of 3087-3200m and characterized as a low porosity and low permeability reservoir that requires hydraulic fracturing for its economic gas recovery. The aim of the study is to develop an optimum multiple hydraulic fracturing design for the horizontal wells considering the geology, rock mechanics, fracturing fluid, and proppant. This hydraulic fracture design work is based on the Unified Fracture Design (UFD) and selected extension works. Excel sheet is the main tool for the analytical study. OptiFrac and OptiFracMS software are employed to design and analyze results. This study examined well log data from seven wells, well test and production test results from four wells, and the field development plan for the Hilala Gas Field in the Ogaden basin in South Eastern Ethiopia.

Understanding reservoir rock's physical, geo-mechanical properties is crucial to the stimulation of hydraulic fracturing. The brittleness Index can be determined from well log and core data. Based on the analysis of the Adigrat reservoir rock's geo-mechanical properties, the Adigrat sandstone formation in Hilala gas field has a high Young's modulus (51.26 MPa) and a low Poisson's ratio (0.21), correlating it to a brittle rock suited for fracture propagation. The calculated average closure stress is 50.45 MPa, and the suitable proppant material is intermediate-strength bauxite proppants.

An optimum fracture half-length of 310.6m and a fracture width of 2.25 mm are attainable for a given proppant number of 0.87 for a single fracture. An optimum number of twelve (12) transverse fractures can economically attain a dimensionless productivity index of 6.18 for an available proppant number (Np) of 8.92 for the 0.2 mD permeability reservoir and drainage width of 1000m.

Keywords: low permeability reservoir, gas reservoir, hydraulic fracturing, fracture design, fracture geometry, brittleness, closures stress, geo-mechanical property, optimum number of fractures.

Chapter-1 Introduction

1.1 Background

The importance of gas production from low permeability reservoirs is rising as conventional gas reserves are being depleted. A well's capacity to produce hydrocarbon or receive injection fluid is limited by the inherent permeability of the reservoir and changes made near the wellbore during drilling operations and other activities. The two main technologies that have made the development of low permeability and unconventional oil and gas formation economically viable are hydraulic fracturing and horizontal well completion techniques (Meyer, Bazan et al.,2010), (Crosby, 2002), (Nolen-Hoeksema ,2013).

Hydraulic fracturing entails creating a fracture in the formation using a fracturing fluid under hydraulic pressure, which is then used to propagate the fracture, and preserving the created fracture open with proppant. The propped fracture serve as conduit pathway between the formation and the wellbore for hydrocarbon production (Jones and Britt, 2009). The fracture created usually has two wings that spread out in opposite directions from the wellbore. The main function of the fracturing fluid is to deliver the force required to generate the fracture in the formation and carry the proppant from the wellbore and into the fracture. Fracturing Fluid are mainly water-based fluid system, principally with the alternative gelled (linear gel or crosslinked) and non-gelled (slick water) composition. Depending on the formation, reservoir pressure, and fluid types; the addition of gas as a foam or a distinct phase could increase the utility of the fracturing fluid. Oil based, alcohol based, and emulsion-based fluid system are examples of other types of fluid systems (Jones and Britt 2009, Miskimins 2019). Proppants are designed to keep the crack open after post-treatment hydraulic pressure is released (Jones and Britt 2009, Miskimins 2019). The proppant filled fracture, creates a narrow but very conductive flow route to the wellbore. This flow path has a very large permeability, often five to six orders of magnitude greater than the reservoir permeability. It is typically narrow in one horizontal direction, but can be quite long in the other horizontal directions covering a considerable height. In low permeability reservoirs, typically intended propped widths are on the order of 0.25 in (6.35 mm) whereas the 'tip-to-tip' length possibly be 3000 ft (914.4m) (Economides, M., Oligney, R., & Valko, P. (2002)).

Hydraulic fracturing enhances fluid flow by creating fractures in the rock formation connecting the reservoir and rock formation (Nolen-Hoeksema 2013). It is a constantly evolving well stimulation technique. It can be customized to enable, increase, accelerate and restore production by lowering flow path resistance in a variety of geological settings ranging from source rock to reservoirs (Miskimins 2019). Hydraulic fracturing is routinely used to artificially increase the productivities of these low permeability and tight gas reservoirs (Crosby, 2002).

The other method that has proven to be far more effective than vertical well for tight formations is horizontal well completion. A horizontal borehole runs horizontally across the target formation until it reached the designated planned depth. Such lateral wellbore facilitates the formation to carry out multiple fracturing treatment for a single well (Yao 2013).

Natural gas wells benefit greatly from hydraulic fracturing. For low-permeability reservoirs (Figure 1.1), the need is obvious: it is the only means to monetize large number of horizontal wells. Additionally, in recent years, horizontal wells with multiple transverse fractures have become the preferred configuration for many low-permeability reservoirs. (Marongiu-Porcu, Wang et al. 2009)

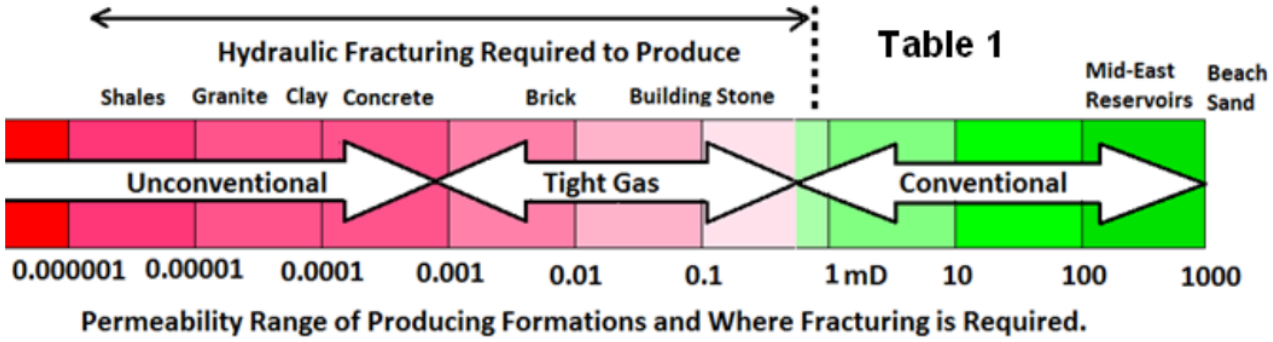

Figure 1. 1 Permeability Range of Producing Formation and Where Fracturing is Required (after King 2012).

Since 1949, hydraulic fracturing has been the primary and comparatively affordable stimulation technique utilized in the petroleum industry for enhanced oil and gas recovery. In Horizontal wellbores, multi-stage and multi-clustered per stage fracture treatment result in a large stimulated reservoir volume (SRV) , which boosts both production and estimated ultimate recovery (EUR) (Meyer, Bazan et al.) Multistage hydraulic fracturing helps to attain further decrease in the

pressure drops as they act as elongated conductive paths extended deep into the reservoir which help easy flow of gas to the fractures (Karem Al-Garadi et, al. 2019).

Any hydraulic fracture can be characterized by its length, conductivity and associated equivalent skin effect. The created and conductive fracture lengths (X_f) may occasionally be distinguished from one another. The created fracture length is related to the length of the fracture that developed during the execution of the hydraulic fracture treatment. The length of the fracture that stays open when the well is in production is known as the "conductive fracture length," and it effectively creates a better conduit for fluid production to the well (Economides, 2013).

Since practically every fracturing decision (such as the choice of fracturing fluid, proppant type, size, and concentration, and pump rate) is an economic one, hydraulic fracturing goals are best realized through economic optimization. Fracturing stimulation can be optimized using a variety of economic and well performance parameters. The most prevalent are net present value (NPV), discounted return on investment, pay out, initial potential, and annualized well performance. However, as each of these characteristics offer a unique set of optimal dimensions; therefore, the optimization criteria should be determined by the corporate goal (Jones and Britt 2009).

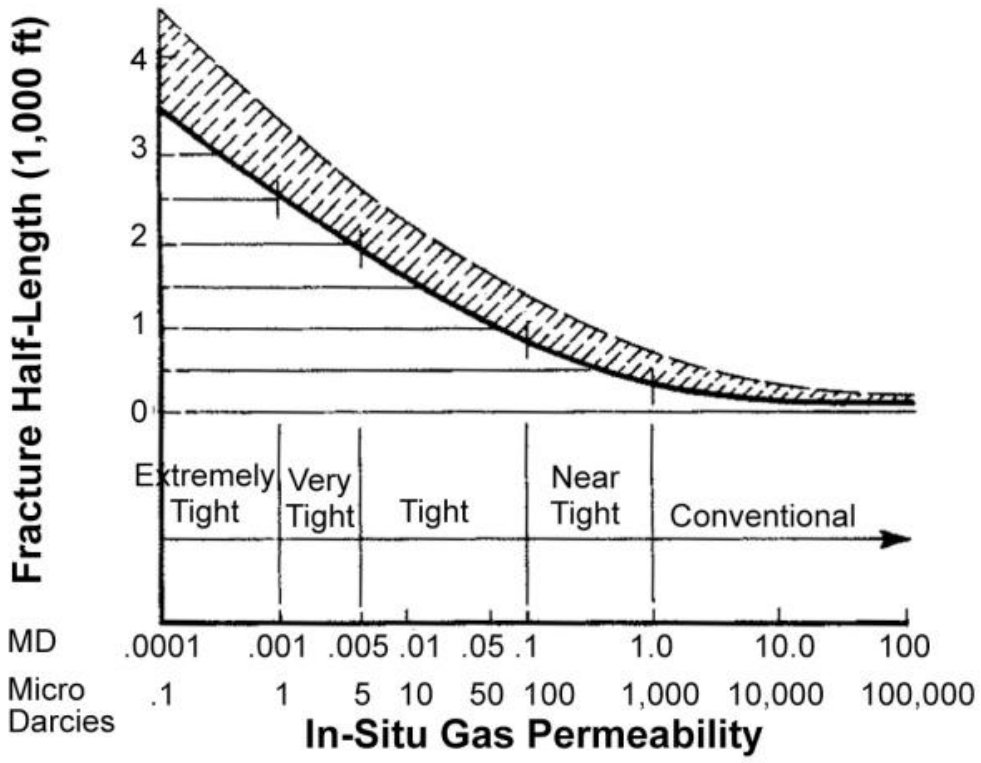

Figure 1. 2 Desired fracture half-lengths for different formation permeabilities (Jones and Britt 2009).

The in-situ gas permeability versus fracture half-length plot in **Figure 1.2**. Show that for a low permeability gas formation higher fracture length is required.

A Fracture needs to be planned for specified formation permeability. Low permeability formations need stimulation because their permeability is simply too low for the well to produce naturally at a profitable rate. Low permeability formation fracture is planned for attaining the optimum length. High permeability formations are meant to have short, highly conductive fractures, to bypass the damage, which typically entail maximizing fracture width (Economides and Martin 2007).

This study focuses on hydraulic fracture stimulation design for horizontal wells in low permeability gas reservoir in Hilala Gas Field as a development option for gas production enhancement.

1.2 Description of the study area

1.2.1 The Hilala gas field

The Hilala Gas Field is located within the Ogaden basin platform in the Somalia National Regional State in Ethiopia. The Ogaden basin located in South Eastern-Ethiopia covers an area of 350,000 square kilometer and a sedimentary deposition thickness of 6000 meters which is divided into multiple blocks for petroleum exploration and development concessions.

1.2.2 Geographical Location

The Hilala Gas Field is located in the Ogaden basin at a latitude of 6˚11’50.226’’N and longitude of 43˚41’29.297’’E in the South Eastern Ethiopia, approximately 700 km form Addis Ababa and about 72 km west of Calub gas field (Figure 1.3). It covers an area of 969 square kilometer.

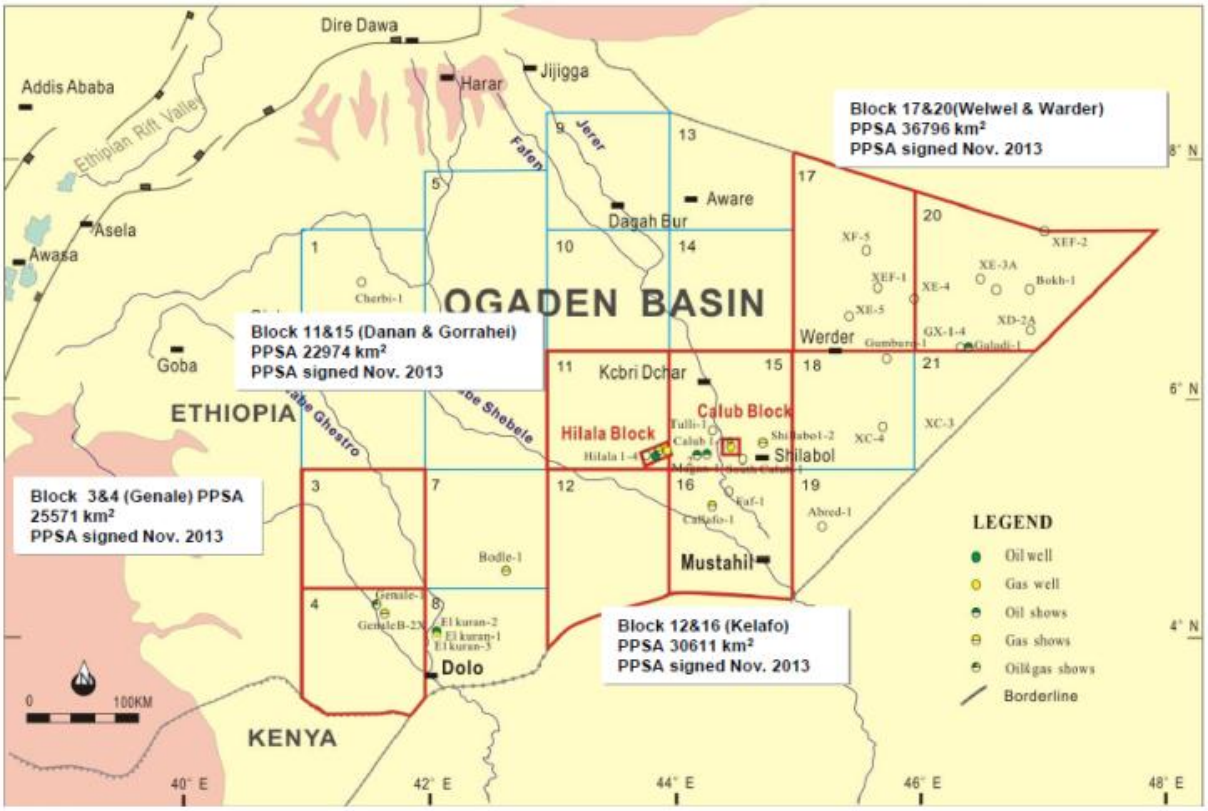

Figure 1. 3 Location of Hilala Gas Field (POLY-GCL Petroleum Investments Limited Ethiopian Branch, 2017)

1.2.3 Regional Geology and Stratigraphy

The Ogaden basin, where the Hilala Gas Field is situated, is impacted by the formation of the Karoo rift of the Paleozoic time, the East African Mesozoic and Cenozoic sub-rifts and the red sea East African Basin of the Cenozoic, which forms a large overlaid basin. With the evolution

and geological movements of the basin, two sedimentary deposits developed from the continental to the sea environment (POLY-GCL Petroleum Investments Limited Ethiopian Branch, 2017).

The Marda and Karan fault zones were created in the Ogaden basin as a result of the regional tectonic movement of Africa. The basin tectonic pattern is controlled by two groups of basement fault in NEE and NW directions. The Ogaden basin exhibits three uplift structural patterns, namely, the North uplift zone, West uplift zone, and the South uplift zones. There are five sets of reservoirs in the Hilala Gas Field in the Ogaden basin with two categories of lithologies. These are the sandstone reservoirs group which includes Adigrat and Calub formations and the carbonate reservoirs categories which includes the Hamanlei and Gabredarre formations.

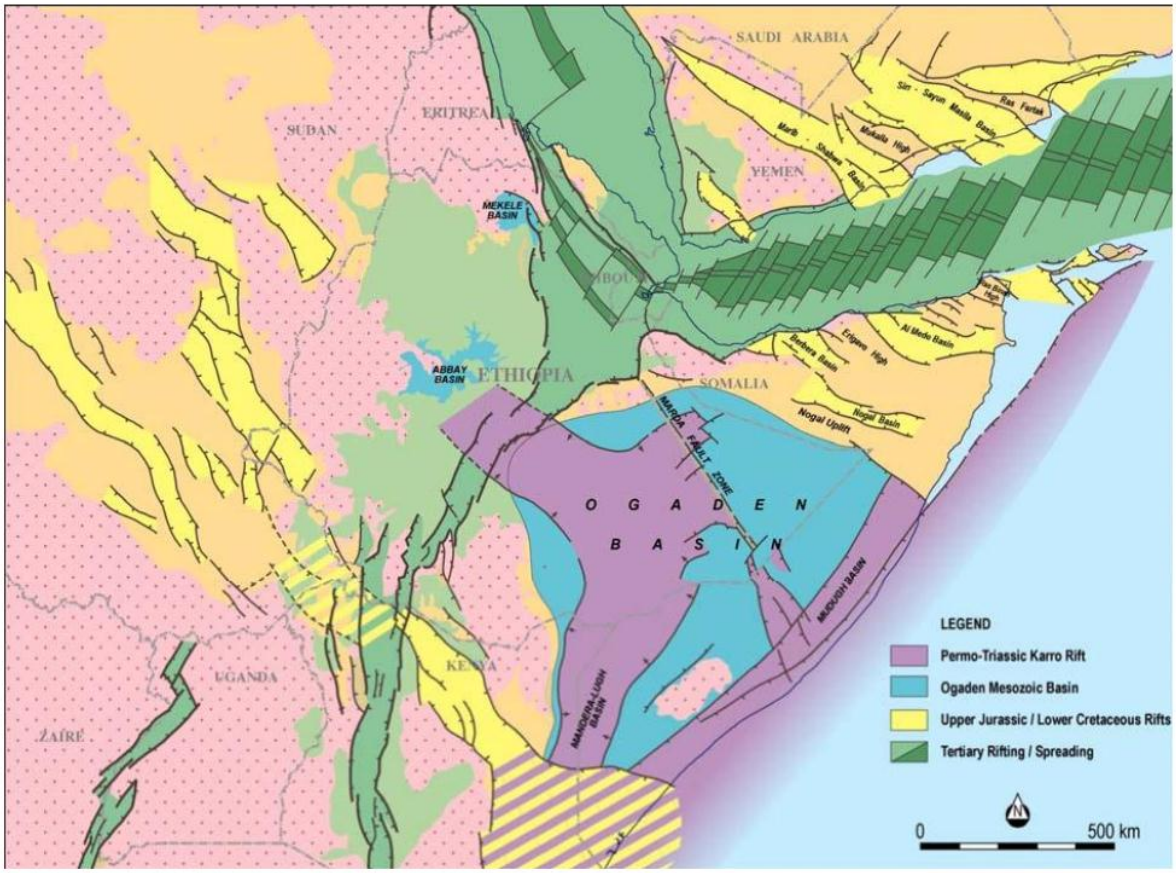

Figure 1. 4 Tectonic Structure of the Ogaden basin (Ministry of Mines, Ethiopia, 2011)

1.2.4 Stratigraphic features of Hilala Gas Field pay zones

The Adigrat reservoir formation, the theme of this study and the main gas producing reservoir is widely and stably distributed in the Hilala field. The average sedimentary thickness of the Adigrat formation ranges from 120 to 160m with an average value 155 m (Figure 1.5). It is composed of gray sandstone, fine sandstone and interbedded with dark grey sandstone.

Stratigraphic Unit					Lithology	Thickness(m)	Lithology Description	Remark
Era	System	Series	Group	Formation	(←West East→)			
Mesozoic	Cretaceous	Middle		Faf		150m-330m Average:200m	At the top of the formation is grayish limestone, part of which presents yellow. Gay green and grayish mudstone with medium hardness is at the bottom of the formation.	Marine Deposit
		Lower		Gorrahei		760m-1110m Average:900m	Overall, dark gray and greenish gray limestone is the main rock type mingled with argillaceous and dolomitic limestone and mudstone grain. At the middle top of the formation presents anhydrite band.	
	Jurassic	Upper		Gabredarre		150m-290m Average:240m	The upper part of the formation is grayish mudstone part of which presents brown, mingled with a little of limestone. Black and grayish green limestone mingled with a little of mudstone is at the bottom of the formation.	
				Uarandab		130m-240m Average:170m	Gray and grayish argillaceous limestone, part of which presents white or semitransparent anhydrite.	
		Middle	Hamanlei	U. Hamanlei		350m-550m Average:440m	Gray and grayish interbeded mudstone and limestone, part of which includes ooid and gray-opaque anhygritein closure.	
				M. Hamanlei		500m-640m Average:550m	At the top of the formation is white-semitransparent anhydrite. The main lithology is brown or grayish-brown interbeded dolomite and limestone. In the middle of it still includes anhydrite.	
				L. Hamanlei		180m-250m Average:230m	At the top of the formation is black and dark gray argillaceous limestone, part of which presents anhydrite. In the middle of it is the grayish and brown limestone. At the bottom of it is black mudstone which distributes steady.	
		Lower		Transition		80m-120m Average:100m	At the top of the formation is black and dark gray argillaceous limestone, part of which presents anhydrite. In the middle of it is the grayish and brown limestone. At the bottom of it is black mudstone which distributes steady.	Continental Deposit
				Adigrat		60m-160m Average:120m	Grayish sandstone is the main lithology. This formation possesses steady balck mudstone barrier bed. Quartz sandstone and quartz-feldspar sandstone are the main sandstone types.	
	Triassic	Upper-Middle	Karroo	Gumburo		230m-750m Average:430m	Gray and dark brown mudstone are the main lithology. Black and brown silts and stone is observed occasionally. At the top of the formation, apparent gray mudstone could be seen. Anhydrite and pyrite can be seen occasionally.	
		Lower		Bokh		280m-550m Average:370m	Dark gray and black thick mudstone distributes widely. Silts and stone could be seen occasionally.	
Palaeozoic	Permian	Upper		Calub		20m-170m Average:80m	This formation and basement is unconformably contacted. Gray heterogranular feldspar-sandstone, conglomeratic coarse sandstone, middle-sized grain sandstone and argillaceous silts and stone are the main rock types.	
Precambrian				Basement			It is constituted with ganite clastic, grain, quartz grain, feldspar, hornblende, kaoline and mica. The grain size is from medium to coarse. At the bottom of it, there is colored mineral. The typical mineral is biotite and hornblend.	Basement

Figure 1. 5 Stratigraphic and Lithologic column of the Ogaden basin (after POLY-GCL Petroleum Investments Limited Ethiopian Branch, 2017)

Adigrat formation is divided into four subzones zones (sandstone groups), sand bodies of A1-A4 with each thickness of 30-50 m. Gas zones are mainly contained in A1, A2 and A3 zones.

Table 1. 1 Adigrat Formation Subzones in the Hilala Gas Field (after POLY-GCL Petroleum Investments Limited Ethiopian Branch, 2017).

Assessment Parameter	*Subzone Adigrat (A1)*	*Subzone Adigrat A2*	*Subzone Adigrat A3*	*Subzone Adigrat A4*	*Total*
Reservoir Lithology	Sandstone	Sandstone	Sandstone	Sandstone	
Formation Thickness (m)	33.3	53.9	26.6	41.7	155
Average Sand Thickness (m)	11.7	22.7	7.0	40.4	81.8
Burial Depth (m)	3081	3116	3152	3162-3261	

The four sandstone groups of Adigrat formation have different thicknesses (Table 1.1). The Adigrat A1 has an average thickness of 33.3 m and the average sand thickness is 11.7 m. The average thickness of the Adigrat A2 is 53.9 m and the average sand thickness is 22.7 m. The Adigrat A3 and A4 have an average thickness of 26.6 and 41.7 m and, sand thickness of 7.0 m and 40.4 m respectively.

1.2.5 Adigrat Reservoir Structure in Hilala Gas Field

The Adigrat formation structure in Hilala Gas Field exhibits an elongated anticline with NEE with an aerial coverage of 30Km long and 7km wide block. There are three crests in the anticline from west to east, which occur at the sites of well West Hilala-2, Hilala-1 and Hilala-6 (**Figure 1.6**)

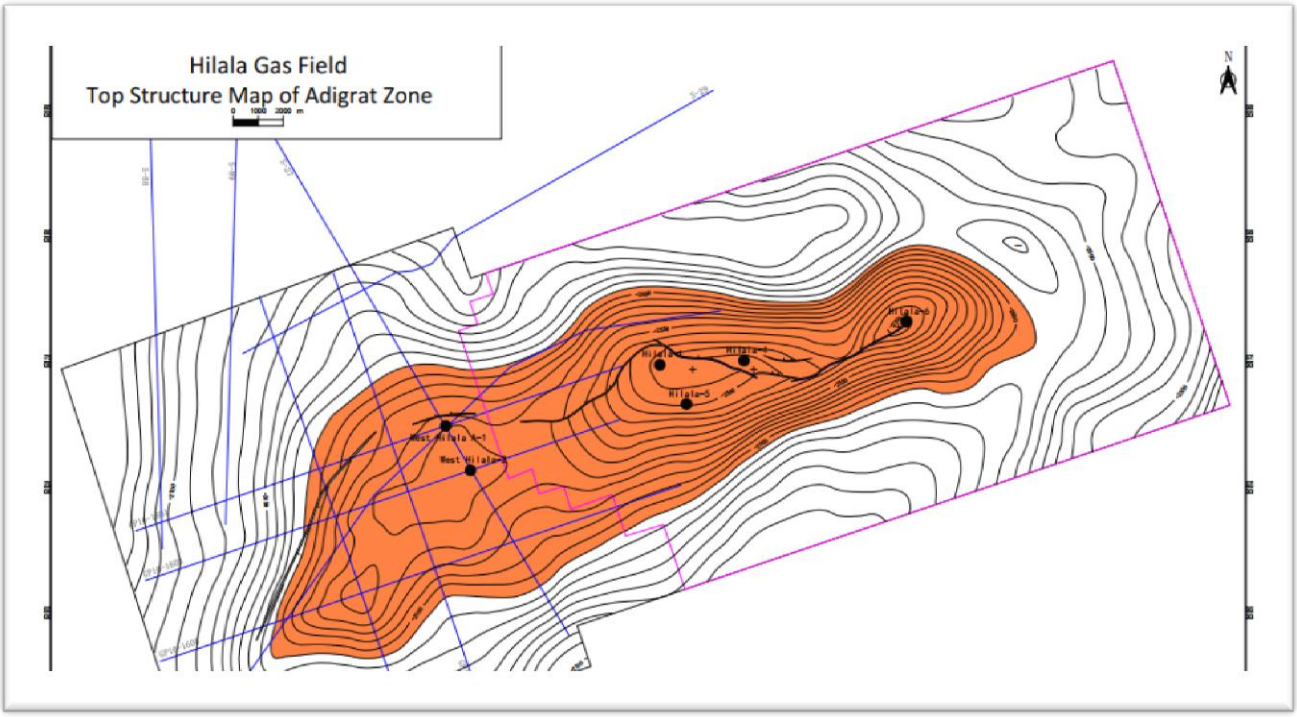

Figure 1. 6 Adigrat reservoir top structure in Hilala Gas Field (after POLY-GCL Petroleum Investments Limited Ethiopian Branch, 2017).

1.2.6 Lithology of Adigrat Reservoir in Hilala gas field

Quartz and felspathic quartz sandstone make up the majority of the Adigrat formation. It has a modest level of compositional and textural maturity, with the predominant grain contact mode being line contact pattern.

1.2.7 Adigrat formation Physical Property in Hilala Gas Field

The Adigrat sandstone physical property study showed that the sandstone core porosity ranges from 8 % to 12% with an average of 10.4%. The core permeability ranges from 0.2 to 2 mD with an average of 1.38 mD. Log interpretation porosity range from 2.6 % to 14% with an average of 9.2 % in A1-A3. The Permeability is from 0.02 to 12.89 mD with an average of 1.3 mD in A1-A3. Hence, Adigrat sandstone reservoir is classified as low permeability and low porosity reservoir (Table 1.2).

Hilala gas field has a geothermal gradient of 2.52 °C/100 m, indicating that it is a normal temperature system with 106.7 °C in the middle of the Adigrat reservoir. Furthermore, as normal pressure gradient, the pressure gradient of Hilala gas field is 1.1 MPa/100m and the pressure is 33.86 MPa with a pressure coefficient of 1.04 at the middle of the Adigrat gas formation (POLY-GCL Ethiopia, 2017).

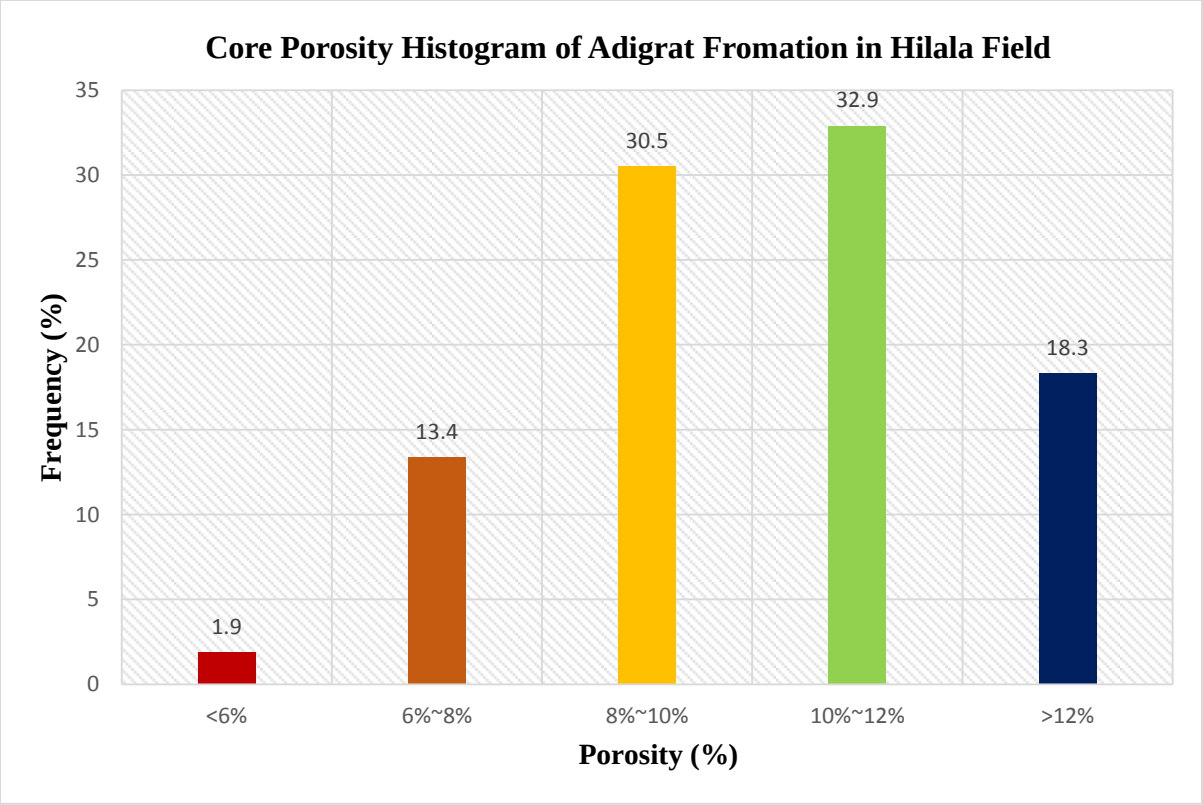

Figure 1. 7 Core Porosity Histogram of Adigrat formation in Hilala Gas Field (POLY-GCL, 2021**)**

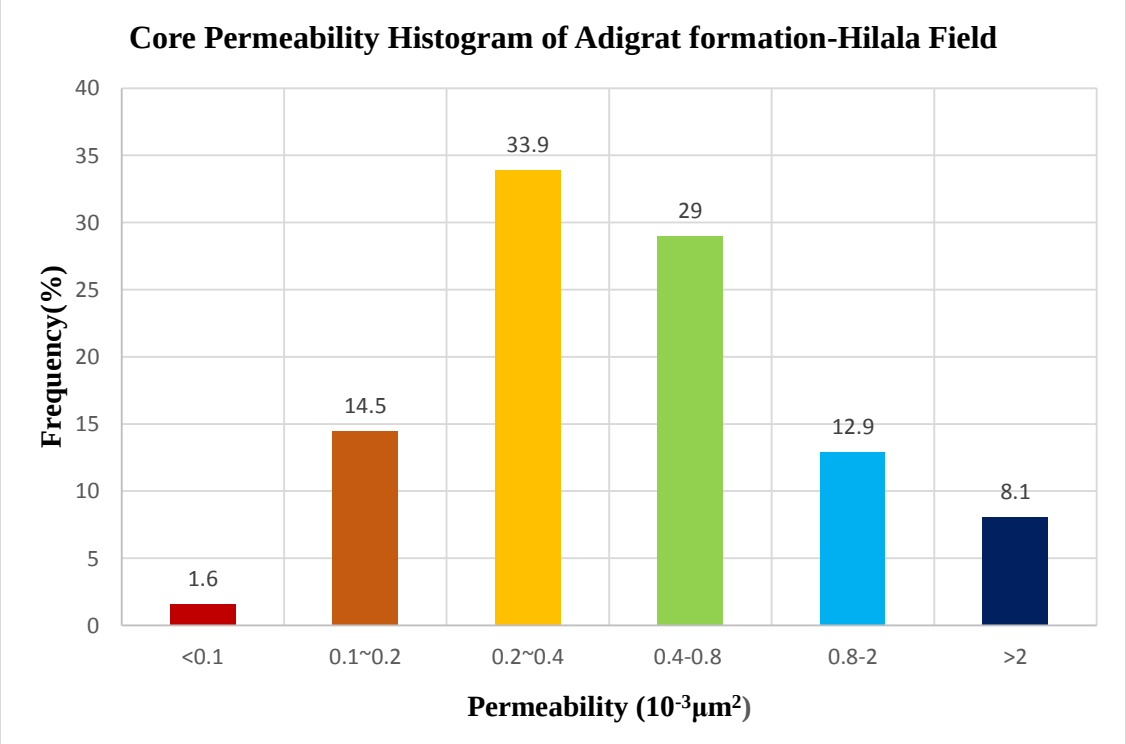

Figure 1. 8 Core Permeability of Adigrat formation in Hilala Gas Field (POLY-GCL, 2021**)**

Table 1. 2 Porosity and Permeability classification of clastic reservoirs (POLY-GCL, 2021**)**

Reservoir Type	Porosity (%)	Permeability ($10^{-3}\mu m^2$)
Ultra-high Porosity and permeability	$\phi \geq 30$	$k \geq 500$
High porosity and permeability	$25 \leq \phi < 30$	$100 \leq k < 500$
Middle porosity and permeability	$15 \leq \phi < 25$	$10 \leq k < 100$
Low porosity and Permeability	$10 \leq \phi < 15$	$1 \leq k < 10$
Ultra-low porosity and permeability	$\phi < 10$	$k < 10$

1.2.8 Reservoir Temperature and Pressure system

The Hilala gas Field's formation temperature and pressure (POLY-GCL, 2021).

$$T=0.0275H+21.12 \quad (1.0)$$

$$R^2=0.9442$$

Where, T is Formation Temperature; H is depth, m.

$$P=0.0114H-1.893 \quad (2.0)$$

$$R^2=0.9821$$

Where, P is formation Pressure, MPa; H is depth.

The geothermal gradient of Hilala Gas Field is 2.5 ˚C/100m, making it a reservoir with normal temperature. The average pore pressure gradient of the field is 1.07Mpa/100m, belonging to normal pressure system. At a depth of 3165m the Formation Temperature and Pore Pressure is about 108.16 ˚C and 34.2 MPa respectively.

1.3 Statement of the Problem

There is a huge commercially recoverable gas reserve in the Ogaden basin of Ethiopia that has been identified for development. Hilala Field, located within this basin system, is considered for gas commercialization in the recent field development plan prepared by private companies and approved by the government. Despite the existence of a significant gas reserve, the recovery factor of such resources is limited by the geological properties of the reservoir formation. Among these formation properties, permeability is critical for an effective hydrocarbon flow.

According to the porosity and permeability classification standards, the Adigrat formation is classified as a low porosity and low permeability reservoir based on its physical reservoir properties. In its natural state, the reservoir with the lowest permeability values cannot produce gas at the optimum level, but hydraulic fracturing can address multiple challenges for efficient

production. The total organic content (TOC), hydrocarbon saturation, reservoir thickness, and other parameters could be attractive enough to develop the resources, but the limiting factor in the production of hydrocarbons will be the ability the fluid to flow from the reservoir to the wellbore. The flow of hydrocarbon fluids is determined by effective permeability, which has to be enhanced in the case of the Adigrat sandstone reservoir. As a well stimulation technique, hydraulic fracturing is one of the most durable innovations that the oil and gas industry has ever invented. Through Hydraulic fracturing as a primary means for production enhancement, commercial gas production from the low permeability formation in the Hilala gas field is possible. The combination of horizontal wells and hydraulic fracturing will greatly expand the ability of producers to profitably recover natural gas and oil from low-permeability reservoirs that otherwise cannot be recovered economically.

1.4 Significance of the study

A complete hydraulic fracturing design would have the potential to enhance production significantly when implemented in tight reservoirs such as the Adigrat sandstone formation. Moreover, stimulation decreases the number of wells to be drilled (well counts) and has an impact on the overall economic investment for any oil and gas development project. For newly emerging countries like Ethiopia in the oil and gas sector, it is crucial to utilize every hydrocarbon deposit using production enhancement technologies such as hydraulic fracturing in an economical way. In this regard, such a study will lay the basis for a development plan, future studies, and the adaptation of improving technologies. The choice to develop a field either with conventional completion or through the application of hydraulic fracturing has a big impact on the number of wells to be drilled and on the infill plan of a field.

This study will constitute an initial contribution to the understanding of multistage hydraulic fracturing designs intended for horizontal wells in Hilala gas fields. It will serve as an initial document for further study, as there is no published work on hydraulic fracturing in the gas field in general.

1.5 Scope of the study

This hydraulic fracturing design study is bound to the low-permeability clastic reservoir of the gas bearing Adigrat formation buried at a depth of 3087-3261 m in Hilala Gas Field, Ogaden Basin, Ethiopia. The overall goal of this horizontal well fracturing stimulation design in Hilala Gas Field is to maximize the reservoir capacity while maintaining a single well's production rate. The aim of this study is to design multistage hydraulic fracturing as a stimulation technique for a horizontal well to increase production. The scope of the study is limited to physical optimization, low permeability reservoir, transverse fracture type, and finite conductivity fractured wells producing under a pseudo-steady state flow regime.

1.6 Objective of the study

1.6.1 General Objective

The general objective of this study is to develop an optimal multiple hydraulic fracturing design for the horizontal well in Hilala Gas Field.

1.6.2 Specific Objectives

The specific objectives of the study are

1) To compute the *reservoir geo-mechanical properties* (Young's Modulus and Poisson's ratio) of the Adigrat formation
2) To determine the *minimum horizontal stress* (*Closure stress*)
3) To determine *Optimal fracture geometry (Optimal* X_f *and* W_f*)* and *optimal dimensionless productivity index* (J_D) that maximize production
4) To determine the *optimum number of transverse hydraulic fractures* in the horizontal well in Adigrat sandstone reservoir

Chapter-2 Literature Review

1.1 Hydraulic Fracturing

Hydraulic fracturing is a method of well stimulation used on oil and gas wells in low permeability reservoirs. It requires the use of special fluids and solid materials to produce fracture or repair damages in the formation. Sands and specially designed fluids are pumped into the reservoir at high pressure and flow rate to fracture the target formation. As the pressure is released after the treatment, the proppant will keep the fracture open which served as a conduit for the flow of fluids from the reservoir to the wellbore (King 2012). Hydraulic fracturing has a wide range of applications. Among these are applications for production enhancement in low and moderate permeability reservoirs(**Figure 2.2**), bypassing wellbore formation damages in high permeability reservoirs, decrease the amount of sand production in loosely consolidated sandstone reservoirs, connecting the formations natural fracture to the wellbore (Guo, Liu et al. 2017). Increased production rate is the most obvious sign of successful treatment as shown in (**Figure 2.2).** The fracture created can operate as conduit for gas, oil or water to flow freely towards the wellbore. The fracture has normally two wings (**Figure 2.1**) ,extending from the wellbore in opposite direction (Jones and Britt 2009). Hydraulic fracturing is induced vertically due to the deep formation and minimal in-situ stress in the horizontal direction (Olayiwola and Rahman 2017).

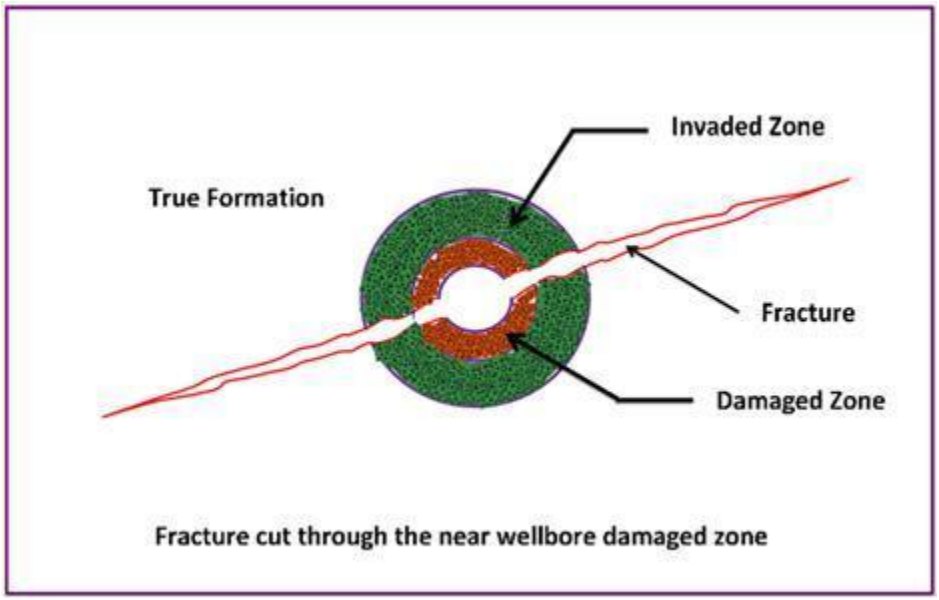

Figure 2. 1 Hydraulic fracture illustration (Energy, 2016)

Hydraulic fracturing is no longer viewed merely as a stimulation technique that is suitable only for low permeability reservoirs in the petroleum industry. Even better, fracturing is no longer seen as a last resort for depleted or unexpectedly poorly performing wells but rather as a critical element of well and reservoir management and essential component of production engineering. Fracturing has become a more popular option to the point where it is now the preferred method of well completion for all type of wells, but particularly for gas well (Marongiu-Porcu 2009, Economides 2013).

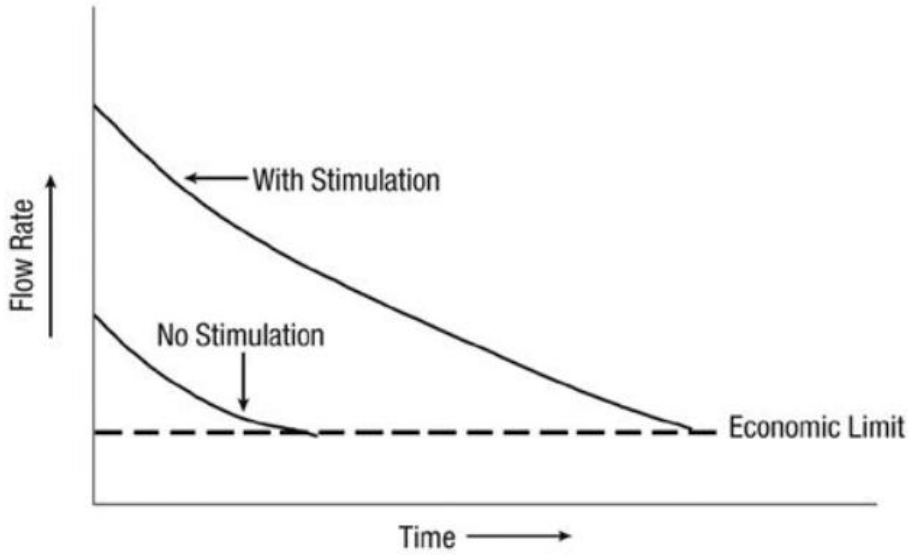

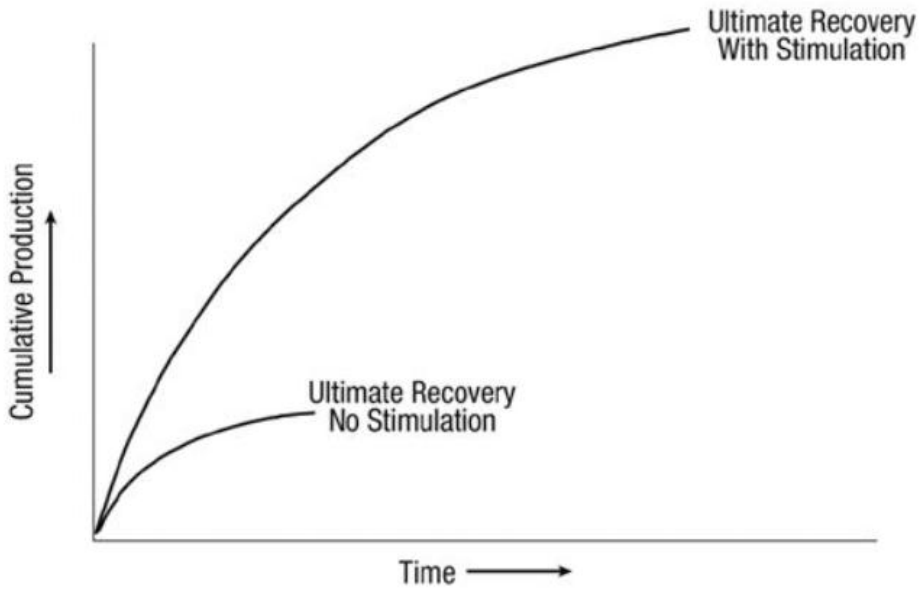

Figure 2. 2. Production enhancement from low permeability reservoirs via hydraulic fracturing (Guo, B., et al. 2017)

Fracturing was first used in the late 1940s (**Figure 2.3**) to improve production from marginal well in Kansas (Olayiwola and Rahman 2017). Following the first concept development through field testing creating the hydraulic fracturing method between 1947 and 1948, the industry followed with a decade of extensive commercial use, but with little significant advances on the process during this early time period. It has been witnessed the widespread acceptance and dissemination of hydraulic fracturing as a functional well stimulation procedure in the last six-seven decades since this initial development era, with significant scientific milestone advances within the fracturing technology community (Olayiwola and Rahman 2017).

Figure 2. 3. First hydraulic fracturing stimulation of a producing well Kansas, USA, in 1947 (Miskimins 2019)

The design and elements of hydraulic fracturing have been fine-tuned over the past seven decades to effectively increase production, typically by multiple folds, particularly in low-permeability reservoirs and source rocks. Hydraulic fracturing wells were typically vertical until the year 2000, with only one fracture per well when stimulation was needed. Between 1950 and 2000, there were roughly one million fracture treatments. Since 2000, the percentage of highly deviated wells has risen dramatically, and fracture treatments have grown from one or two per

well to a range of 20 to more than 200 in a single well that might now be 3 miles (4.8 km) long. (Miskimins 2019).

There are typically four processes involved in the hydraulic fracturing treatment as shown in **Figure 2.4**: pumping a pad fluid (fluid only, no proppant), injecting a series of slurries (fluid and proppant) with varying concentrations of proppant, displacing the proppant-laden slurry at least to the point of entry into the formation, and stopping pumping to allow the formation to be drained and closed before the well is started. (Yao 2013, Miskimins 2019).

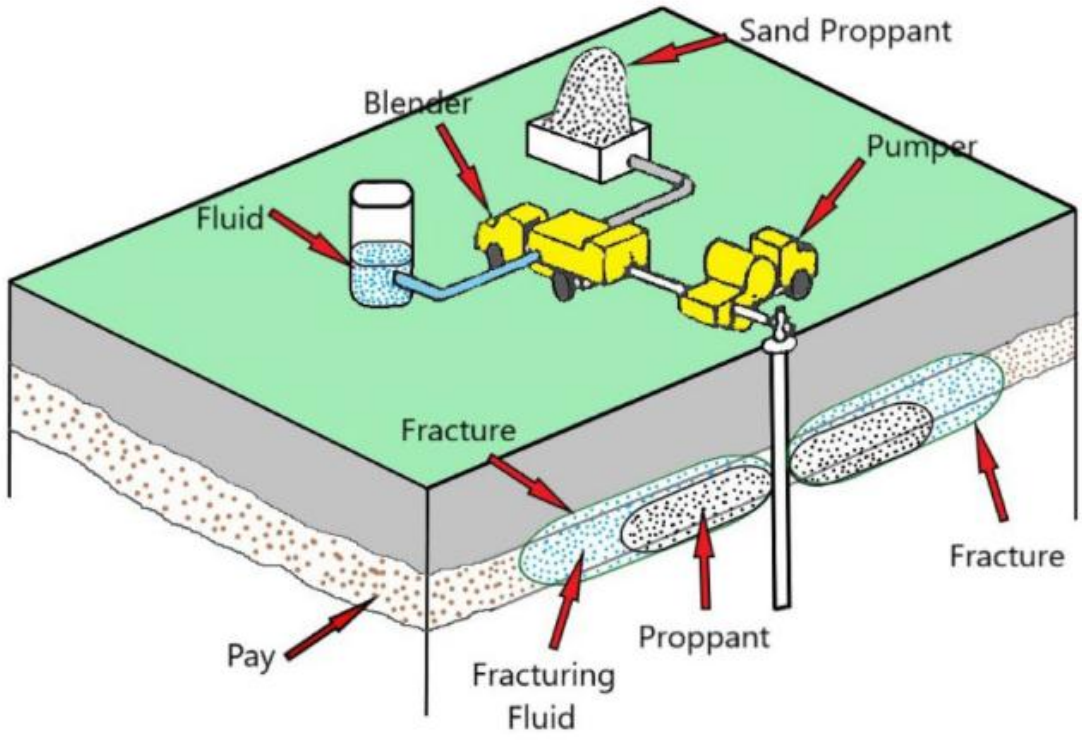

Figure 2. 4. Hydraulic Fracturing process (Miskimins 2019, Esfandiari, M., & Pak, A. (2023))

In the late 1980's, Texas operators began to combine horizontal wells with massive hydraulic fracturing (MHF) treatments. Hydraulic fracturing technology evolved from a single-stage operation to multi-stage (40 plus) fracturing. The multi-stage fracturing (**Figure 2.5**) process starts at the toe of the long horizontal wellbore and progresses to the heel. For each stage, the corresponding wellbore section is isolated, and then, water is pumped to fracture the formation. Sand carried along with the water can prop the fracture (Yao 2013). In unconventional oil and

gas reservoirs, four to six fractures are produced concurrently in each stage and to develop the reservoir fully, there could be up to 40-50 stages (Gokaraju, 2014).

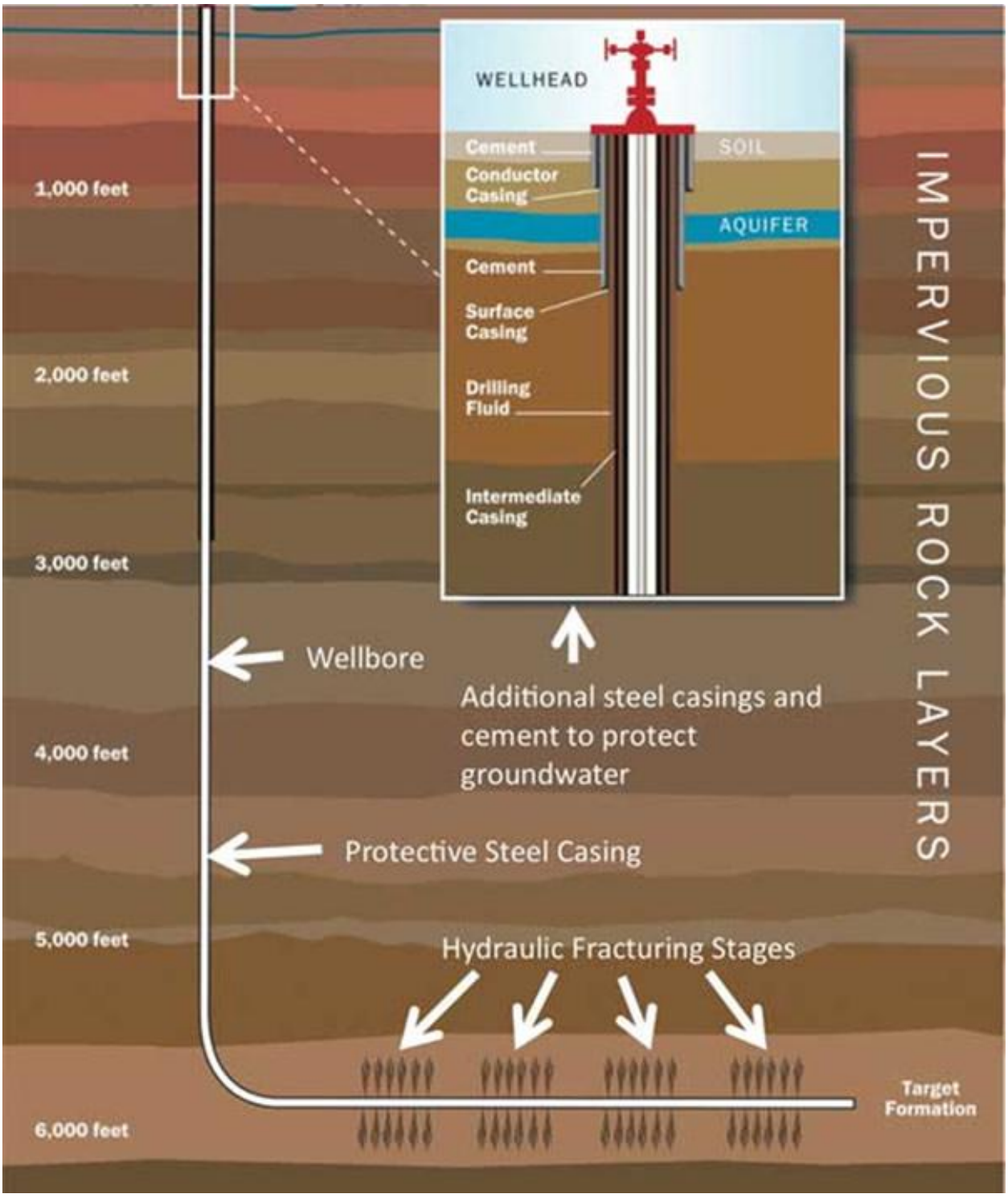

Figure 2. 5 Multistage fracturing in horizontal wells (Survey K.G, 2012)

Multistage hydraulic fracturing has been shown to be more effective than the other techniques through a number of factors. First, more "superhighways" are provided by numerous hydraulic fractures than by a single-stage fractured vertical wells. Second, the increasing stages can significantly increase the contacted reservoir area. Third, there are always open natural fractures in tight and low permeability formations. The interaction of hydraulic fractures with the natural-fracture network increases the stimulated reservoir volume (SRV) (Yao 2013).

1.2 Hydraulic Fracture Mechanics

The principles of rock, fracture, and fluid mechanics play a significant role in the comprehension and engineering design of hydraulic fracturing treatment. The rock mechanical properties determine the stress magnitude and its distribution at depth, whereas its elastic property determines the geometry of the fracture (such as fracture height and width) that are formed and the vertical height migration (Valkó and Economides 1995). Hydraulic fracture can be designed to provide optimum results. However, the design cannot ensure that the procedure will be successful. The in-situ stress situation determines the direction in which a fracture will propagate. Similar geo-mechanical factors govern the fracture geometry and, leak off (Jones and Britt 2009).

Formations that are candidate for hydraulic fracturing are found at great depth, overlain by rock formation of considerable thickness. The overburden causes the formation of interest to be subjected to stress caused from depositional mechanism and tectonic phenomena.

Reservoir formations are confined and under in-situ stress which strongly influence the geometry of fractures initiated from horizontal wells. Three in situ stresses (**Figure 2.6**) that are mutually orthogonal are applied to reservoir rocks: the vertical stress (σv); the maximum horizontal stress (σH); and the minimum horizontal stress (σh) which controls the direction of the fracture (Crosby , Rahman et al. 2002). Most often, the maximum principal stress is the vertical stress—often equal to the weight of the overburden—while the maximum horizontal stress is generally the intermediate principal stress. hydraulic fracture propagates as a vertical fracture in the direction of the intermediate stress (the maximum horizontal stress (Jones and Britt 2009)

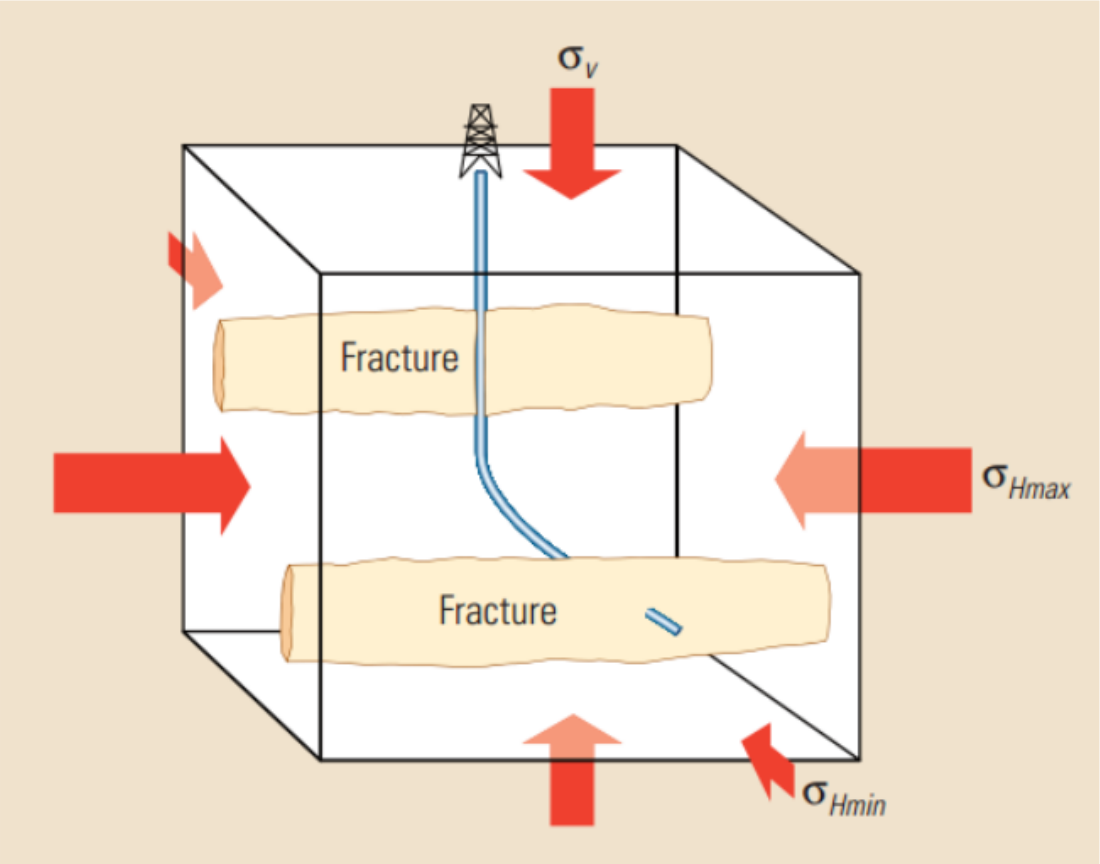

Figure 2. 6. The three principal in-situ stresses and hydraulic fracture (Yang 2014).

1.2.1 Rock Mechanics in Hydraulic fracturing

A rock section responds to a load in reversible or irreversible ways. The genesis and spread of fracture indicate that the material has responded in irreversible ways. Rock property characterization is crucial for calculations of rock deformation, fracture, failure and stress caused by the hydraulic fracturing process (Miskimins, 2019). Some of the interest areas in hydraulic fracturing include the width and closure stress calculation, proppant embedment and breaking calculations, among others. In-situ stress and formation thickness determine fracture height. Calculation of rock deformation, fracture, failure and stress created by the hydraulic fracturing process depend on the ability to characterize rock properties (Economides, M., Oligney, R., & Valko, P. (2002); Miskimins, 2019; Jones, 2009).

Given that the elastic theory still provides a sufficient description of stress, linear elasticity is a valuable tool when investigating fracture. A linear elastic material has an elastic constant that can be measured in a static or dynamic experiment. The static experiment with uniaxial loading

is shown in the **Figure 2.7** below. The Young's modulus (E) and Poisson's (v) ratio are parameters determined from the experiment.

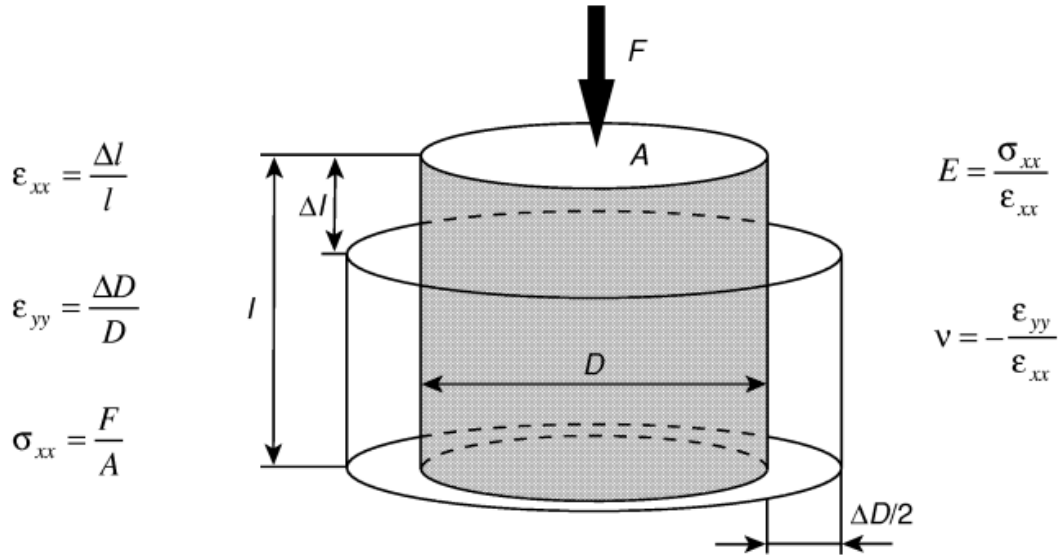

Figure 2. 7. Uniaxial Loading experiment demonstration (Economides, M., Oligney, R., & Valko, P. (2002)).

The sample shorten when a force is applied along the loading direction. Hooke's law state that under uniaxial compression, the stress induced is proportional to the strain.

$$E=\frac{\sigma xx}{\varepsilon xx} \tag{3.0}$$

$$\upsilon=-\frac{\varepsilon yy}{\varepsilon xx} \tag{4.0}$$

where, E is Young's modulus, υ is Poisson's ratio σ_{xx} is the vertical stress, ε_{xx} is vertical strain and, ε_{yy} is horizontal strain.

1.3 Rock Mechanical Properties Determination from Log Data

High rock brittleness value is required for hydraulic fracturing design in the target depth interval for oil and gas development. Rock mechanical properties such as the Young's modulus and Poisson's ratio and other elastic rock properties can be determined using sonic log data (Suranto, 2021). Acoustic wave propagation velocities are typically recorded in terms of interval transit time (the reciprocal of the velocity). Compressional and shear interval transit time logs are applicable for determination of rock mechanical property, fluid and lithology identification

(Aron, J., & Murray, J., 1978). The elastic rock property, namely, the Poisson's ratio and Young's modulus can be utilized to distinguish the brittle and ductile zone from complete sonic data.

In a classical acoustic logging, only the compressional interval transit time (Δtp) is measured. The compressional arrival is simply detected because it arrives early and at spacings generally used it stands out against the background noise preceding it. Estimation of the shear interval transit time (Δts) could be made as this way arrives late (Aron, J., & Murray, J., 1978).

The sonic log data is presented as slowness or the travel time per unit distance mostly travel time per foot which is called the delta T (Δt) , usually measured in μs/ft.

The conversion equation between the slowness and velocity is expressed $\Delta t=\frac{10^6}{V}$ where Δt is in μs/m and v is in meter per second (m/s).

The shear wave (S wave) velocity is calculated using the well-known Castagna equation (1993) Dvorkin, J. P. (2008).

$$Vs=0.804Vp-0.856 \quad (5.0)$$

Young's Modulus and Poisson's ratio Estimation

The following are two methods for calculating dynamic Young's modulus and static Young's modulus using compressional wave velocity (Vp) and Shear wave velocity (Vs) (Khan, I., Ismail, A., & Ali,I. (2018)).

$$E_{dynamic}=\rho Vs^2\left(\frac{3Vp^2-4Vs^2}{Vp^2-Vs^2}\right)x10^{-6}GPa \quad (6.0)$$

$$E_{stat}=0.96Edynamic-2.64\ GPa \quad (7.0)$$

Moreover, the sonic log and density log data results of transverse slowness and density of sandstone formation is used to estimate Poisson's ratio through the following equations

$$\text{Poisson's ratio}(\upsilon_{dynamic}) =\frac{1}{2}\left(\frac{\Delta Vs^2-2\Delta Vp^2}{\Delta Vs^2-\Delta Vp^2}\right) \quad (8.0)$$

$$\upsilon_{static}=1.2437\ \upsilon_{dynamic} \quad (9.0)$$

Where;

Vp= Primary wave velocity (m/μs), Vs=Secondary wave velocity (m/μs)

ρ=rock density (g/cm^3) ,*E*=Young's modulus (Pascal)

2.3.2 Brittleness Index Calculation

Fracturing ability of a rock is not only dependent on in situ stresses but also governed by rock mechanical properties (e.g., tensile strength, Young's modulus, Poisson's ratio), rock physical properties, and mineral contents. The general guideline for the rock mechanical properties on hydraulic fracturing is that high Young's modulus value and low Poisson's ratio match to a brittle rock, which in turn expedient the hydraulic fracture propagating (Zhang, 2019).

Rickman et al., (2008) applied the brittleness index (B) to quantify rock brittleness. This brittleness index combines the effect of Young's modulus and Poisson's ratio of the rock and can be expressed in the following equation (Zhang,2019).

$$B = 50x\left(\frac{E-Emin}{Emax-Emin}+\frac{v-vmax}{vmin-vmax}\right) \quad (10.0)$$

Where

B is the brittleness index (%).

E is the static Young's modulus of the rock

E_{max} and E_{min} are the maximum and minimum Young's moduli respectively (constant), E_{max}=55.2 GPa E_{min}=6.9 GPa ; v is the Poisson's ratio of the rock , vmax and vmin are the maximum and minimum Poisson's ratio, respectively ; V_{max} =0.4, V_{min}=0.15 (Zhang, 2019).

A high index of brittleness (e.g., B ≥60), i.e. a brittle rock has a high Young's modulus and low Poisson's ration, while a ductile rock has a low brittleness index. When combined with formation closure and breakdown pressures, the brittleness index can be used to help hydraulic fracturing design. It is important to note that the rock's brittleness is influenced by both rock mechanical properties and physical properties (e.g., bulk density, porosity, the mineral contents). In addition, a high Young's modulus may indicate a high degree of brittleness, but it may also indicate low porosity (Zhang, 2019).

2.4 Analytical Fracture Models

Hydraulic fracturing models are used to comprehend the hydraulic fracturing processes i.e fracture initiation, rock deformation, fluid flow in the fracture, proppant transport to the created fracture and fluid loss into the formation. Fracturing model are mainly used for predicting the

fracture geometry and proppant placement, to conduct sensitivity analysis and, perform treatment optimization (Guo, Liu et al. 2017).

Generally, hydraulic fracturing models fall into three main types. The 2D fracture model, 3D fractures model and the unconventional fracture model. During and after the fracture treatment, fracture growth evaluation and fracture geometry estimation is made based on the analysis of the'' net pressure''. The ''net pressure'' is defined as the change in pressure inside the fracture and the minimum closure stress.

$$P_{net}=P_f-\sigma_{closure} \tag{11.0}$$

Where P_{ne} is the net pressure, P_f is the fluid pressure inside the fracture and, σ_{min} is the minimum closure stress.

2.4.1 The PKN Model

Perkins and Kern developed an analytical method for the vertical fracture propagation (**Figure 2.8**) assuming a fixed fracture height and an elliptical cross section in the vertical plain. Additionally, they claimed that only the maximum width at any point along the fracture length is proportional to the net pressure on the elliptical width profile of the fracture proposed by Sneddon and Elliott (1946) ,(Guo, Liu et al. 2017).

$$W_{max}(x)=\frac{2(1-v^2)Pnet(x)hf}{E} \tag{12.0}$$

Where, $W_{max}(x)$ is the maximum fracture width at position x along the fracture length. $P_{net}(x)$ is the net pressure at position x, and h_f is the fixed fracture height. The net pressure $P_{net}(x)$ is a function of position x along the fracture with maximum value occurring at the wellbore where x=0.

The solution of the maximum fracture width at point x for a symmetrical bi wing fracture is given by

$$W_{max}(x)=3\left[\frac{(1-v^2)\mu qi(xf-x)}{E}\right]^{1/4} \tag{13.0}$$

Where X_f is the fracture half-length. and

$$P_{net}=\frac{3(\mu qiXf)^{1/4}[\frac{E}{1-v^2}]^{3/4}}{2hf}$$

The maximum fracture width at the wellbore (x=0) in an oil field is as follows

$$W_w=[\frac{(1-v^2)\mu qiL}{E}]^{1/4} \quad (14.0)$$

Where W_w is the maximum fracture width at the wellbore in in., μ is in cP, qi is in bbl/min, L is in ft, v is Poisson's ration (0.2-0.3 for most petroleum formations), and E is in psi.

Nordgren (1972) add storage dominated (without leak off effect) and high leak off approximated analytical solution which now known as PKN model.

The storage dominated approximation of Nordgren model, is given as

$$X_f=58.07\left[\frac{Eqi^3}{(1-v^2)\mu hf^4}\right]^{1/5} t^{4/5} \quad (15.0)$$

$$X_f=0.99\left[\frac{(1-v)^2\mu qi^2}{Ehf}\right]^{1/5} t^{1/5} \quad (16.0)$$

Where X_f is the fracture half-length and W_w is the maximum fracture width at the wellbore all in oil field units.

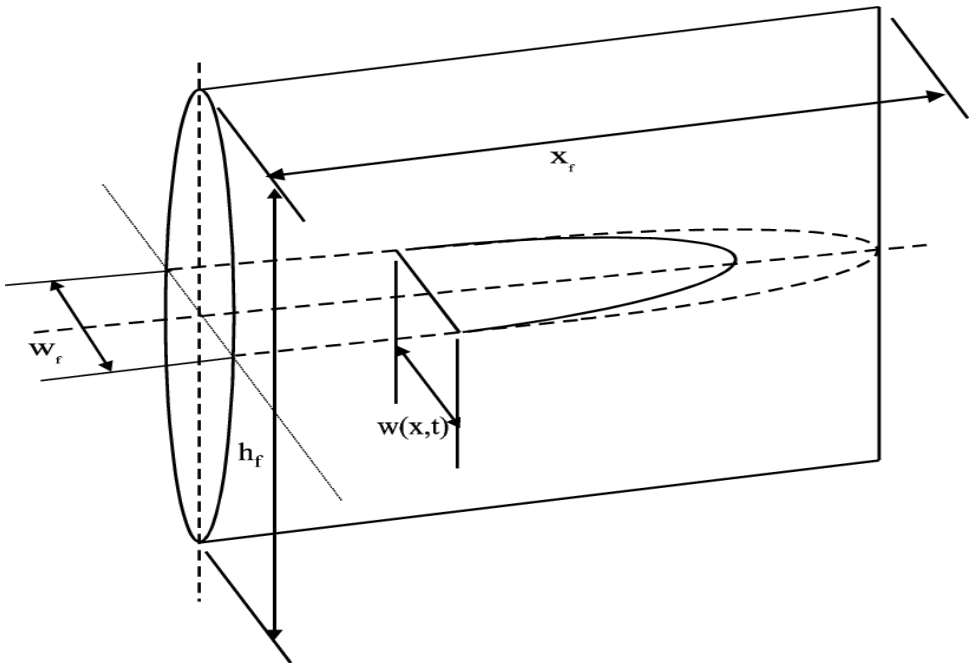

Figure 2. 8. The PKN fracture geometry (MM Rahman et al., 2010)

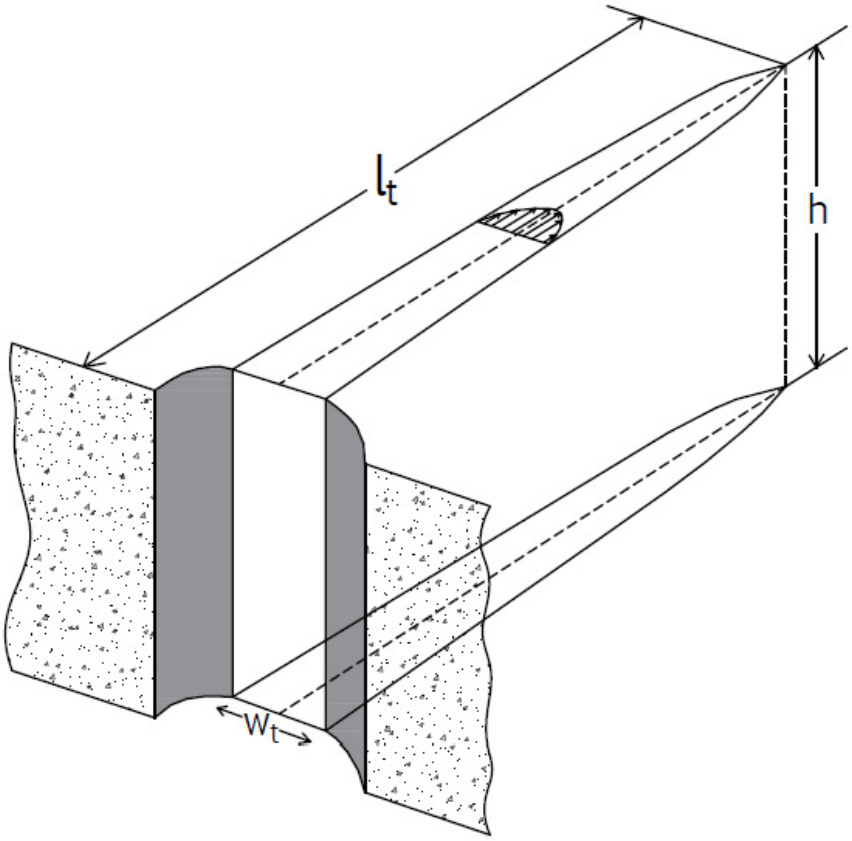

Figure 2. 9. KGD constant height fracture model (Wasantha, 2017)

2.4.2 The KGD Model

The KGD fracture model assumes a rectangular cross section in a vertical plane with the formation stiffness centered in the horizontal plan (Wasantha, 2017). Accordingly, the fracture width at the wellbore (wt) and the fracture length (lt) are expressed as

$$l_t = a\left[\frac{GQ^3}{(1-v)\mu}\right]^{1/6} t^{2/3} \quad (17.0)$$

$$w_t = b\left[\frac{Q^3(1-v)\mu}{G}\right]^{1/6} t^{2/3} \quad (18.0)$$

where, Q =constant injection rate, G is the shear modulus, v is the Poisson's ratio, μ is the viscosity of the fluid, t is the time and a and b are constants. `

The execution of these 2D models differ mostly in how they handle fracture compliance: The PKN model yields an elliptical cross section versus height under the assumption of constant pressure in the fracture and a sliding opening at the layer interface for the KGD model. The PKN model is more suited for usage in fracture with a high length / height aspect ratio because the shortest fracture dimension typically drives fracture compliance, while the KGD model performs

better when the length to height ratio is low. (Miskimins 2019).The general consensus is that the PKN model applies best to fractures that are longer relative to their height , whereas the KGD fracture model applies better when fracture are shorter relative to their height (Jones and Britt 2009).

2.5 Horizontal well Fracture Propagation

Horizontal wells can be drilled in any direction for various benefits. In Hydraulic fracturing propagation, two limiting wellbore fractures have received considerable attentions mainly governed by the direction of minimum principal stress. When a horizontal well is fractured, either longitudinal or transverse fracture results.

(1) *Longitudinal (axial) fracture* that propagate in planes parallel with wellbore axis; formed where the horizontal wells are drilled perpendicular to the minimum horizontal stress or along to the maximum horizontal stress.

(2) *Transverse fracture propagates* in plane orthogonal to wellbore axis-formed where horizontal well is drilled along the minimum horizontal stresses or perpendicular to the preferred fracture plane.

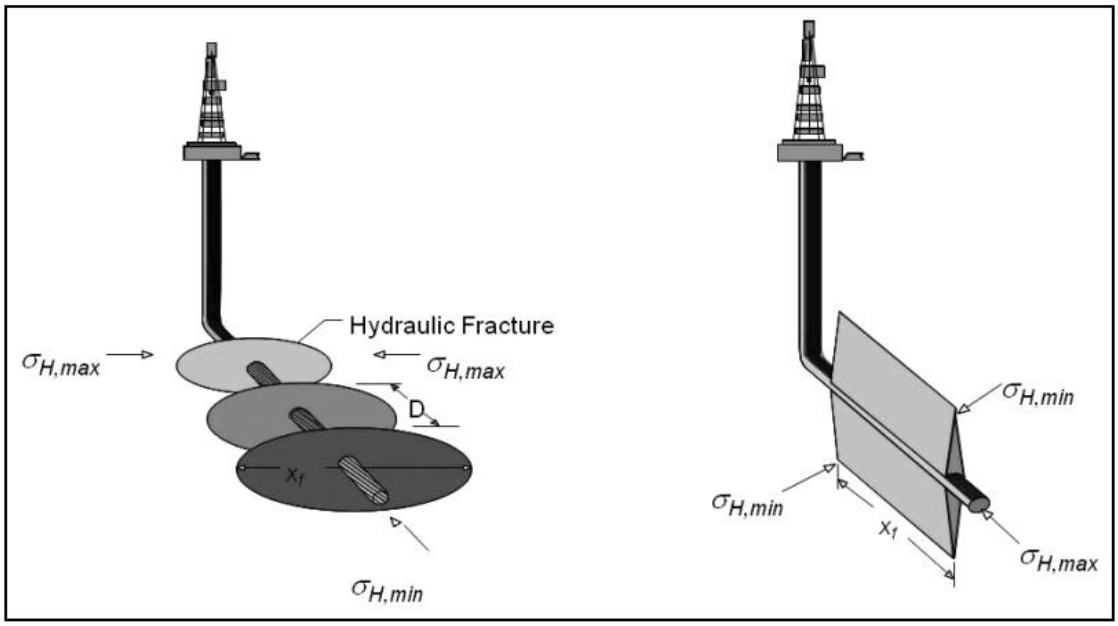

Figure 2. 10. Multiple transverse fracturing on the left and Longitudinal on the right (Liu, 2012)

In horizontal wells in gas reservoirs, transverse fractures are favored when the reservoir permeability is less than 0.5 md; if the gas reservoir has a permeability larger than 0.5 md, longitudinal fractures are preferable to identical wells with transverse fractures (Economides, Marongiu-Porcu et al. 2010).

2.6 Fracturing Materials

Fracturing fluid (including additives) and proppant are the two main materials needed to establish a conduit for production of hydrocarbons at the wellbore. The fluid's system function is to initiate, propagate, and transport the proppant, while the proppant role is to maintain the conductive pathway to the wellbore once the treatment is complete and well is restored to production. The volume and quantity of these two materials must be defined as part of the fractured design (Jones and Britt 2009).

The fluid and additive work together to form the hydraulic fracture and then to deliver the proppant into the created fracture. Once the proppant is in place, and confined by the fracture closure, the carrier fluid and additive are degraded and flow back out of the fracture –''fracture clean up'' creating the desired significant productive flow path (Economides, M., Oligney, R., & Valko, P. (2002)). The fracturing fluid must possess particular physical and chemical characteristics in order to successfully stimulate the target formation. The fracturing fluid should be compatible with the formation material and fluids, be able to suspend proppant and transport it deep into the created fracture, capable of developing the required width via its viscosity. In addition, it should possess properties of low leak off, easy to remove from the formation, stable and maintain its viscosity throughout, possess low frictional pressure and It should be simple to prepare in the field (Miskimins 2019)

2.6.1 Proppants

Proppants are solid material employed in hydraulic fracturing to hold and maintain the created fracture apart to create a conductive channel to the wellbore, after the end of treatment and the fracturing fluid has leaked off. The composition, physical property, proppant pack permeability, long-term degradation of the proppant and movements of formation fines in the fracture as well as effects of post closure polymer concentration in the fracture are some of the factors affecting the fracture conductivity (Economides and Nolte 1989). Because the proppant must counterpart earth's stress to keep the fracture open, material strength is critical; the proppant material must

be strong enough to withstand the closure stress. Other parameters looked into proppant selection include size, shape, composition, and to a lesser extent, the density of the proppant. (Economides, M., Oligney, R., & Valko, P. (2002)). The difficulty in selecting the appropriate proppant for fracturing lies in studying and knowing the reservoir properties and the intended fracture geometry to be created, and then combining that knowledge to the choosing of proppant and its performance properties. Eventually, the decision is an economical one- weighing of cost of deploying a specific type and volume of proppant against the value regained (Miskimins 2019)

The two major classes of proppants are natural sand and man-made ceramic or bauxite proppants. Sands are used for lower stress applications, in formations approximately 8000 ft (2438.4m) preferably, considerably, less. Man made proppants are used for higher stress situation in formation generally deeper than 8000 ft (2438.4m).

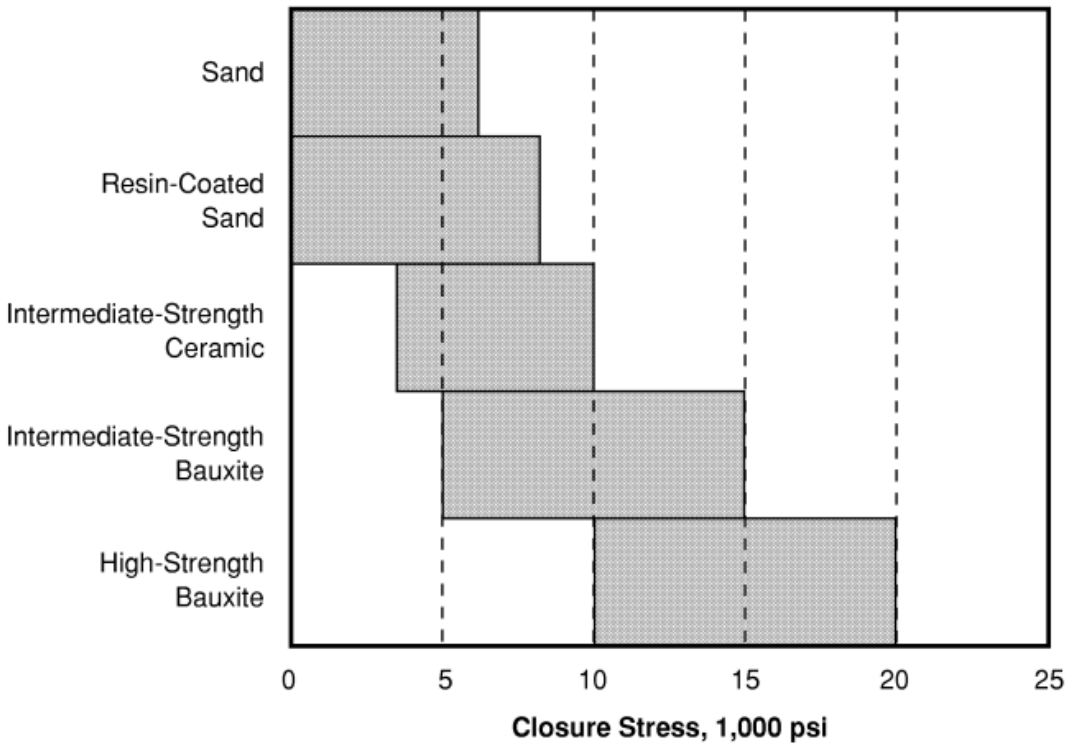

Figure 2. 11. Proppant Selection guide (Economides, M., Oligney, R., & Valko, P. (2002)).

2.6.1.1 Physical properties of Proppant

Proppant possess several physical properties that affect its performance. Some of the physical properties include grain size and grain size distribution, sphericality and roundness, crush resistance, density, acid solubility and turbidity etc. The grain size of the proppant affects the fracture conductivity and its transport inside the fracture. The grain size of the proppant is measured in mesh-size ranges, which is well-defined by the quantity of openings across one linear inch of screen. For a large particle size, the mesh size number is small. Comparatively ,30/50 mesh proppant is smaller than 20/40 mesh proppant. Regularly used industrial proppant size include 12/20, 16/30, 20/40, 30/50, 40/70 etc (Guo, Liu et al. 2017).

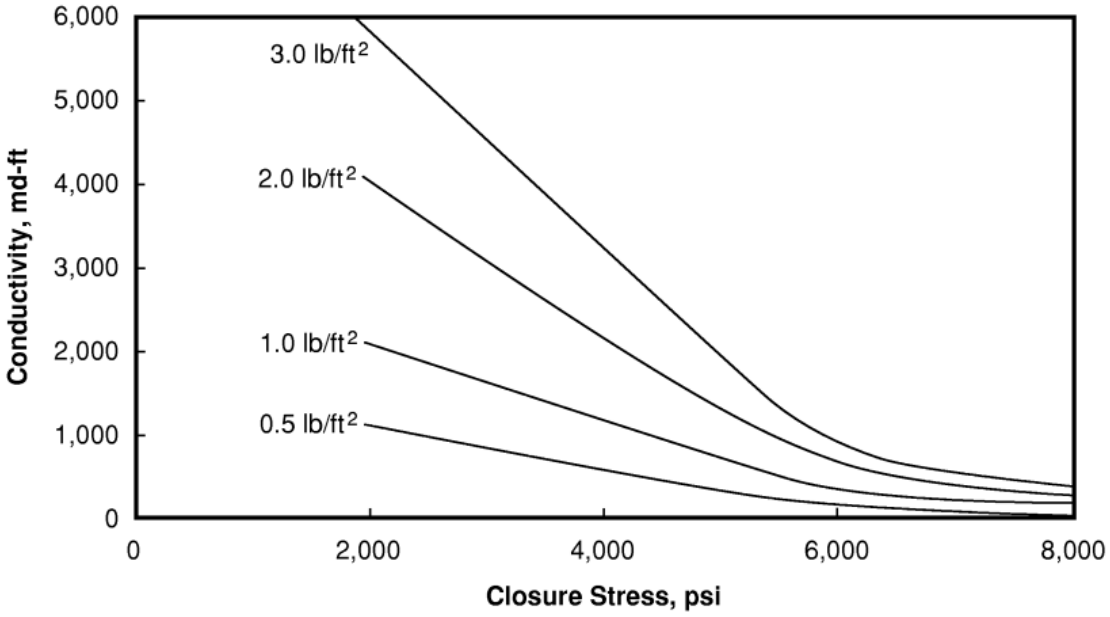

Figure 2. 12. Fracture conductivity for various areal proppant concentration (20/40 mesh) (Economides, M., Oligney, R., & Valko, P. (2002)).

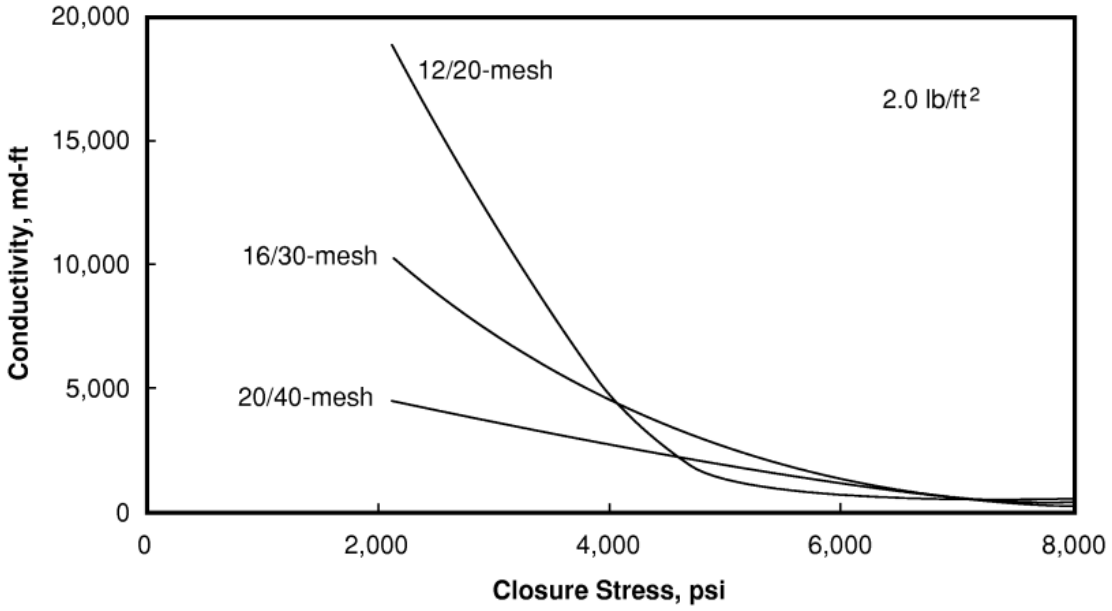

Figure 2. 13. Fracture conductivity for various mesh size (Economides, M., Oligney, R., & Valko, P. (2002)).

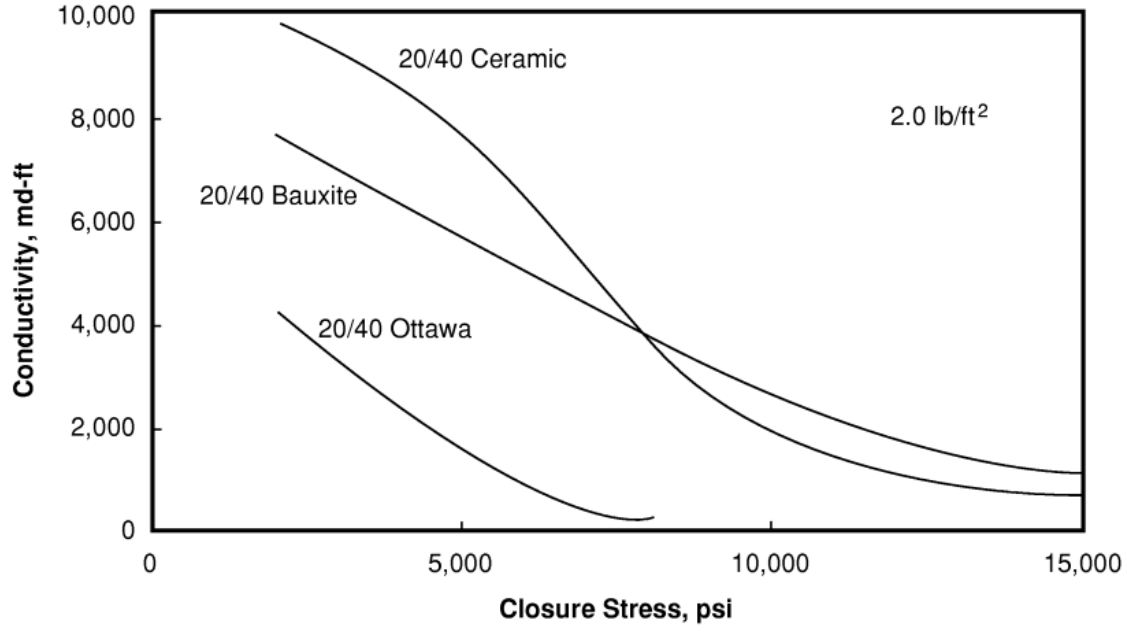

Figure 2. 14. Fracture conductivity for various proppants (Economides, M., Oligney, R., & Valko, P. (2002)) .

Figure 2. 15. 40/70 White sand **40/70 Brady sand (Miskimins 2019)**

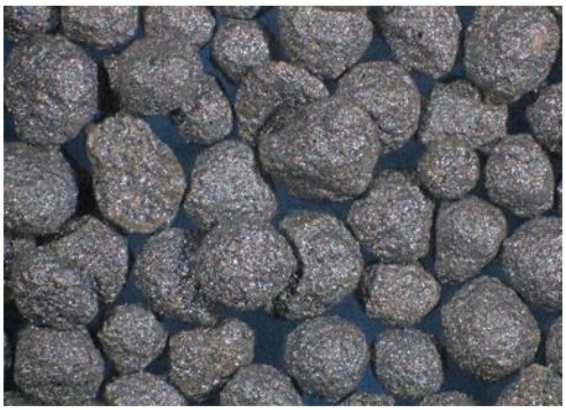

Figure 2. 16.High-strength ceramic **ISP ceramic (Miskimins 2019)**

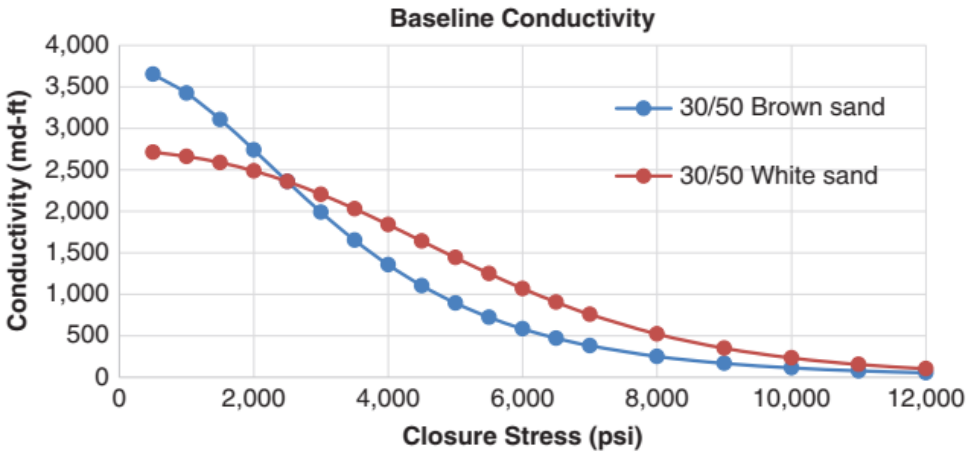

Figure 2. 17. Typical baseline conductivities—white and brown sands (Miskimins 2019)

2.7 Effective Closure stress Calculation

During the selection of the required proppant, it is essential to know how much the closure pressure will be. Eaton's equation is used to determine the closure stress (minimum horizontal stress) at depth in the reservoir. It is generally expressed form:

$$S_h=\frac{v}{1-v}(Sv-Pp)+Pp \tag{19.0}$$

Where v is Poisson's ratio, Sv is the absolute vertical stress, and Pp is the reservoir pore pressure. The absolute vertical stress Sv is roughly the weight the overburden per unit area. In the integral form it is expressed as

$$Sv=\int_0^H \rho dH \tag{20.0}$$

where ρ is the density of the overlying strata.

Density log makes it simple to calculate the density from the surface to the formation of interest. In practice the value is found to range from 0.1 to 1.1 psi per foot of depth. If there is no other information, the value is assumed to be 1 psi/ft (Economides, M., Oligney, R., & Valko, P. (2002)), (Valkó and Economides 1995).

The reservoir pore pressure must be subtracted from the total vertical stress in order to determine the effective vertical stress, which is expressed as

$$\sigma_v = Sv - \alpha P_p \quad (21.0)$$

where α is Biot's constant (value between 0.7 to 1) or the ''*poroelastic''* constant, to take into account the reservoir fluid are not in a closed box (free to move out of control under consideration) this constant term added to the pore pressure (Economides, M., Oligney, R., & Valko, P. (2002)).

The reservoir rock will experience a horizontal stress as a result of the overlying vertical stress. The magnitude of the horizontal stress is calculated by

$$\alpha_h = \frac{v}{1-v}\sigma v \quad (22.0)$$

where, α_h is the effective horizontal stress

2.8 Hydraulic Fracturing Fluid

The Proppant is subsequently transported into the created fracture by the fracturing fluids, which transmit hydraulic pressure from the pump to the formation. Factors to consider when selecting the fluid include availability, safety, ease of mixing and use, viscosity characteristics, compatibility with the formation, ability to clean up from the fracture and, cost (Economides, M., Oligney, R., & Valko, P. (2002)).

The two available hydraulic fracturing fluids are

1) Guar based crosslinked Gel Systems-Viscosity water based

2)Friction reducer water (FR/Slickwater)- Low friction water based

The comparative advantage of the two fracturing fluids is shown in **Table 2.1** below

Table 2. 1 Comparison of Friction Reducer water (FR/Slickwater) and Guar based Crosslinked Gel (after Dobbs J., 2020**).**

Utilization	FR/HVFR/Slick water	Advantage	Guar based croslinked gel	Advantage
Hydraulic equipment Horsepower	15,000 - 25,000 HHP		4,000 - 15,000 HHP	
Investment size	Larger		Lower	X
Pumping equipment rate	50-120 barrels/minute		20 - 75 barrels/minute	
Investment size	Larger		Lower	X
Water	More		Less	X
cost example: DJ basin	$500,000/job		$155,000/job	X
Saline or reproduced water	<12,000 ppm TDS		>100,000 ppm TDS	X
Pump parts & pipes Rate of erosion	High		Low	X
Chemical additives	1	X	3	
Friction - Velocity	Lower - Higher	X	Higher - Lower	
Viscosity				
FR/slickwater	2 - 5 cps			
HVFR/slickwater	5 - 30 cPs			
Ultra - Light Gel, guar based			100 -200 cPs	X
Light gel, Guar based			300 - 500 cps	X
Proppant transport	Lower, based on velocity		Higher, based on viscosity	X
Frac width	Reduced width		Required width	X
Screening out early	yes		no	X
Large size & amount of proppant	no		yes	X

2.9 Fracture Height Design

The basic goal of hydraulic fracturing is to create and sustain a stable fracture with high conductivity in order to enhance the productivity of the well and its ultimate recovery (Jones and Britt 2009, Miskimins 2019).The selection and placement of proppant are the critical components of a successful stimulation treatment. The importance of fracture height formation from different fracturing executions is illustrated in **Figure 2.18** below. In (a), the fracture created after the initiation is very small, and *hf* is small and did not cover the required area. In (b), the fracture goes beyond the reservoir area and covers other intervals. In (c), the fracture grows outside of the intended zone and hits an aquafer zone. In all these illustrations, the importance of fracture design and understanding rock mechanics is illustrated. The potential productivity benefit of the fracture is determined by the formation's ability to convey fluid to the fracture and the fracture's potential to deliver the fluids to the wellbore.

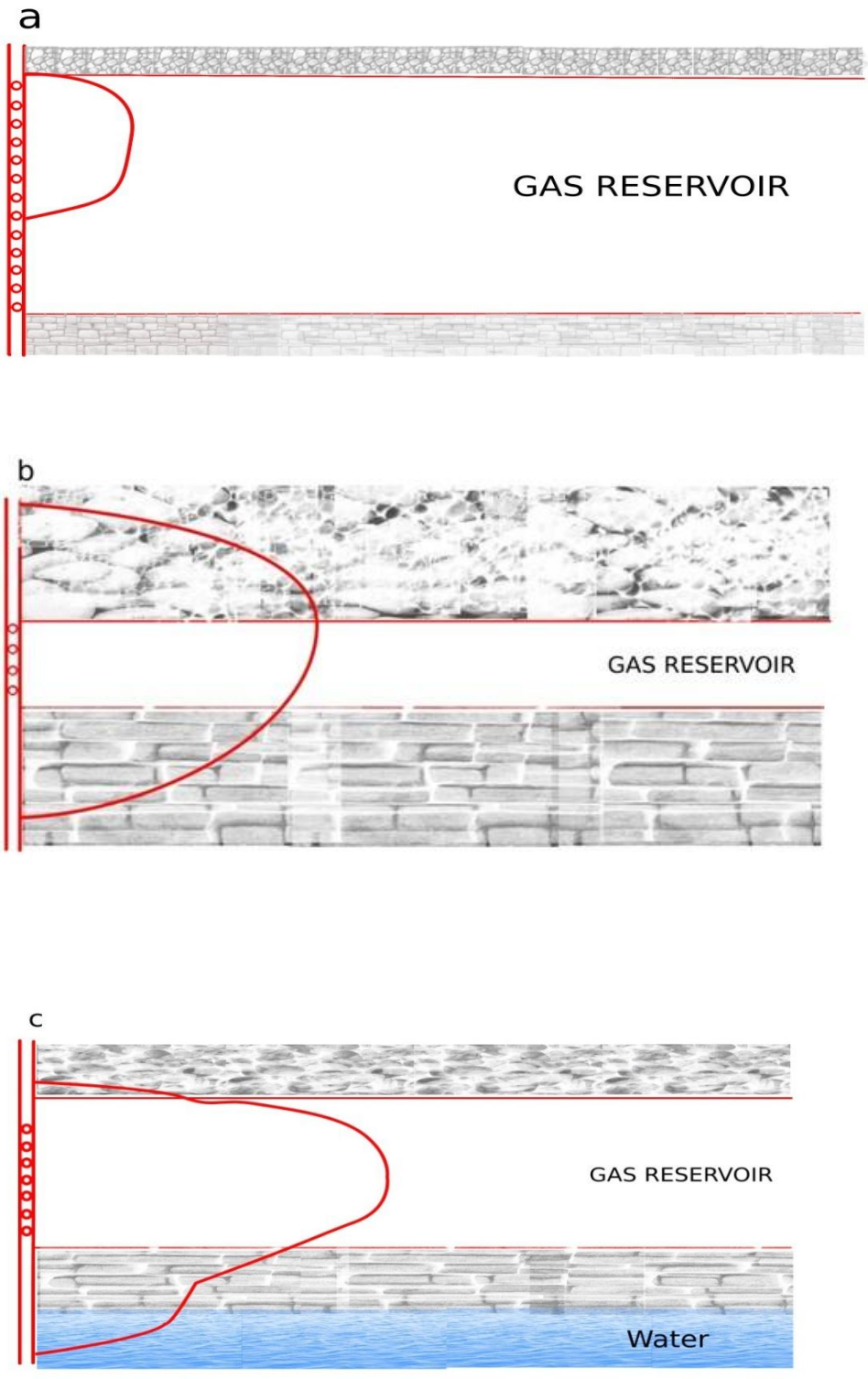

Figure 2. 18. Importance of fracture height in fracture design (after Economides, 1989)

2.10 Productivity Index

The productivity index, which is widely used to measure well property, is a measure of the well potential or ability to produce. The improved in productivity can be used to either increase the production rate or decrease the pressure decline.

Productivity index (PI) most commonly denoted by J is expressed as

$$J = \frac{q}{\Delta P} \tag{23.0}$$

Where ,

J= Productivity index

q=production rate, q= $\frac{2\pi kh\Delta p}{\alpha 1 \beta \mu} qD$

ΔP=Driving force (pressure drawdown),

$$\Delta P = \frac{\alpha 1 \beta q \mu}{2\pi kh} PD \tag{24.0}$$

Where, k is the formation permeability, h is the pay thickness, β is the formation volume factor, μ is the fluid viscosity and α is the conversion constant.

According to (Economides, M., Oligney, R., & Valko, P. (2002)), The pseudo-steady state productivity index is pivotal from the perspectives of fracture design. (J).

$$J = \frac{q}{\acute{P} - Pwf} = \frac{2\pi kh}{\alpha 1 \beta \mu} JD \tag{25.0}$$

where J_D is the dimensionless productivity index

Moreover, there are several approaches to integrate the stimulation effect in the productivity index. one way to incorporate it is via the idea of '' pseudo-skin''

$$J_D = \frac{1}{ln\left[\frac{0.472re}{rw}\right] + sf} \tag{26.0}$$

Or alternatively through the equivalent wellbore radius,

$$J_D = \frac{1}{ln\left[\frac{0.472re}{\acute{r}w}\right]} \tag{27.0}$$

J_D=is a function of drainage -volume geometry and fracture parameters.

Equation (27.0) is most convenient and wide-ranging when considering fractured wells non-circular and with more general drainage areas.

The capacity of the rock formation to deliver fluids to the fracture and the fracture's ability to deliver fluids to the wellbore determines the potential productivity benefit offered by the fracture. The generally used term for this relationship between fracture conductivity and reservoir capacity is call dimensionless fracture conductivity *(Cf_D)* (Miskimins 2019).

$$C_{fD}=\frac{Kf*W}{K*Xf} \tag{28.0}$$

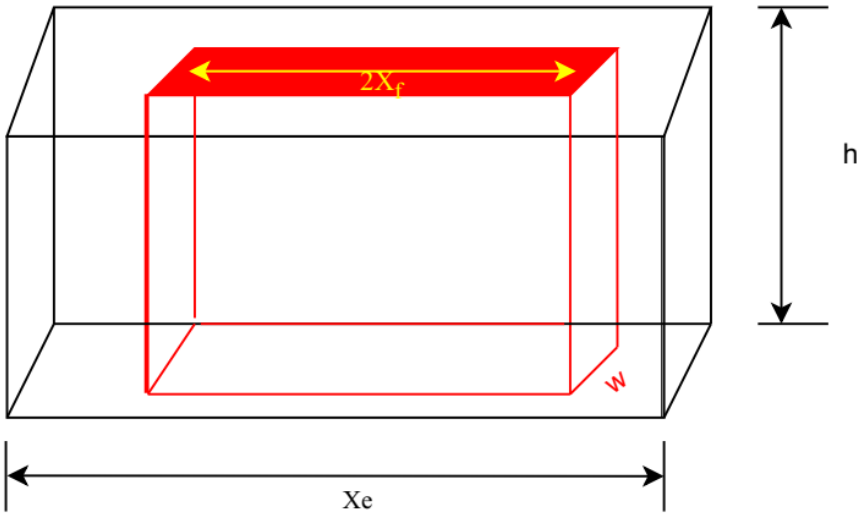

Figure 2. 19. Fracture demonstration for a rectangular drainage area (Economides, M., Oligney, R., & Valko, P. (2002)).

Assume that the fracture inside the rectangular prism **Figure 2.19** is a fracture intersecting the outside rectangular drainage area from bottom to top in a vertical well,

The performance is known to depend on the penetration ratio in the x direction

$$I_x=\frac{2Xf}{Xe} \tag{29.0}$$

and on the dimensionless fracture conductivity (C_{fD}).

Where X_f is the fracture half-length, X_e is the side length of the square drainage area, K is the formation permeability K_f is the proppant pack permeability, and w is the average (propped) fracture width.

2.11 Optimization of Hydraulic Fracturing

A common hydraulic fracturing design optimization procedure starts from a fracture size, usually denoted by, but not limited to, the fracture half length. A fracture propagation model then describes the hydraulic fracturing geometry definitely including the width and, with an appropriate model, the fracture height.

The key to formulating a meaningful technical optimization problem is to realize that the fracture penetration and the dimensionless fracture conductivity (through width) are competing for propped volume.

For a fixed proppant volume, the longer the fracture, the narrower the fracture is. Longer fractures expose higher areas for production and narrower fractures give higher friction losses. Consequently, there is an optimal fracture length and width that would maximize the dimensionless productivity index of fractured wells.

combining equation (30) and (31) , a new term called dimensionless proppant number (Np) is introduced by (Economides, M., Oligney, R., & Valko, P. (2002))..

Dimensionless variables are a key aspect of the unified fracture design (UFD). By far the most essential aspect in unified fracture design is the dimensionless proppant number, Np which can also be expressed as

$$N_p = I_x^2 C_{FD} = \frac{4KfXfW}{KXe^2} = \frac{4KfXfWh}{KXe^2h} = \frac{2KfVf}{K\,Vres} = \frac{2Kf}{K}\frac{Vp}{Vr} \qquad (30.0)$$

Where, Np is dimensionless proppant number, K_f is proppant or fracture permeability, X_f is fracture half-length, w is fracture width, Xe drainage side length. V_f is the propped volume, *Vres*, reservoir volume. According to equation (32) above the proppant number is the weighted ratio of propped fracture volume (two wings) to the reservoir volume, with a weighting factor of two times the proppant to formation permeability contrast.

In the above definition of proppant number (Np), K_f denotes the permeability of the proppant pack which is a design important parameter. The manufacturer provides nominal value for proppant package permeability and allowed it to be decreased by a factor. It is crucial to note that the permeability of the proppant pack, K_f, is normally reported from laboratory testing. However,

actual downhole circumstances such as formation fine migration, fracture fluid damage, and effects of non-Darcy flow drastically affect the result. The conductive length, is considered to be made up of two equal half lengths (X_f) extending in opposite direction from the well, just for the purpose of fracture design and well productivity estimates (Economides, Hill et al. 2013). There are three main strategies to improve fracture conductivity: increase proppant concentration in order to create wider fracture, use a bigger proppant with higher permeability and use a stronger proppant to lessen crushing and enhance conductivity (Economides, M., Oligney, R., & Valko, P. (2002)).

Figure 2.20 shows J_D represented as a function of dimensionless fracture conductivity, C_{FD} with I_x as a parameter. However, it is not helpful in solving an optimization problem involving a fixed amount of proppant.

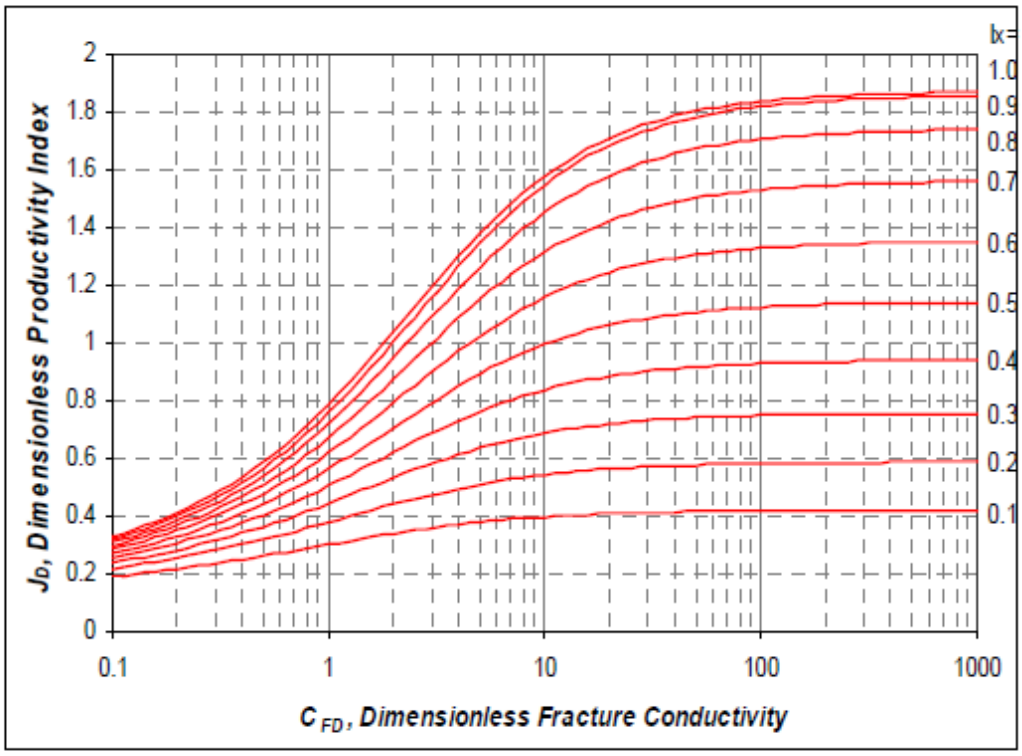

Figure 2. 20. McGuire-Sikora type -J_D versus I_X for pseudo steady state condition (J.I Rueda, 2004)

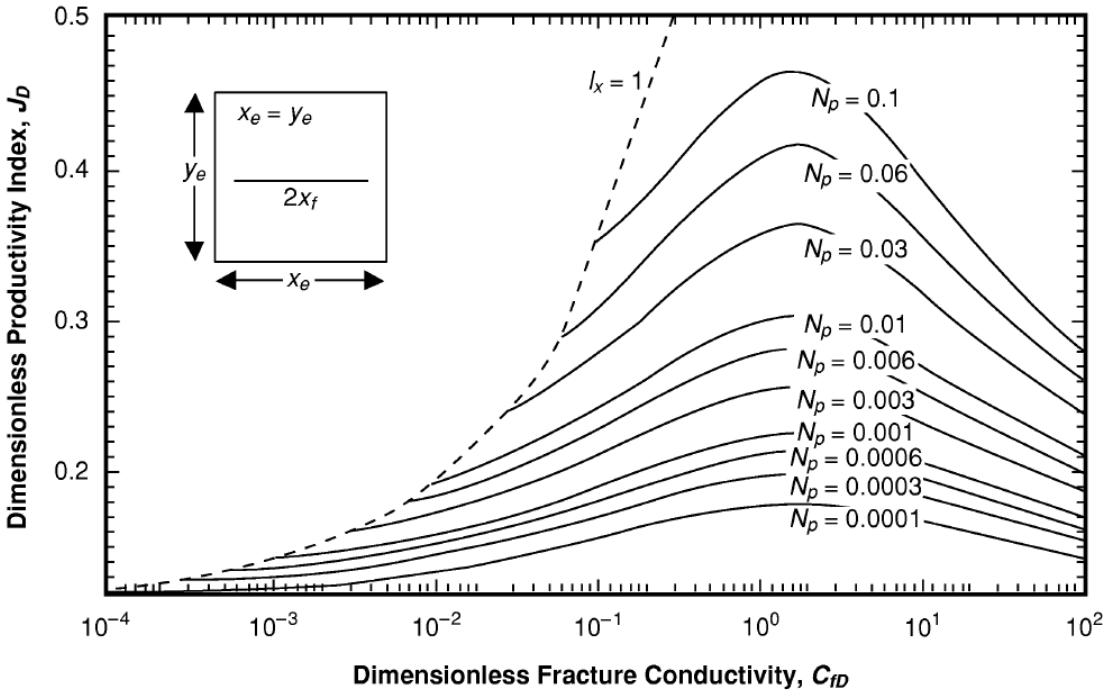

Figure 2. 21. Dimensionless productivity index (Nprop<0.1) (Economides, M., Oligney, R., & Valko, P. (2002)).

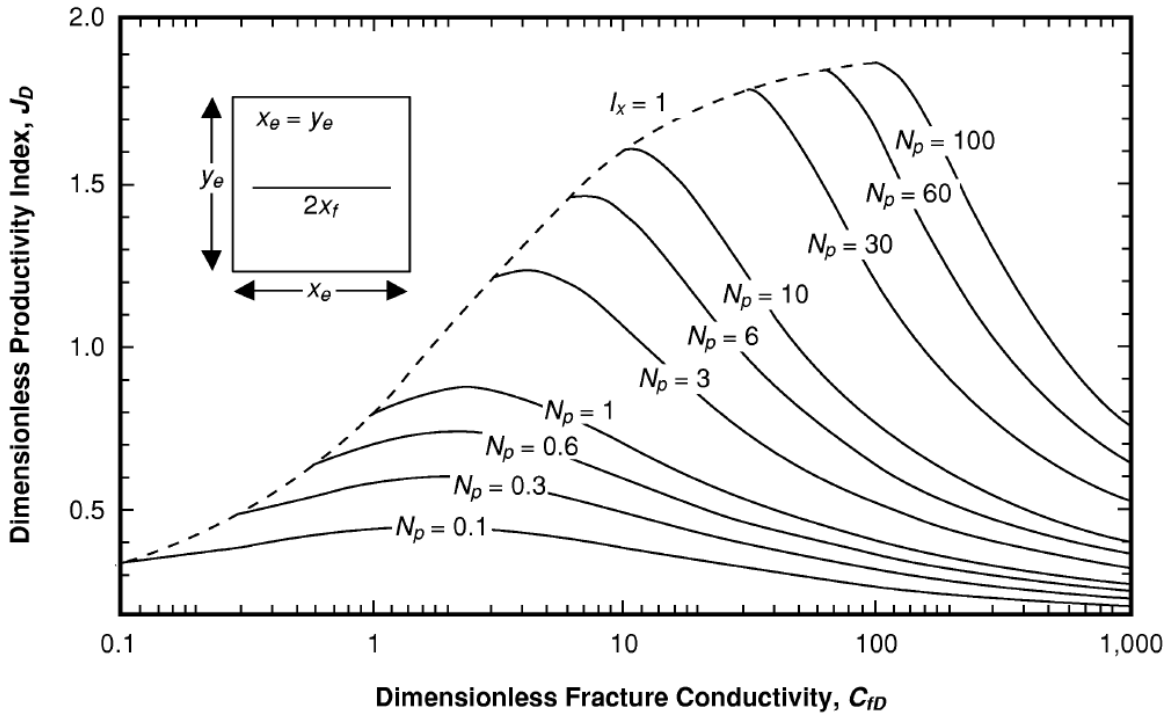

Figure 2. 22. Dimensionless productivity index (Nprop>0.1) (Economides, M., Oligney, R., & Valko, P. (2002)).

In actuality, it would be quite challenging to even achieve a proppant number greater than unity. In fact, the optimum C_{fD}, for a large proppant number determines an optimum penetration ratio close to unity (Economides, M., Oligney, R., & Valko, P. (2002)

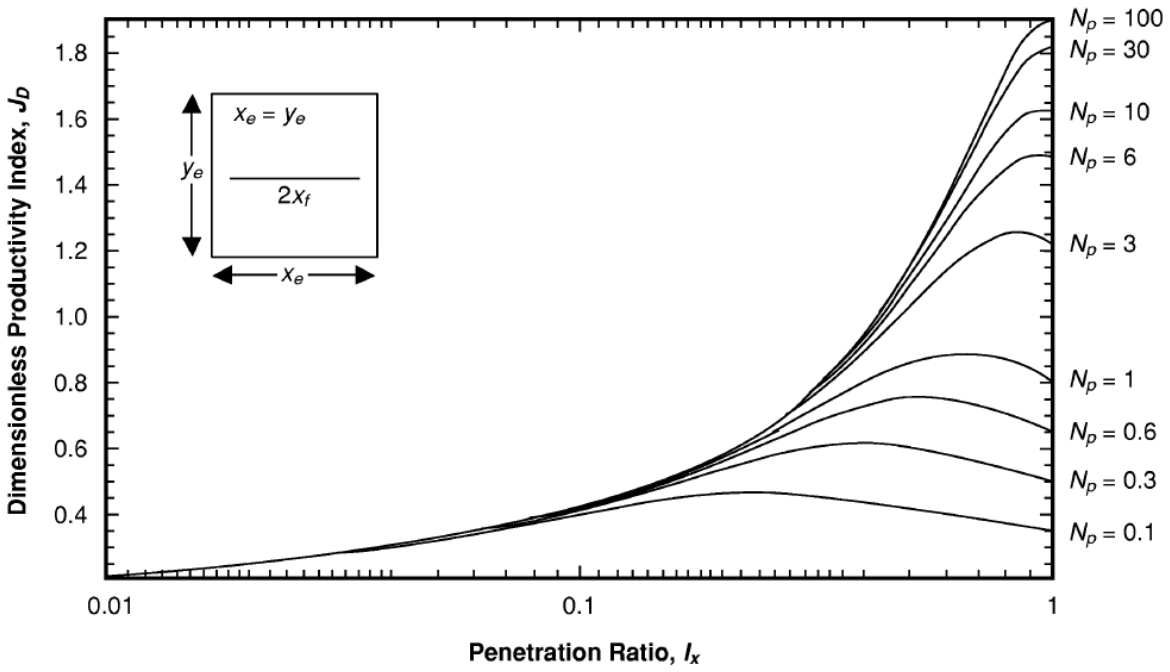

Figure 2. 23. Dimensionless productivity index as a function of penetration ration, with proppant number as a parameter (for Nprop> 0.1) (Economides, M., Oligney, R., & Valko, P. (2002)).

2.12 Optimum Fracture Design

The J_D can be represented using *Np* as a parameter as shown in **Figure 2.21- Figure 2.23**, for a given value of *Np*, there exists a well-defined dimensionless fracture conductivity (C_{fD}) at which the dimensionless productivity index (J_D) is maximized. Since a given proppant number reflects a fixed amount of proppant number reaching the pay, the dimensionless fracture conductivity found beneath the peak of each individual curve is the optimal length-width compromise ((Economides, M., Oligney, R., & Valko, P. (2002)), Rueda, 2004). The optimal C_{fD} and Np can be used to determine the fracture dimension that will maximize J_D

$$I_{x\_opt}=\sqrt{\frac{Np}{CfD\_opt}} \tag{31.0}$$

$$X_{f\_opt}=\frac{Xe}{2} Ix\_opt \tag{32.0}$$

$$W\_opt=CfD\_opt\frac{K}{Kf}X_{f\_opt} \tag{33.0}$$

In the hydraulic fracture design and optimization , assuming a single fracture in a square drainage area as shown in **Figure 2.19,** the proppant number (Np) is calculated as follows from Guk et al,. (2014)

I. The volume of the reservoir (V_r) will be

$$V_r = h_{net} x_e^2 \quad (34.0)$$

II. The fracture permeability (K_f)

$$K_f = K_{prop}\ X\ Gel\ Damage \quad (35.0)$$

III. The Proppant mass in the Payzone (Mf)

$$M_f = Mp\frac{hnet}{hf} \quad (36.0)$$

IV. Fracture volume in the payzone (V_f)

$$V_f = \frac{Mf}{SGprop(1-\phi prop)} \quad (37.0)$$

V. $Np = \frac{2Kf}{K}\frac{Vp}{Vr}$

Where

GelDamage =the proppant permeability reduction due to gel damage (%).

h_{net} =the net reservoir thickness in m

I_x =the penetration ratio, dimensionless

J_D=Dimensionless productivity index, dimensionless

K=permeability in mD (millidarcy)

M= mass in Kg

Np= Dimensionless proppant number, dimensionless

SG=specific gravity, dimensionless

V=volume, m^3

W=width in mm.

2.13 Optimal number of fractures in a horizontal transverse fracture

Guk et al. (2014) have developed systematic and comprehensive approach to the design of transverse hydraulic fracturing on horizontal wells on the basis of UFD which includes optimization of number of stages, fracture half-length and conductivity.

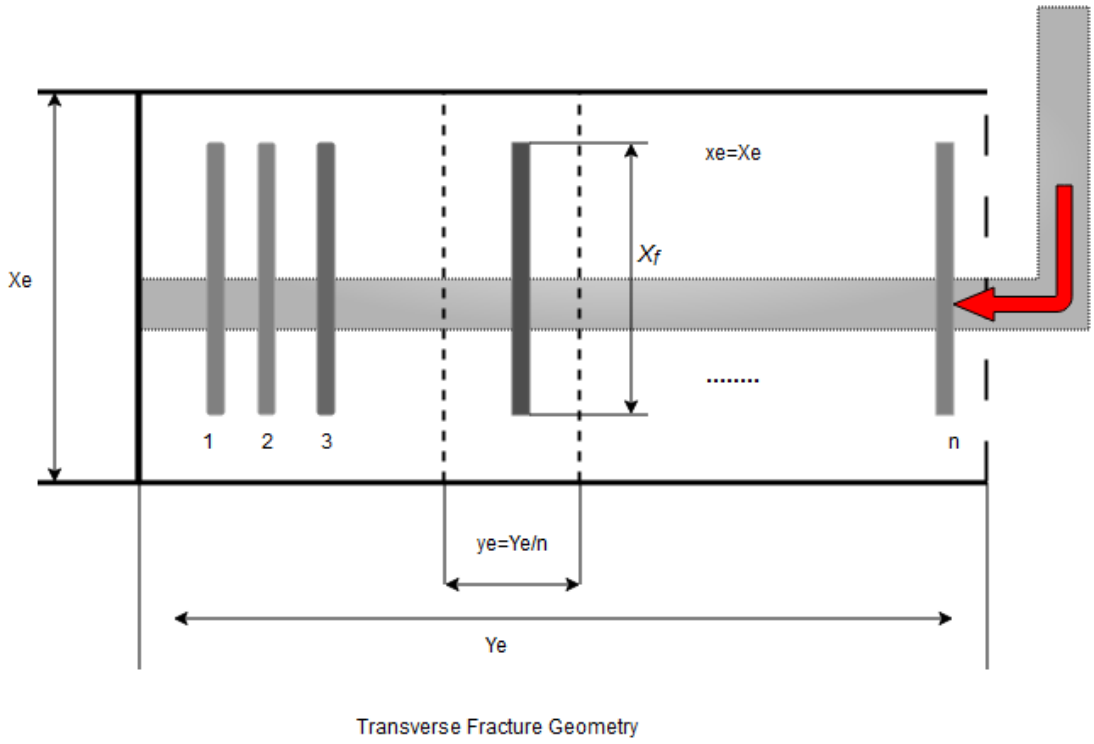

Figure 2. 24 Transverse Fracture Geometry in Horizontal well (after Guk et al., 2014**)**

From **Figure 2.24**, the total productivity index of a well will be equal to the productivity index of each fracture multiplied by the number of fractures.

$$J_{Dtot} = n(J_{Di}) \qquad (38.0)$$

Where

$J_D$tot= Total productivity index of multiple fractures

J_{Di}= Productivity index of individual fractures

n=Number of fractures

In **Figure 2.24**, all fractures were assumed to be identical and have identical drainage area. Hence, the number of proppant (Np) of the whole system is equal to the Np of each fracture.

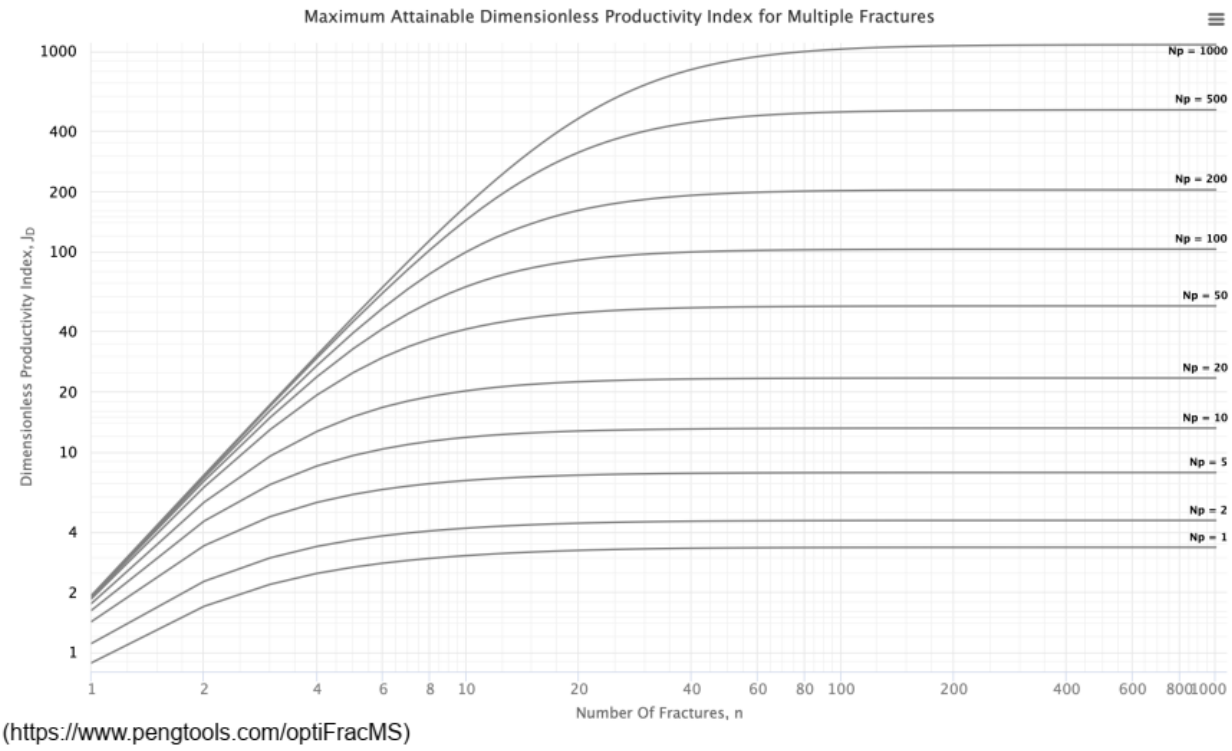

Figure 2. 25 Maximum Attainable Dimensionless Productivity Index for Multiple Fractures (Guk et al.,2014**)**

In Figure 2.24, the dimension of each fracture produced in the rectangular drainage Xe x $\frac{Ye}{n}$ in a pseudo-steady state flow regime and $y_{eD} = \frac{Ye}{nXe}$, there is an optimal value of inverse aspect ratio (x_{eD}) which yields the maximum J_D of a single fracture for each value of proppant number ($x_{eD} = \frac{nXe}{Ye}$).

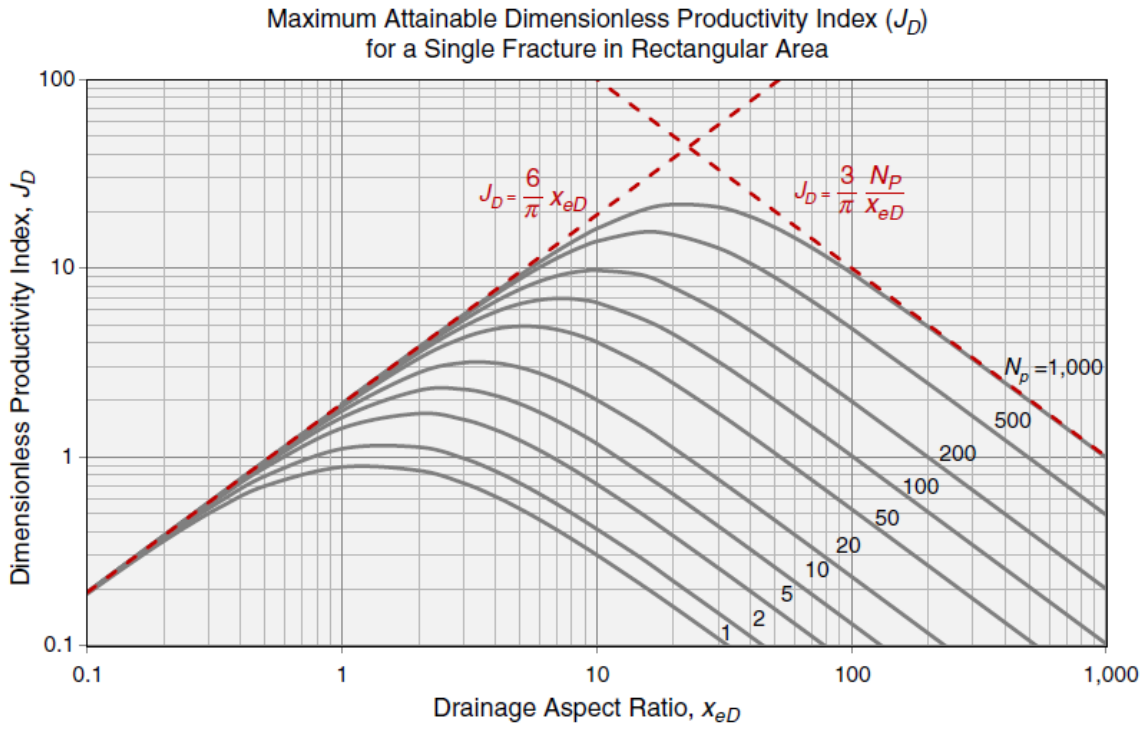

Figure 2. 26 Maximum Attainable Dimensionless Productivity Index(J_D) for a Single Fracture in a Rectangular area (Guk et al.,2014**)**

There are two asymptotes (left and right) which represent fully penetrated fracture with infinite conductivity ($J_D=\frac{6}{\pi}$xeD),the fracture technical potential, the case of infinite proppant number and another with low conductivity ($J_D=\frac{3}{\pi}\frac{Np}{xeD}$) (Guk et al,2014).

For the assumed identical fractures having identical drainage area, $x_{eD}=n\frac{Xe}{Ye}$.If the total drainage area is assumed to have a square shape (Xe=Ye), then x_{eD}=n. Substituting this x_{eD} in the two asymptotes gives JD=$\frac{6}{\pi}$n and JD=$\frac{3}{\pi}\frac{Np}{n}$ respectively for a single fracture. For multiple fractures, the asymptotes are transformed into JD=$\frac{6}{\pi}n^2$ and JD=$\frac{3}{\pi}Np$ respectively, with the resulting curve shown below.

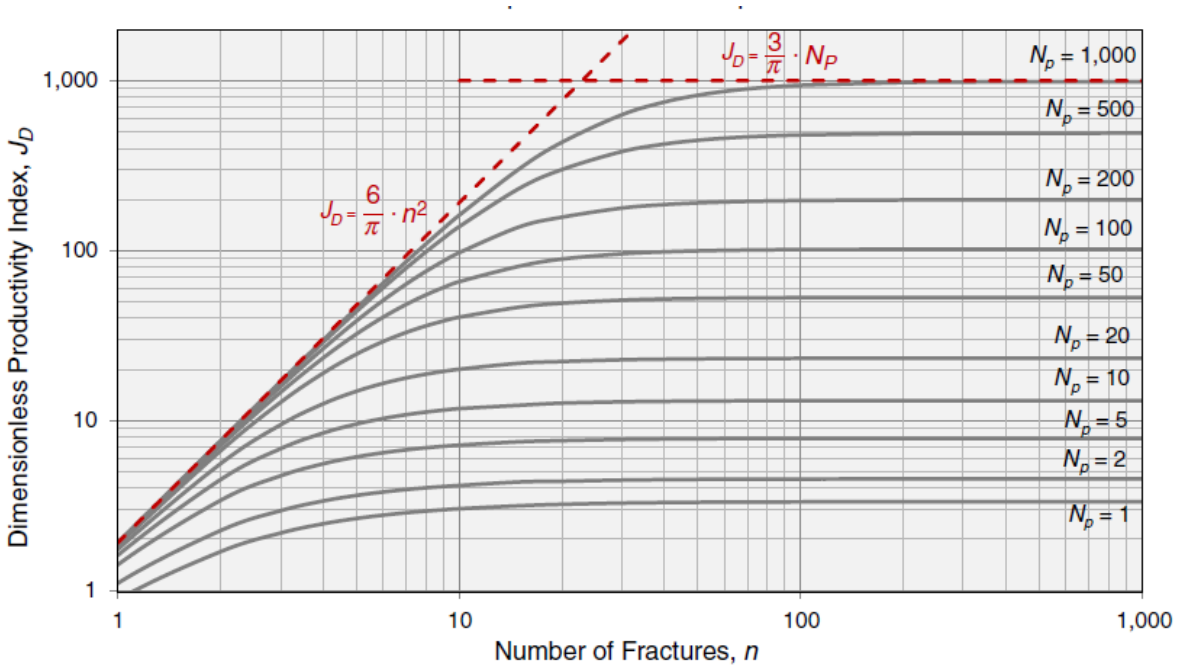

Figure 2. 27 Maximum attainable dimensionless productivity index for horizontal wells with multiple fracture-effect of choke skin accounted (Guk et al.,2014**)**

2.14 Choke skin effect

Because of the flow convergence in the vertical fracture to the horizontal wellbore there is an additional pressure loss expressed in equations (39.0 and (40.0) from Mukherejee and Economides (1991), providing the value for the effect of the choke skin (Guk et al., (2014).

$$Sc=\frac{kh}{kfw}\left[ln\left(\frac{h}{2rw}\right)-\frac{\pi}{2}\right] \quad (39.0)$$

which can be re-arranged as

$$Sc=\frac{Ix}{NpyeD}*\frac{2h}{xe}\left[ln\left(\frac{h}{2rw}\right)-\frac{\pi}{2}\right] \quad (40.0)$$

The Dimensionless Productivity Index (J_D)

The dimensionless productivity index (J_D) of a single fracture intersecting a horizontal well can be calculated using the equation developed by Wei and Economides (2005) as presented by Guk et al., (2014) in equations (41.0) through (43.0) below

$$J_{DTH}=\frac{1}{\frac{1}{JDV}+Sc} \quad (41.0)$$

The dimensionless productivity index of horizontal well with multiple transverse fractures (J_{DMFHW}) will be

$$J_{DMFHW}=\frac{n}{\frac{n}{JDMV}+Sc} \quad (42.0)$$

Where J_{DMV} is the dimensionless productivity index of multiple fractures without accounting the choke skin effect.

Combining equation (41.0) and (42.0) and noting that $n=\frac{1}{yeD}$ for square drainage area

$$J_{DMFHW}=\frac{1}{\frac{1}{JDMV}+\frac{Ix}{Np}*\frac{2h}{xe}\left[ln\left(\frac{h}{2rw}\right)-\frac{\pi}{2}\right]} \quad (43.0)$$

The choke skin effect for a horizontal well with multiple hydraulic fractures depend on two additional dimensionless parameters: $\frac{xe}{h}$ and $\frac{h}{rw}$ (Guk et al, 2014).

The Practical constraints is expressed as

$$I_{xmax} = \frac{Np}{n} x \frac{kxe}{2kfWmin} \quad (44.0)$$

Where,

Np is proppant number, *n*, number of fractures, *xe* is the drainage width, *kf* is fracture permeability and W_{min} is the minimum fracture width.

Chapter 3- Methodology

Hydraulic fracturing design assumes the determination of optimal half-length and width for a given proppant type and mass. Factors that affect this fracture design include the geology, geomechanics, and reservoir properties of the field, which, among other things, encompass several important aspects of the fracture design process. This analytical study has provided optimum parameters for planned transverse hydraulic fracturing in the horizontal wells of the Adigrat sandstone formation. Based on well log data and core analysis results, critical fracture design features such as rock geo-mechanical properties (Young' modulus and Poisson's ration), closure stress, brittleness index, and fracture geometry with the PKN fracture model assumption are estimated. The geology and geo-mechanics of the Hilala Gas Field provide a means of appropriate reservoir candidate selection, making them as important as the design process itself. This fracture design study work is based on the unified fracture design (UFD) (Economides, M., Oligney, R., & Valko, P. (2002)) and extension works by Guk et al, (2014). Since the fracture length and width compete with each other for the fixed proppant volume, there should be an optimum fracture width and length that would maximize the dimensionless productivity index of fractured wells. The Unified Fracture Design (UFD) methodology is used to determine the optimal width and length for any given amount of proppant number (Np). In this study, an excel sheet is used as the main tool to solve the formation's geo-mechanical properties, brittleness index, and closure stresses. OptiFrac and OptiFracMS software are also employed to design and analyze fracture geometry and optimum design results. The design process is simplified by the use of workflows that ensure critical steps are followed when arriving at the results.

The well log data of seven wells, well test and production test results of four wells, and field development plan of the Hilala Gas field in the Ogaden basin have been analyzed. Geological and reservoir properties are gathered from recently drilled wells in the 30km long and 7 km wide, gently trending NEE structure of Hilala Gas Field (Appendix 1.1). The four wells that are located along the fault line and selected for this study are shown in **Table 3.1.**

Table 3. 1 Selected Wells From Hilala Gas Field (after POLY-GCL, 2019)

No.	Well	Formation	Interval (m)	Production rate ($10^4 m^3/d$)
1	Hilala-SS	Adigrat	3105.0-3155.0	10.77
2	Hilala-SM	Adigrat	3097.2-3159.2	4.6-6.0
3	Hilala-AM	Adigrat	3131-3162.1	22.11
4	Hilala-HT	Adigrat	3200.9-4057	21.89

The general work flow for the design of the multistage hydraulic fracturing of the Adigrat formation in Hilala Gas Field is presented in **Figure 3.1**. This overall design study is undertaken in four main steps, while a separate methodology for each objective is developed describe how the results are attained.

The first step consists of a geological study description and characterization of the target formation for candidate selection to perform fracturing. The compositional analysis of the Adigrat formation and the existence of natural fractures were conducted from a previous study in Hilala Gas Field.

Secondly, the geomechanics and stress parameters of the target reservoir in Hilala Field is analyzed. Hydraulic fracturing is pressurization of the rock formation through an engineered fracturing fluid to break the formation and increase the flow of hydrocarbons. The stress parameters of the geomechanics part control the breakdown, propagation of the rock formation, and height migration of the fracture. Density and sonic log data results are used to calculate the geo-mechanical characteristics (Poisson's ratio, Young's modulus, and Brittleness Index) of the Adigrat rock formation. The calculation work flow is presented in **Figure 3.2.**

Then the Closure stress (Minimum horizontal stress) is determined at 3165m in the middle of the Adigrat formation, which helps to understand the types of proppants required to support the created fracture and the selection of fluid types compatible with the formation.

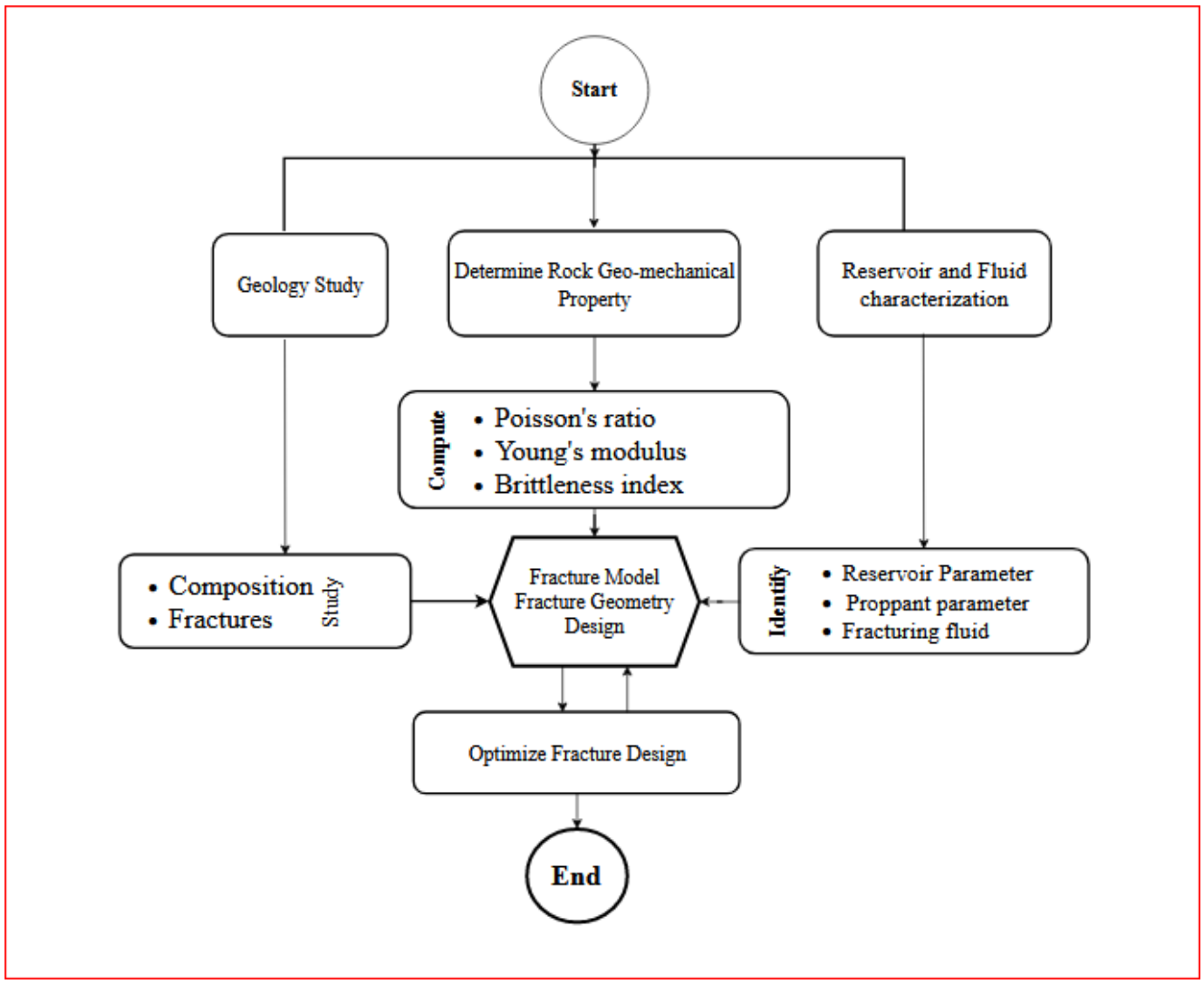

Figure 3. 1 General design work flow of the multistage hydraulic fracturing of horizontal well in Hilala Gas Field

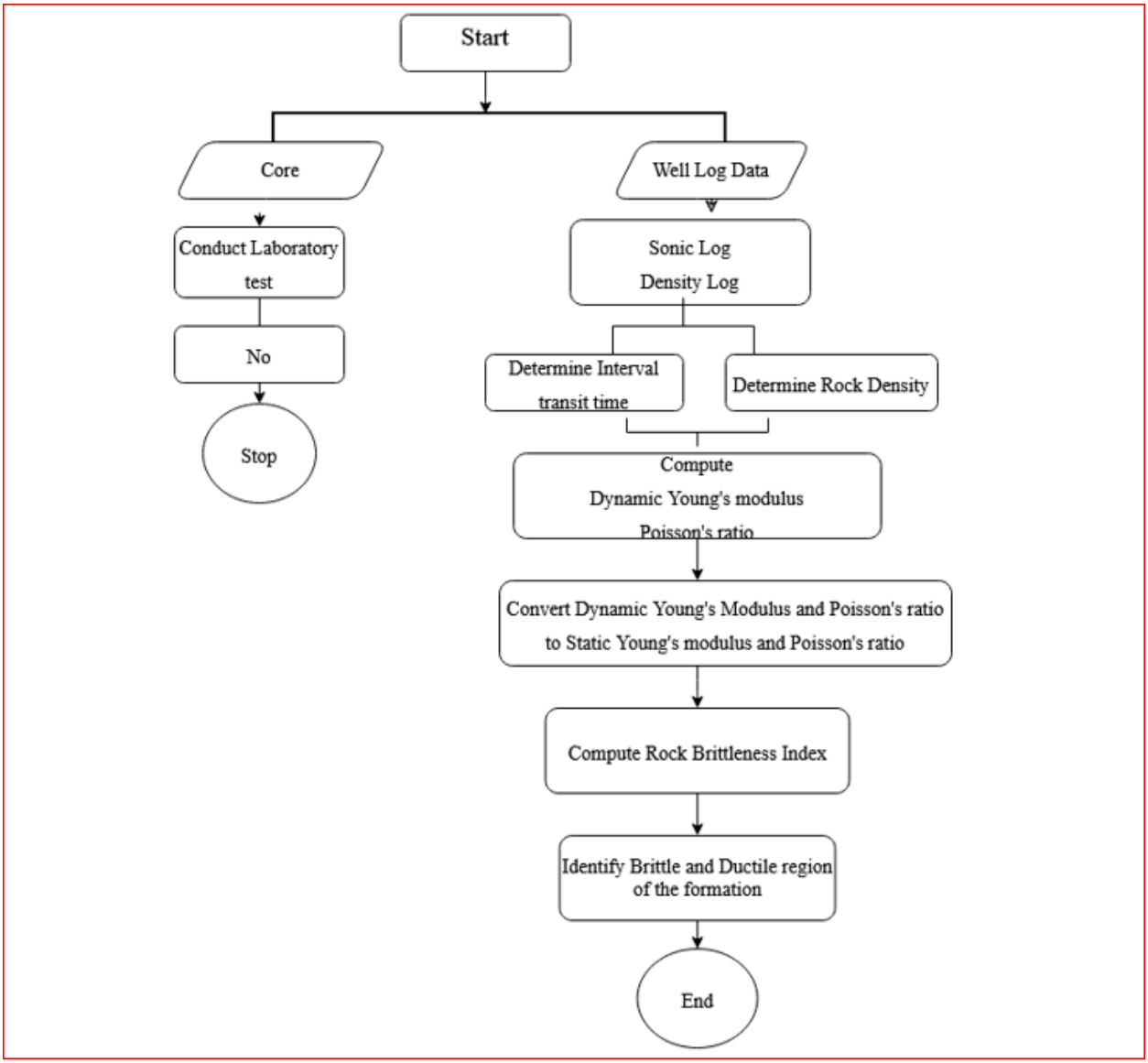

Figure 3. 2 Determination of rock geomechanical property from sonic and density log

The third step is the literature review work, which has assisted in understanding the fundamentals of hydraulic fracturing and advancements in vertical and horizontal wells, available fracture propagation models, and the concept of unified fracture design (UFD). The perceptions of single and multistage fracture for horizontal wells and fracture mechanics are explored at this step. The review work provides methods and techniques for the fracture geometry calculation, closure stress determination, and computations of the optimal productivity index of this design study.

The fourth and final step is the fracture design and optimization step. It incorporates optimizing the fracture geometry design using the Unified fracture design (UFD), the fracturing fluid, and proppant design.

3.1 Fracture Design and Optimization Methodology Approach and Tools

The Excel sheet is the main tool employed in this study. Two fracturing software packages (OptiFrac and OptiFracMS) are used to generate the *type curve* results with the methodology of the Unified fracture design (UFD) and extension works by Guk et al., (2014).

3.1.1 Determination of the Magnitude of Minimum Horizontal stress (Closure stress)

The Eaton's method in **equation (19.0)** is applied to determine the closure stress at the target depth of 3165m**.** The Pore pressure is determined using **equation (2.0)** for the Hilala gas field at the Adigrat formation (depth, H=3165 m).

Based on the proppant selection guide in **Figure 2.13** and the calculated Closure stress of the Adigrat formation in Hilala Gas Field ($P_{Closure}$ =55.32 MPa), the 20/40 TX brown bauxite sand proppant is selected for the purpose of this design study.

Table 3. 2 Proppant property 20/40 TX brown bauxite at closure pressure ($P_{closure}$) of 55.32MPa

No.	Parameter	Value	Unit
1	Bulk volume	61710	Kg/m^3
2	Mean Diameter	0.64	mm
3	Specific Gravity	2.65	
4	Proppant Permeability (K_f)	61710	mD
5	Porosity	0.42	

Table 3. 3 Reservoir and Proppant parameters for the Fracture design of Adigrat formation

Parameters		
1. Proppant Parameters@55.32Mpa $P_{closure}$		
• Proppant type	20/40 TX brown bauxite	
• Proppant Permeability (K_f)	61710	mD
• Mass of proppant (Mp)	2000	tons
• Gel Damage	0.001	%
2. Reservoir Parameters		
• Reservoir Permeability (k)	0.2	mD
• Reservoir net thickness (h_{net})	81.8	m

• Fracture height (X_f)	90	m
• Drainage width (Xe)	1000	m
3. Output		
• Dimensionless Productivity index (J_D)		
• Dimensionless fracture Conductivity (C_{fD})		
• Fracture Geometry (X_f,W_f)		

For the **single fracture** geometry (fracture half-length and width) design, the PKN fracture model and UFD method are used for the designated transverse fracturing under this study. The fracture half length and width are calculated using the PKN fracture model combined with the stress parameters. Accordingly, a constant fracture height of 90 m is assumed, in the Adigrat formation thickness of 155m (81.8 m net thickness), and a permeability of 0.2 mD is selected from the permeability frequency graph in **Figure 1.8**. The proppant is selected from Catalog **Appendix 2.** OptiFrac software is used for single fracture optimization.

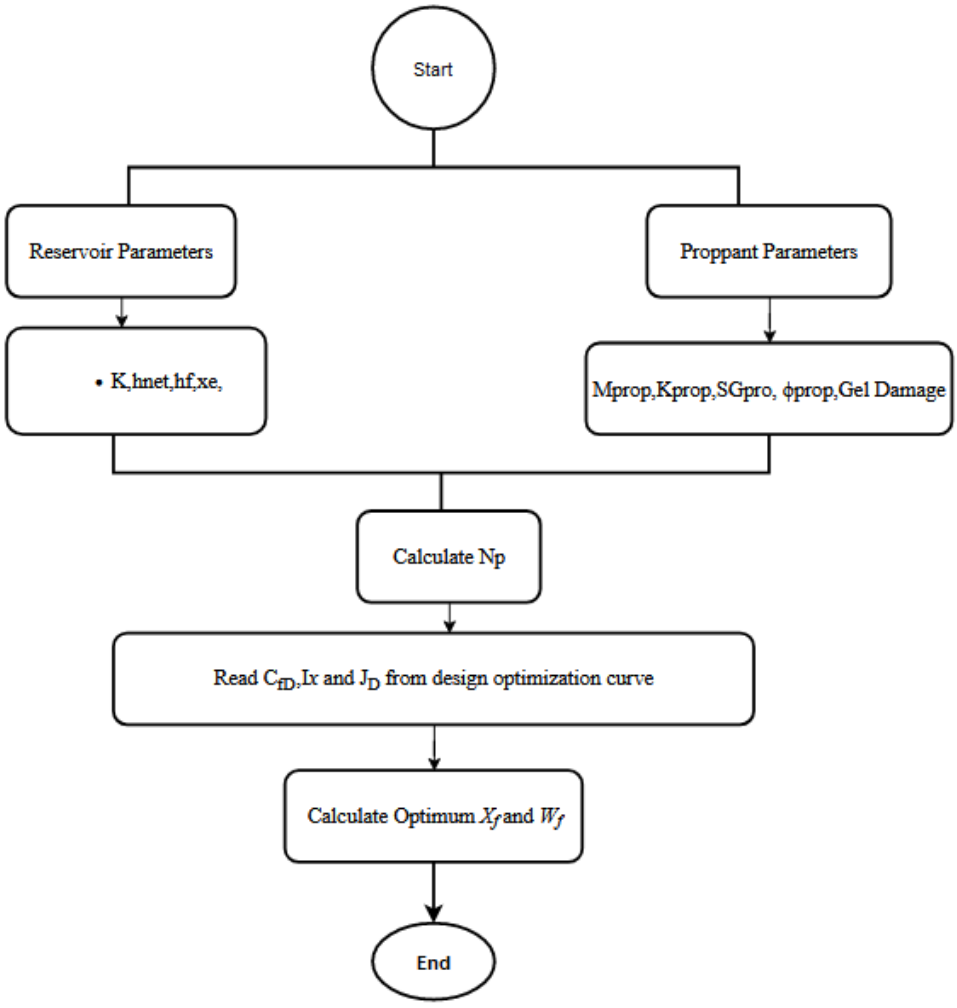

Figure 3. 3 Fracture design optimization work flow (Modified after Guk et al., 2014).

The dimensionless proppant number (*Np*) is calculated using the Unified Fracture Design (UFD) method using equation (30.0). The dimensionless proppant number is used as a parameter in the dimensionless productivity index (J_D) versus dimensionless fracture conductivity (C_{fD}) to determine the optimum penetration ratio and optimum value of the conductivity.

Finally, the optimal values of the dimensionless conductivity and proppant number are used to determine the fracture dimensions that maximize the dimensionless productivity index using equations (31.0-33.0).

Multistage fracturing Geometry

With type curves and provided reservoir and proppant parameters, the optimal number of fractures (n) and their geometry are calculated in the transverse hydraulic fractures of the horizontal wells. For the design and optimization of the number of transverse fractures in the horizontal wells, analytical methods and OptiFracMS software are used. The procedure to calculate the optimal number of fractures and fracture geometry required to maximize the well productivity index is shown in **Figure 3.4**.

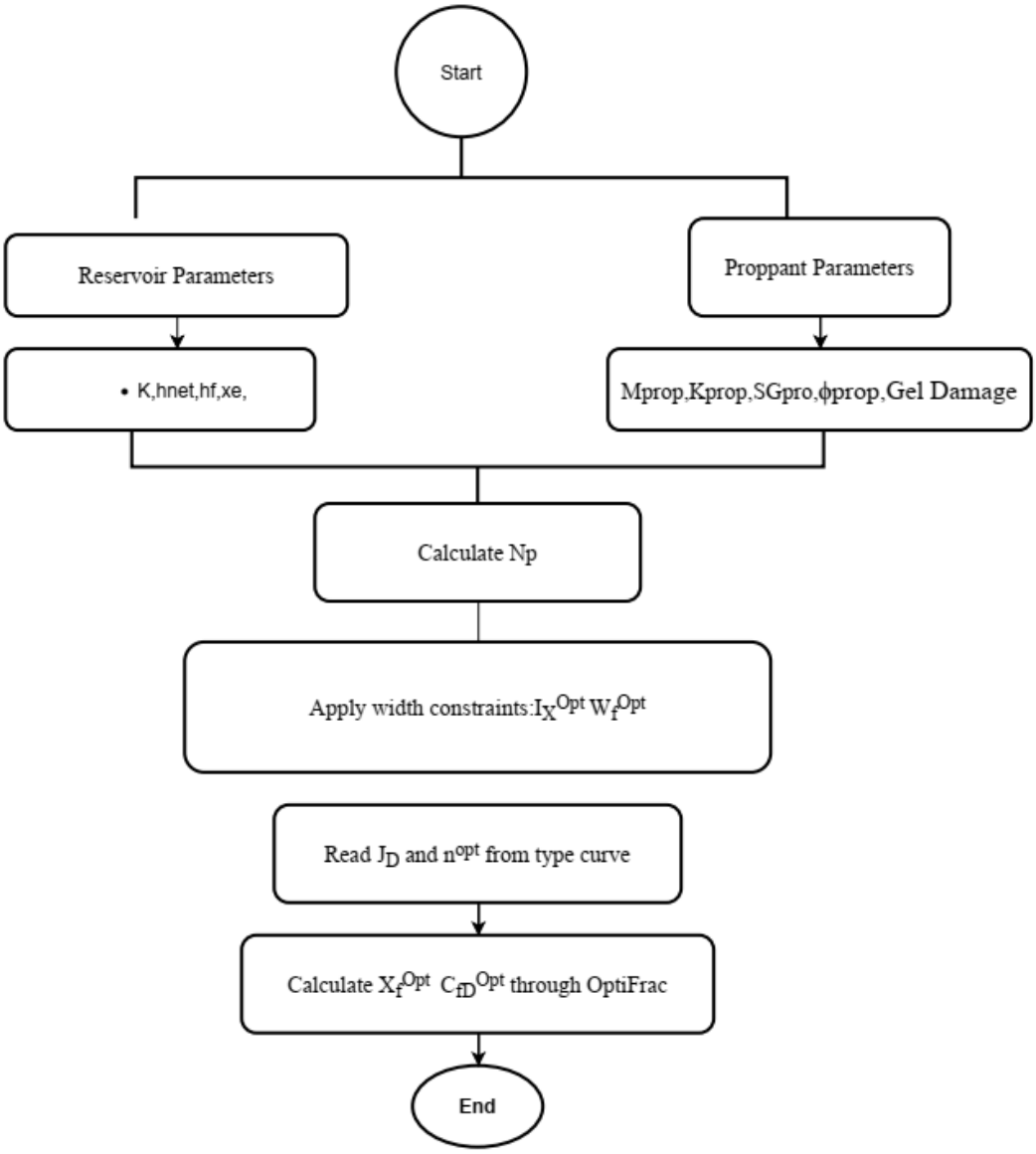

Figure 3. 4 Fracture Optimization design work flow

The proppant number (N_P) is determined from equation (30.0), with the steps illustrated in equations (34.0) through (37.0). Next, the Np is used to determine the number of fractures (n) from the *type curve* in Figure (2.25-2.27). Applying the minimum fracture width with three proppant grains of 20/40 Texas Brown intermediate-strength bauxite, the minimum fracture width is 1.93 mm. The 'maximum practical penetration ratio' equation (44) developed by GUK et al., (2014), is then used to determine the optimum penetration ratio (I_X^{Opt}).

Using the relationship between Penetration ratio (I_x), dimensionless fracture conductivity (C_{fD}) and Proppant Number (Np), the optimum fracture dimension is now determined by applying equations (31.0) to (33.0).

Chapter-4 RESULTS AND DISCUSSIONS

Based on the methodology designed, the following are the results and discussions presented with reference to the aim of the study, which is to determine the geo-mechanical properties of the Adigrat reservoir, the fracture geometry, and fracture number for an enhanced gas productivity of the horizontal wells in the Hilala Gas Field.

4.1 Rock Geo-mechanical Properties

4.1.1 Transverse Slowness determination based on log data

Table 4.1 shows the calculation results of shear velocity (V_s) for the Sandstone, Pelitic sandstone, and Mudstone of the Adigrat formation computed from compressional slowness. The shear velocity (Vs) is obtained using the Castagna et al., (1993) method for clastic rocks in equation (5.0).

Table 4. 1 The Density, interval transit time and velocity of Adigrat formation in Hilala gas field

Lithology	Density (kg/m^3)	Compressional Slowness (Δtp) (μs/m)	Compressional Velocity (Vp) (m/s)	Transverse slowness (Δt_s) (μs/m)	Shear velocity (V_s) (m/s)
Sandstone	2500	203.4	4916.13	322.94	3096.57
Pelitic sandstone	2550	230	4354.29	378.09	2644.85
Mudstone	2600	262.5	3810.00	453.05	2207.24

The Adigrat Formation lithology consists of mudstone, sandstone, Pelitic sandstone, and a small amount of gritstone and gypsum rocks.

The Adigrat sandstone in Hilala field has a density of 2500 Kg/m^3, compressional interval transit time of about 203.4 μs/m (4916.13 m/s) and a transverse slowness of about 322.94 μs/m (3096.57 m/s). The density of the Pelitic sandstone is 2550 kg/ m^3 , the interval transit time 230 μs/m (4354.29 m/s) and the transverse slowness is 378.09 μs/m (2644.85 m/s). The formation mudstone density is 2600 kg/m^3 and has compressional slowness of about 262.5 μs/m (3810.0 m/s) and transverse slowness of 453.05 μs/m (2207.24 m/s).

4.1.2 Young's Modulus and Poisson's ratio

Table 4.2 shows the calculation results of Young's modulus (dynamic and static) and Poisson's ratio calculated using equations (6.0) through (9.0). Dynamic moduli derived from well log or core data are not in line with the actual engineering needs. Hence, calculated results are changed to static moduli to represent the rock deformation under the high stress of subsurface conditions using equations (7.0) and (9.0).

Table 4. 2 Dynamic and static Young's Modulus, Static Poisson's ratio of Adigrat formation

Lithology	Compressional Velocity (ΔVp) (m/s)	Transverse Velocity(ΔVs) (m/s)	Dynamic Young's Modulus ($E_{dynamic}$) in GPa	Static Young's Modulus (E_{static}) in GPa	Static Poisson's ration
Sandstone	4916.13	3065.57	56.15	51.26	0.21
Pelitic sandstone	4354.29	2644.85	43.08	38.72	0.26
Mudstone	3810.00	2207.24	31.06	27.70	0.31

As shown in **Table 4.2**, Sandstone has a static Young's modulus of 51.26 GPa and a Poisson's ratio of about 0.21. The Pelitic sandstone has a Young's modulus value of 38.72 and a Poisson's ratio of about 0.26. The mudstone has a Poisson's ratio of 27.70 GPa and a Poisson's ratio of 0.31. Generally, Sandstone has the highest Young's modulus value and lowest Poisson's ratio, and Mudstone has the highest Poisson's ratio and lowest Young's modulus.

4.1.3 Brittleness Index

Table 4.3 presented the Brittleness Index (%) of Adigrat formation in Hilala Gas Field determined using equation (10.0)

Table 4. 3 Britleness Index (%) of the Adigrat formation in the Hilala Gas Field

Lithology	**Young's modulus (GPa)**	**Poisson's ratio**	**Brittleness index (%)**
Sans atone	51.26	0.21	83.92
Pelitic sandstone	38.72	0.26	60.94
Mudstone	27.70	0.31	39.53

Figure 4.1 Shows the rock brittleness index of the Adigrat reservoir rock formation in the Hilala Gas Field. Sandstone has the highest brittle index (83.92%), followed by Pelitic sandstone

(60.94%) and mudstone (39.53%). A brittle rock has a high Young's modulus and a low Poisson's ratio (e.g., Sandstone), while a ductile rock has a low Young's modulus and a high Poisson's ratio (e.g., Mudstone). When combined with formation closure pressure and breakdown pressure, the brittleness index is used to help hydraulic fracturing design.

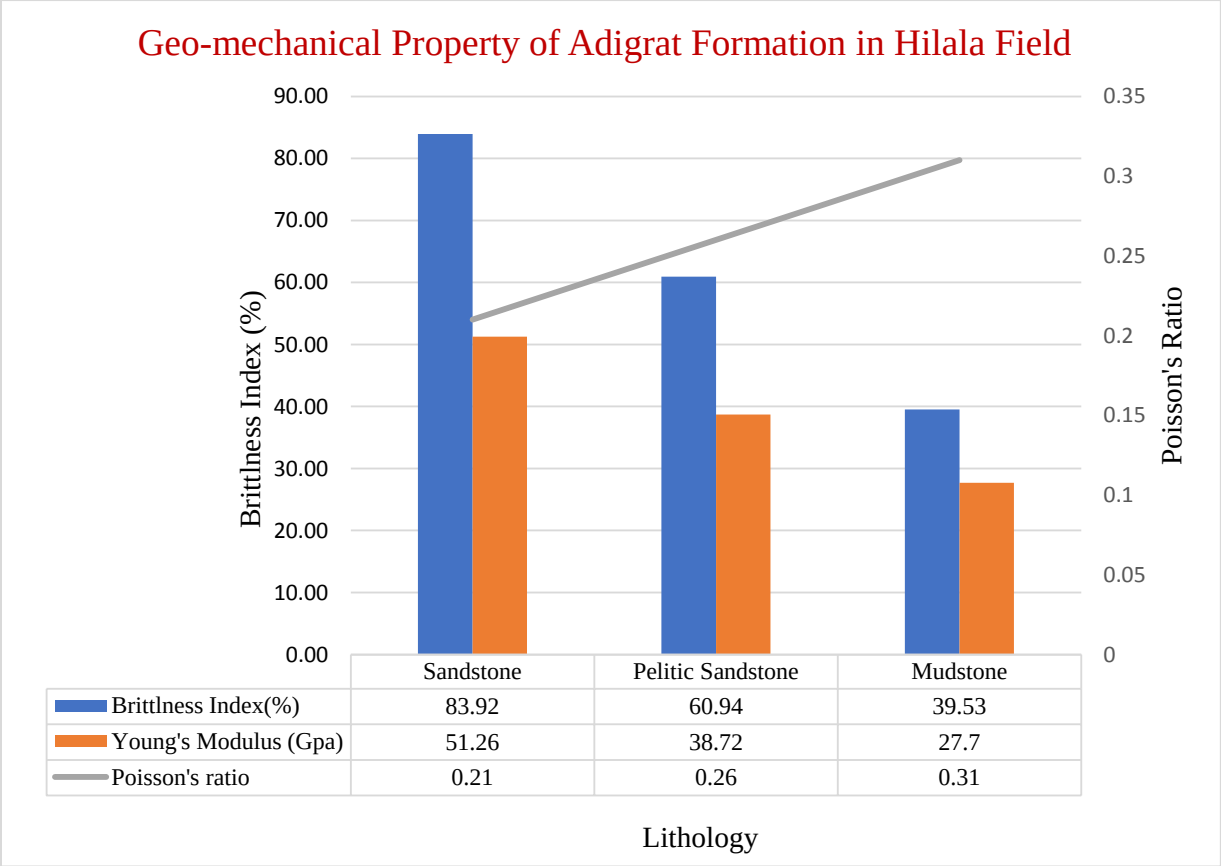

Figure 4. 1 Rock geo-mechanical properties (Poisson's ratio, Young's modulus and Brittleness index) of Adigrat formation in Hilala gas field

4.2 Minimum Horizontal Stress (Closure Stress)

The formation Brittleness Index(B) combined with formation closure pressure is used to design hydraulic fracturing.

Table 4. 4 Minimum Horizontal Stress (Closure Stress) of the Adigrat formation

Lithology	Density (Kg/m^3)	Gravity(m/s^2)	Depth(m)	Poisson's ratio (v)	Pore Pressure (MPa)	Absolute Vertical Stress (Sv)	Closure stress (MPa)
Sandstone	2500	9.87	3165	0.21	34.2	78.10	45.86
Pelit.Sandstone	2550	9.87	3165	0.26	34.2	79.66	50.16
Mudstone	2600	9.87	3165	0.31	34.2	81.20	55.32

In **Table 4.4** The closure stress in Adigrat formation in Hilala Gas Field is between 45.86 MPa-55.32 MPa with an average value of 50.45 MPa at 3165m depth. This closure pressure is the dominant variable to select the proppant type. The proppant material must be strong enough to resist this closure stress.

Figure 2.11 Illustrates a proppant selection guide based on the closure stress at the depth of the reservoir. Accordingly, natural sand can only withstand a maximum closure stress of 5000 Psi (34.48 MPa).

4.3 Fracture Design and Optimization

4.3.1 Single Fracture Design and Optimization

Table 3.3 shows the reservoir and proppant parameters for the fracture design in the Adigrat formation in the Hilala Gas Field. An optimal fracture geometry, dimensionless fracture conductivity, and productivity index are the expected outputs of the fracture design.

Figure 4.2 shows the plot of the fracture performance curve in which the fracture dimensionless productivity index (J_D) as a function of dimensionless fracture conductivity (C_{fD}) for a pseudo-steady state flow regime, with proppant number (N_p) and Penetration ratio (I_x) as a parameter, are represented in a combined manner. The curves in the black lines denote fixed amount of proppant reaching the pay. Each individual curve is linked to the fracture dimensionless productivity index at a well-defined dimensionless fracture conductivity. The red lines signify the dimensionless penetration ratio at which the maximum value is unity. The combination of the red and black *type curves* is useful for fracture design and evaluation.

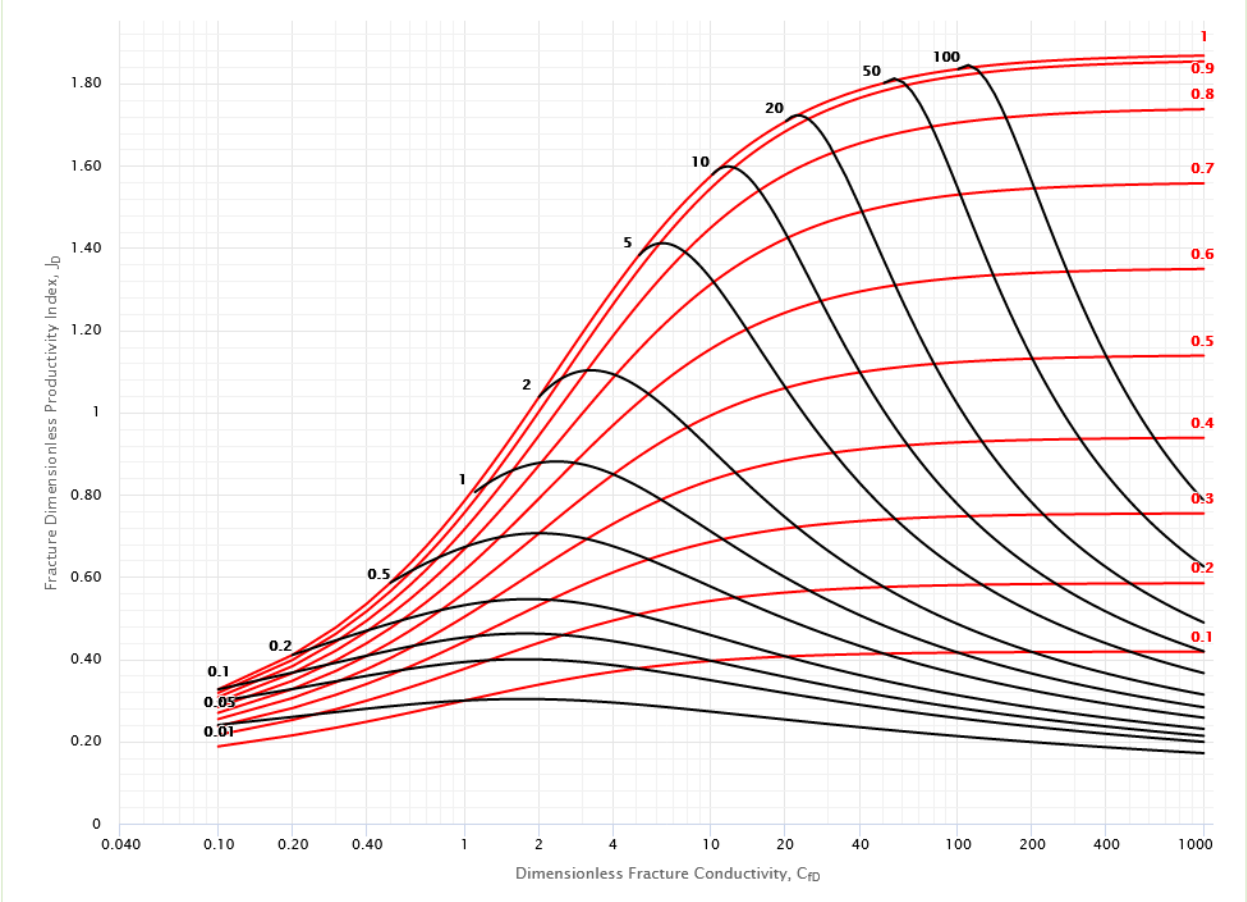

Figure 4. 2 Fracture Dimensionless productivity index as a function of Dimensionless Fracture Conductivity and I_x as a parameter in a pseudo steady state.

For the single fracture in a square area, the proppant number (Np) is determined using equation (30.0) steps stated starting from equation (34.0) through equation (37.0) for the reservoir and proppant input parameters stated in **Table 2.2.** In **Figure 4.2**, the peak of each proppant's curve for the dimensionless fracture conductivity shows the ideal balance between length and width. Using the optimal value of the proppant number (Np), the optimal fracture conductivity ($C^{Opt}{}_{fD}$), and the optimal penetration ratio ($I_x{}^{Opt}$), the Optimal productivity index ($J_D{}^{Opt}$) is determined. The dimensionless fracture conductivity index (C_{fD}) is 2.25, at which the dimensionless productivity index is maximal (0.84) for the available proppant number (Np) =0.87, as shown in **Table 4.5** and **Figure 4.5.** It is now possible to calculate the fracture size (dimensions) that optimizes the dimensionless productivity index (J_D) using the previously determined dimensionless fracture conductivity (C_{fD}) and proppant number (N_P) using the design work flow

in **Figure 3.3**. The optimal values of the penetration ratio (Ix_opt), the fracture half-length (X_f_opt) and fracture width (W_opt) are calculated using equations (31.0) through equation (33.0). The optimal values are 0.62, 310.6 m and 2.27 mm for the penetration ratio, fracture half-length and fracture width respectively as presented in **Table 4.5.**

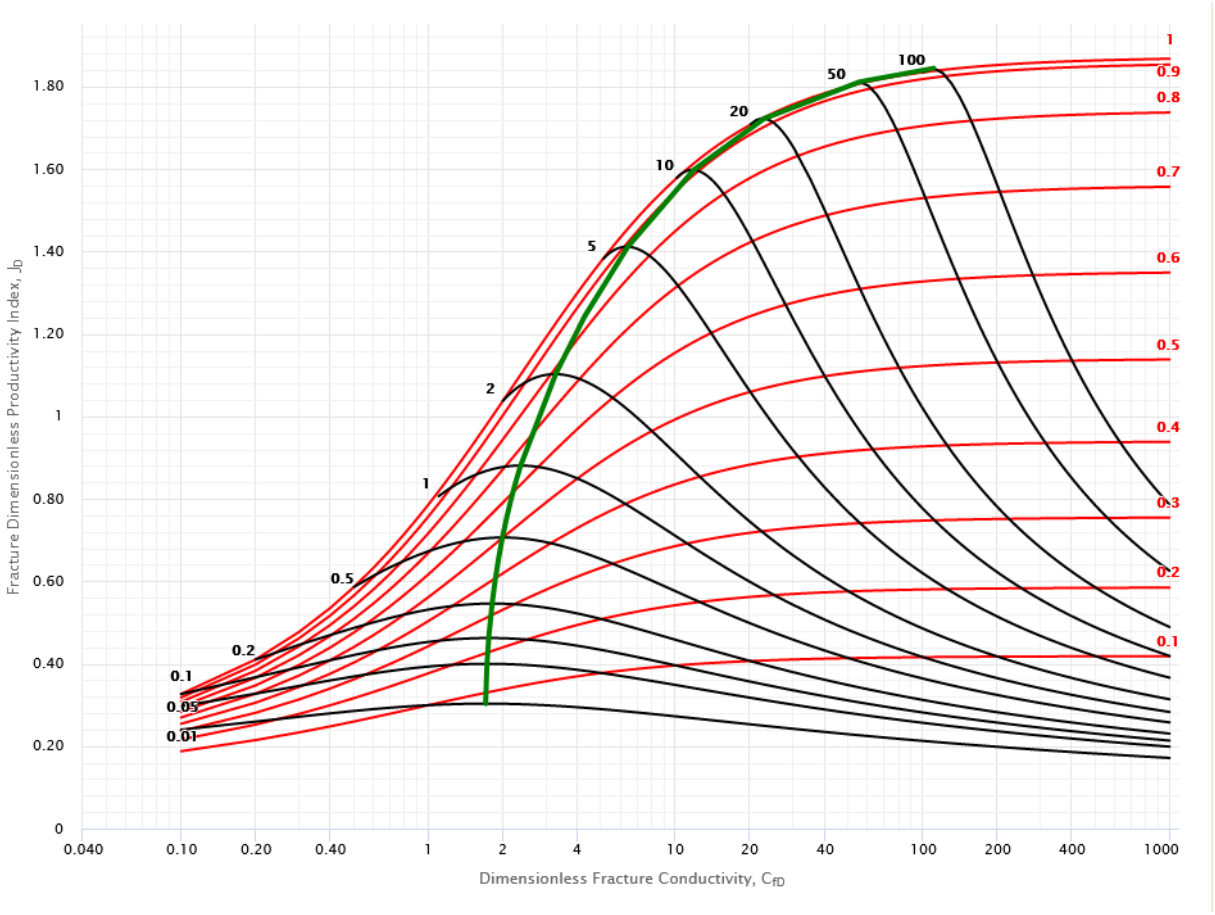

Figure 4. 3. Design Optimization Curve (Green line)

The "Design Optimization Curve", which is the green line in **Figure 4.**3 joining the highest value of the proppant number (*Np*), displays the planned design and the fracture dimensionless productivity index (J_D) value for various quantities of proppant number (*Np*).

In this study, the optimum fracture dimensions (X_f optimum, W_f optimum, and I_x optimum) outputs for the given proppant and reservoir parameters in **Table 3.3** are shown in **Table 4.5.**

Table 4. 5 Achievable fracture performance output

No.	Parameter	Representation	Output	Unit
1	Dimensionless productivity Index	J_D	0.84	
2	Dimensionless fracture conductivity	C_{fD}	2.25	
3	Fracture Half-length	X_f	310.6	m
4	Fracture width	W_f	2.27	mm
5	Fracture penetration	Ix	0.62	
6	Net pressure	P_{net}	18.7	atm
7	Reservoir Volume	Vr	81800000	m^3
8	Fracture Volume	V_f	115.3	m^3
9	Proppant Number	Np	0.87	

Among the key results from the graph and demonstrated in **Table 4.5** for the pseudo-steady state flow regime in the design and optimization processes that are target of this study are the optimal values of fracture geometries (fracture width and fracture half-length). The optimum values of the fracture width and length are 2.27 mm and 310.6 m, respectively. The maximum possible dimensionless productivity index (J_D) for Np=0.87 is 0.84 at a C_{fD} of 2.25.

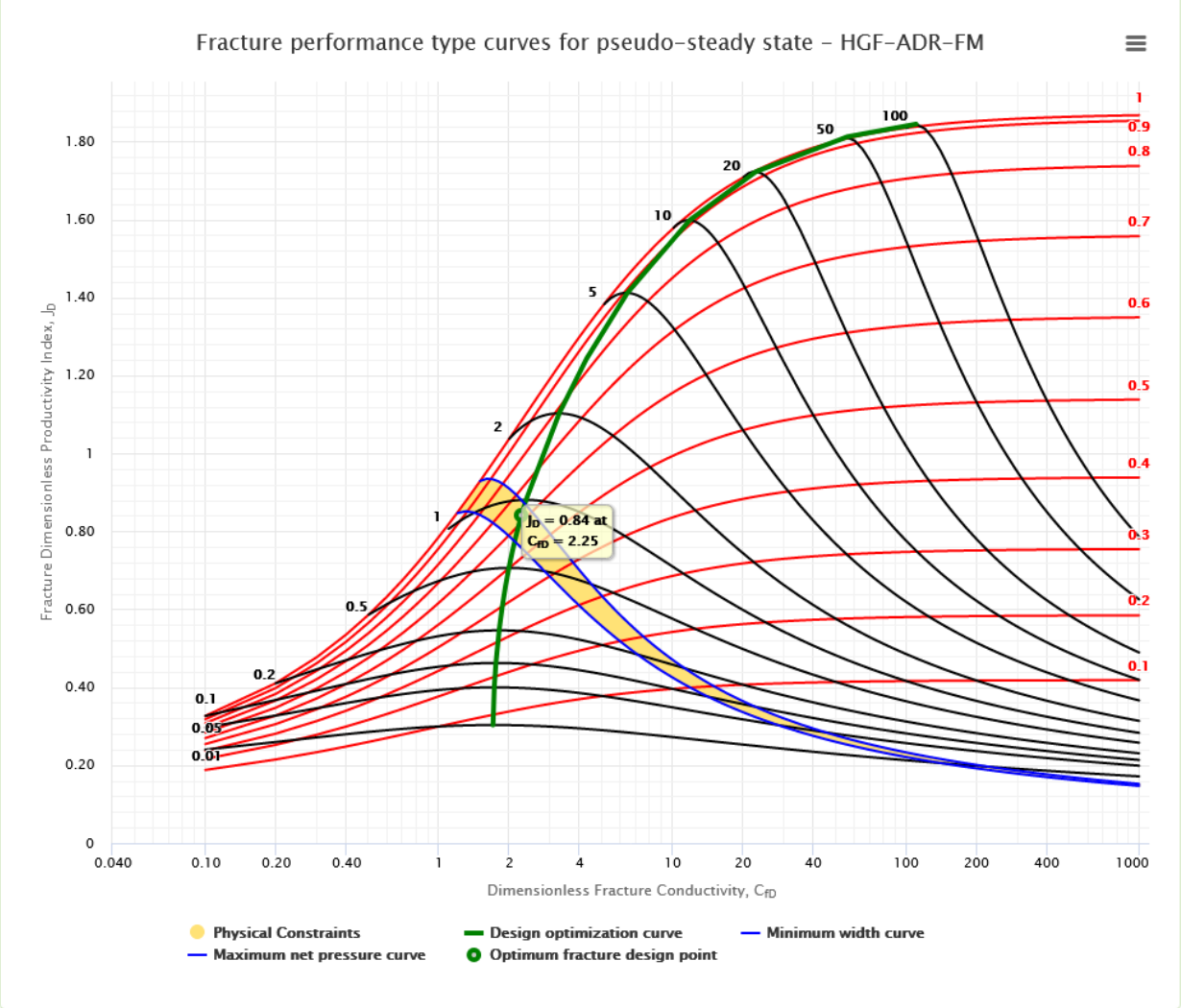

Figure 4. 4 Fracture performance type curves for pseudo-steady state flow regime in Adigrat formation with Optimum design point

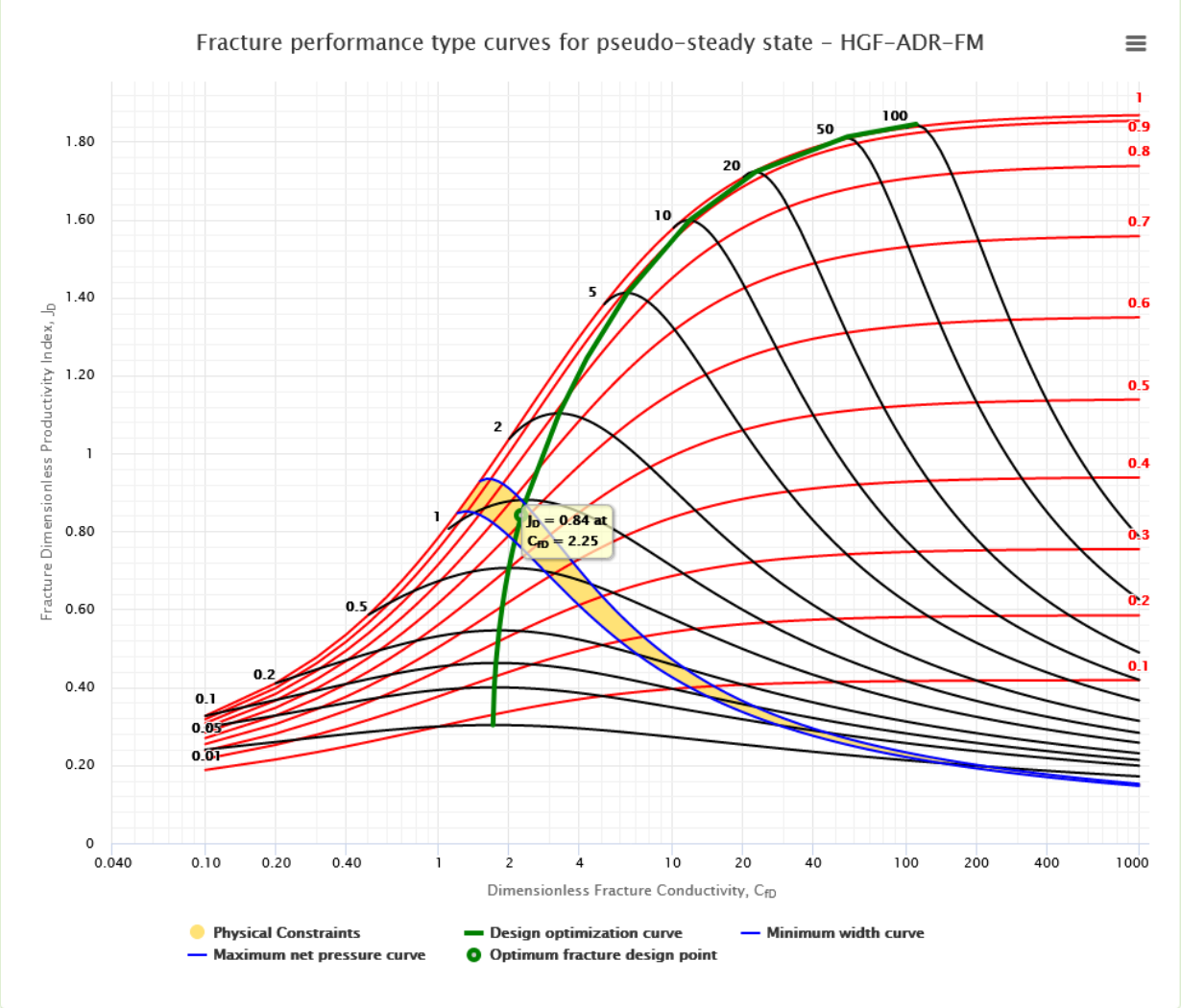

Figure 4. 5 Fracture performance type curves for pseudo-steady state flow regime in Adigrat formation- "working area"

In **Figure 4.5** above, the space between the minimum width curve and maximum net pressure curve is referred to as the 'working area' denoted by the yellow zone. This area should have the best design value.

4.4 Optimum Number of Transverse Fractures

Figure 4.6 presents the maximum attainable dimensionless productivity index for multiple fractures. The total number of fractures is plotted as a function of dimensionless productivity index, with the proppant number as a parameter. The highlighted, bold black curve is the optimal dimensionless proppant number (Np) determined using equation (30.0) without width or choke skin effect. The dimensionless productivity index (J_D) versus the number of fractures (n) for Np=8.92 flatten out to the horizontal asymptote. This is the technical potential of the well with multiple fractures in a square well drainage in which the fractures each drain a rectangular area, with a technical potential of $J_D=\frac{3}{\pi}Np$ similar to the one developed by Guk et al., (2014).

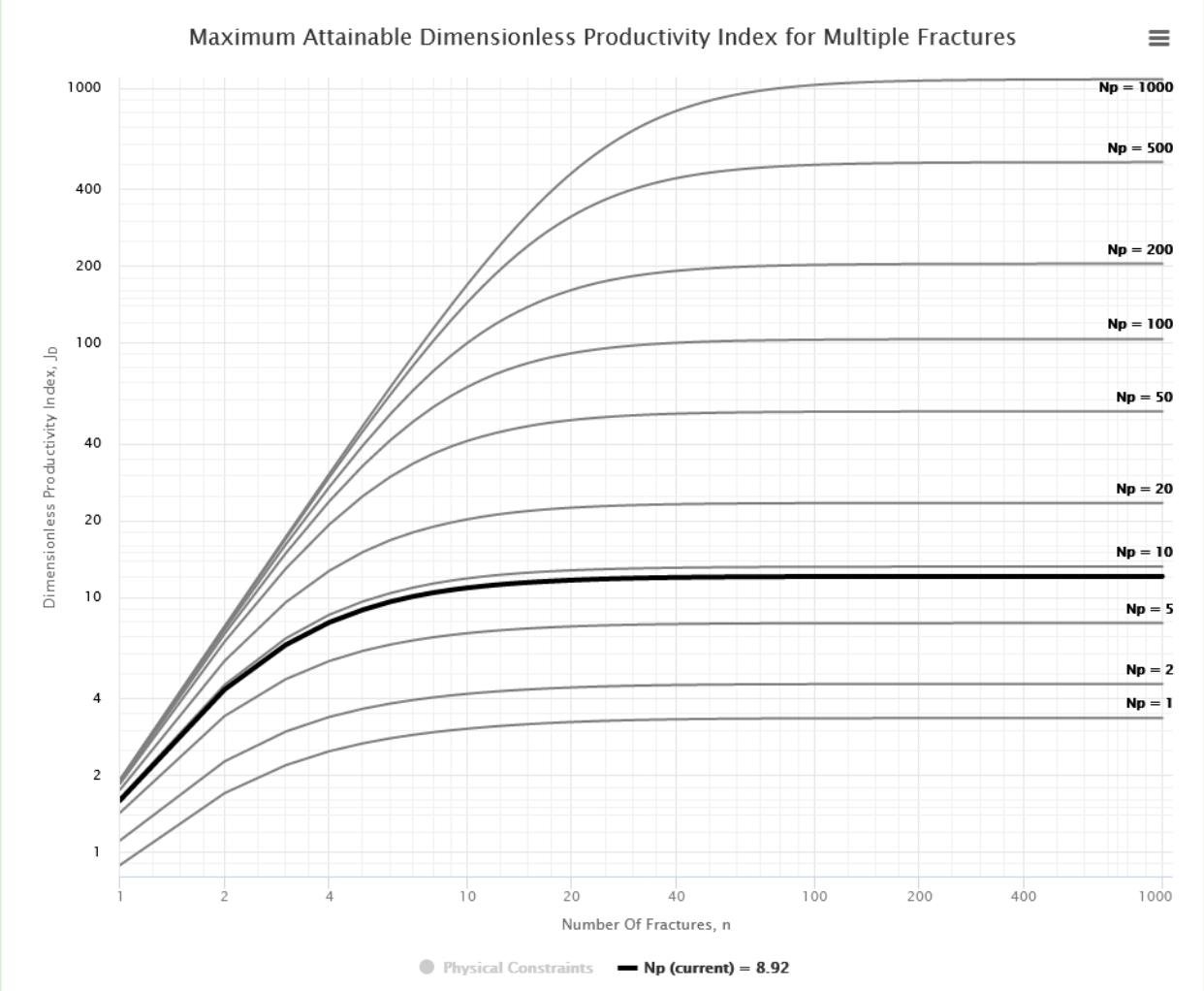

Figure 4. 6 Maximum attainable dimensionless productivity index of horizontal well with multiple fracture in a square area without skin effect

When width constraint and width effect are considered and their effects are incorporated into **Figure 4.6**, The maximum attainable dimensionless productivity index versus number of fracture type curves look like those shown in **Figure 4.6** the maximum practical penetration ratio is calculated using equation (44.0). The Optimal (maximum) penetration ratio is 0.62. Using the relationship between proppant number (Np), penetration ratio (Ix), and dimensionless productivity index (C_{fD}) in equation (31.0) the optimum dimensionless fracture conductivity (C_{fD}) is determined, which in turn helps to determine the fracture geometry in equations (32.0) and (33.0). The optimum results for the reservoir and proppant input parameters of **Table 3.3** are shown in **Table 4.6.**

Table 4. 6 Optimum design values for Horizontal well

No.	Parameter	Name	Optimal Value	Metric units
1	Reservoir Volume	V_r	81.8	10^6 m^3
2	Fracture Height	h_f	90	m
3	Proppant Number	N_p	8.92	
4	Dimensionless Productivity Index	J_D	6.18	
5	Number of Fractures	N	12	
6	Dimensionless Productivity Index	C_{fD}	1.90	
7	Fracture Half-Length	X_f	312.4	m
8	Fracture Width	W_f	1.93	mm
9	Fracture Penetration	I_x	0.62	
10	Net Pressure	P_{net}	15.9	atm
11	Width Constraint		Ok	

From **Figure 4.7**, for the value of proppant number (Np) of 8.92, the dimensionless productivity index (J_D) increases as more fractures are created up to the asymptote line (J_D~12). The increase in fracture will have an effect on the width and fracture half-length of the fracture. The increase in the number of fractures will create a slender fracture. To avoid this effect and to be practical, three 20/40 proppant grains (3 times the proppant mean diameter, which is 3x0.643=1.93) are required to maintain the fracture permeability and minimum fracture width. The values for the minimum width are shown in **Table 4.7**.

To demonstrate the effect of minimum width-constraint on the maximum attainable J_D, three scenarios for this complex were investigated at three different reservoir permeability.

Table 4. 7 Effects of minimum width constraints on optimal attainable J_D demonstration

No.	Cases	K(mD)	Xe(m)	K_f(D)	W_{min} (mm)-20/40 TX brown sand	$\frac{KXe}{2K_fWmin}$
1	A	0.2	1000	61.710	1.93	0.84
2	B	0.4	1000	61.710	1.93	1.68
3	C	0.8	1000	61.710	1.93	3.36

The constraint in **Table 4.7,** when applied to **Figure 4.6** gives a maximum attainable dimensionless productivity index for multiple fractures as shown **Figure 4.7**.

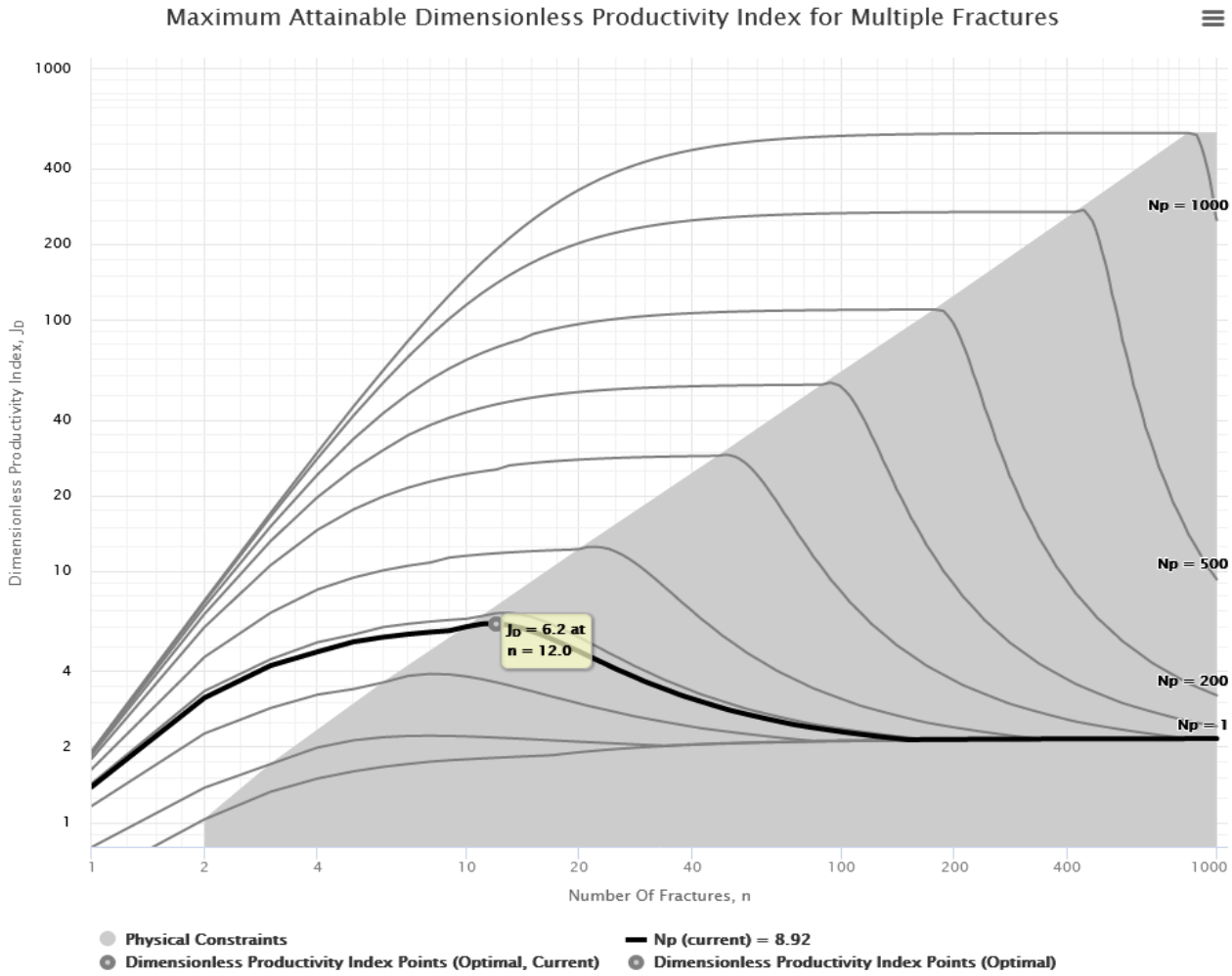

Figure 4. 7 Maximum attainable dimensionless productivity index for multiple fractures in a square area with choke skin and minimum width constraint

Figure 4.7, shows that the dimensionless productivity index, $J_{D,}$ no longer reaches the asymptote, to the technical maximum of the $\frac{3}{\pi}Np$ developed by Guk et al., 2014. As the number of fractures increases, however, the productivity index rapidly declines. The fracture length is shortened to sustain the minimum width. For the dimensionless proppant number (Np) of 8.92, with an increasing number of fractures (n) greater than 12, there is a smaller volume per fracture.

Chapter-5 Conclusions and Recommendations

5.1 Conclusion

The Adigrat reservoir in the Hilala Gas Field consists of sandstone, pelitic sandstone and a small amount of gritstone and gypsum rocks. Understanding the physical and geo-mechanical properties of the reservoir rock is crucial to the design and execution of hydraulic fracturing. These properties can be determined from core data or well log data. The Adigrat reservoir in the Hilala gas field is generally classified as low porosity and low permeability reservoir. To optimize the productivity of this formation, horizontal well completion combined with hydraulic fracturing are considered as development options in the detailed study and analysis considered in this study. The geological and geo-mechanical properties of the gas field provide us with the required rock properties for the selection of hydraulic fracturing design parameters and materials needed, such as fracturing fluids and proppants. Analysis of the geo-mechanical properties shows that sandstone has a static Young's modulus of 51.26 GPa and a Poisson's ratio of about 0.21; pelitic sandstone has a Young's modulus value of 38.72 and a Poisson's ratio of about 0.26; and, Mudstone has Young's modulus of 27.70 GPa and a Poisson's ratio of 0.31. Generally, the sandstone has the highest Young's modulus value and the lowest Poisson's ratio than the pelitic sandstone and mudstone, implying higher brittleness index. The mudstone has the highest Poisson's ratio and the lowest Young's modulus, inferring the lowest brittleness index.

The brittleness and ductility of the reservoir formation determine the fracture initiation, propagation, and length and width of the fracture. Therefore, the estimation of these geo-mechanical properties is very important during fracture design. The rock brittleness index of the sandstone is the highest (83.92%) followed by the pelitic sandstone (60.94%) and the mudstone (39.53%). Sandstone, which is more brittle than other types of rocks, has the lowest Poisson's ratio and the greatest Young's modulus, making it easier to initiate and propagate hydraulic fracture. The ductility of mudstone is due to its clay content.

As the brittleness index is critically important for fracture design; the other necessary parameter determined for the Adigrat formation is the closure stress value of 55.80 MPa, the pressure value at which the proppant is required to have the strength to resist the crushing force when the treatment pressure is released. This closure stress is a dominant variable during the selection and

use of proppant material, conductivity, and overall optimization process. For Adigrat formation, which has a closure stress of 8092.98 psi (55.80 MPa), the suitable and economical proppant material is intermediate-strength bauxite. The multiple hydraulic fracture design for the transverse horizontal well of the Adigrat formation in Hilala Gas Field in the Ogaden basin is done by integrating the available geological, geo-mechanical, and reservoir engineering data of drilled and tested wells in the gas field at the target depth of around 3165m.

Combining the geological, geo-mechanical, reservoir, and proppant parameters as well as fluid parameters, the productivity index and conductivity are functions of the reservoir geo-mechanical parameters and proppant permeability, which in turn are affected by the closure stress. The optimal values of the dimensionless productivity index and conductivity for the single fracture in a square reservoir are 0.84 and 2.25, respectively. Moreover, the optimum fracture width (w_f) and half-length (X_f) geometries are 2.27mm and 310.6 m of the available 0.87 proppant number (Np). The Productivity index of multistage fracture with transverse intersection in horizontal is higher than that of single fracture optimization. The optimum number of transverse fractures for the multistage fracture in the Adigrat formation in Hilala Gas Field is twelve (12) fractures for the drainage width of one thousand (1000) meters. The dimensionless productivity index is 6.18 for the available proppant number (Np) of 8.92. The productivity index first increases with increasing fracture and proppant volume. However, there is an optimal number of fractures (optimum n=12) that yields the optimum productivity index for the available proppant number. The fracture width and penetration ratio compete for the available proppant when more and more fractures are formed, resulting in narrow fractures.

5.2. Recommendation

In this study, a pseudo-steady state flow regime, 2D PKN fracture geometry, and a constant fracture height are assumed. A 3D fracture model could incorporate various parameters to evaluate the result. Due to time and resource constraints, this study is restricted to physical optimization, and detailed economic optimization of the hydraulic fracturing design is not performed. Therefore, economic optimization of the design study is suggested as compulsory for economic decision-making.

References

1) Aron, J., & Murray, J. (1978, October). Formation Compressional and Shear Interval Transit Time Logging by Means of Long Spacings and Digital Techniques. In *SPE Annual Technical Conference and Exhibition* (pp. SPE-7446). SPE.
2) Bagci, S., et al., (2017). Optimization of hydraulic fracturing and production enhancement: Case studies for us shale plays and tight sand reservoirs, OnePetro.
3) Crosby, D. G., et al., (2002). "Single and multiple transverse fracture initiation from horizontal wells." Journal of Petroleum Science and Engineering **35**(3-4): 191-204.
4) Crosby, D. G., Rahman, M. M., Rahman, M. K., & Rahman, S. S. (2002). Single and multiple transverse fracture initiation from horizontal wells. *Journal of Petroleum Science and Engineering*, *35*(3-4), 191-204.
5) Dobbs, J. (2020, May 29). *What Are The Most Effective Hydraulic Fracturing Fluids*. Guar Resources. Retrieved March 3, 2023, from https://www.guarresources.com /effective-fracturing-fluids/
6) Dvorkin, J. P. (2008). Yet another V S equation. *Geophysics*, *73*(2), E35-E39.
7) Economides, M., Oligney, R., & Valko, P. (2002). Unified fracture design: bridging the gap between theory and practice. Orsa Press.
8) Economides, M. J., et al., (2013). Petroleum production systems, Pearson education.
9) Economides, M. J., et al., (2010). Fracturing horizontal transverse, horizontal longitudinal and vertical wells: criteria for decision, OnePetro.
10) Economides, M. J. and T. Martin (2007). Modern fracturing: Enhancing natural gas production, ET publishing Houston.
11) Economides, M. J. and K. G. Nolte (1989). Reservoir stimulation, Prentice Hall Englewood Cliffs, NJ.
12) Gokaraju, D. (2014). "Impact of fracture spacing and mechanical parameter anisotropy on fracture width in horizontal wells in shales."
13) Guk, V., et al., Optimizing Number of Fractures in Horizontal Well, OnePetro.
14) Guo, B., et al., (2017). Petroleum Production Engineering, 9780128096123, USA, Gulf Professional Publishing.

15) Jones, J. R. and L. K. Britt (2009). Design and appraisal of hydraulic fractures, Society of petroleum engineers Richardson, Texas, USA. (Survey, 2012)
16) Khan, I., Ismail, A., & Ali, I. (2018, September). Identification of brittle and ductile zones in sandstone reservoir using well log analysis; a case study, Southern Indus Basin, Pakistan. In *IOP Conference Series: Materials Science and Engineering* (Vol. 414, No. 1, p. 012021). IOP Publishing.
17) King, G. E. (2012). Hydraulic fracturing 101: What every representative, environmentalist, regulator, reporter, investor, university researcher, neighbor and engineer should know about estimating frac risk and improving frac performance in unconventional gas and oil wells, OnePetro.
18) POLY-GCL Petroleum Investments Limited Ethiopian Branch. (2017). *Field Development Plan*
19) Marongiu-Porcu, M., et al., Economic and physical optimization of hydraulic fracturing, OnePetro.
20) Marongiu-Porcu, M., et al., Delineation of application: physical and economic optimization of fractured gas wells, OnePetro.
21) Meyer, B. R., et al. Optimization of multiple transverse hydraulic fractures in horizontal wellbores, OnePetro.
22) Miskimins, J. L. (2019). Hydraulic fracturing: fundamentals and advancements, Society of Petroleum Engineers Richardson, Texas, USA.
23) Nolen-Hoeksema, R. (2013). "Elements of hydraulic fracturing." Oilfield Review **25**(2): 51-52.
24) Olayiwola, S. O. and M. M. Rahman (2017). "Optimizing economic number of transverse fractures in horizontal well: A systematic design for maximum tight gas recovery." Adv Pet Explor Dev **13**(2): 32-42.
25) Rickman, R., Mullen, M., Petre, E., Grieser, B., & Kundert, D. (2008, September). A practical use of shale petrophysics for stimulation design optimization: All shale plays are not clones of the Barnett Shale. In *SPE Annual Technical Conference and Exhibition* (pp. SPE-115258). SPE
26) Suranto, A. M., Buntoro, A., Prasetyadi, C., & Wibowo, R. A. (2021). Feasibility Study on the Application of Dynamic Elastic Rock Properties from Well Log for Shale

Hydrocarbon Development of Brownshale Formation in the Bengkalis Trough, Central Sumatra Basin, Indonesia. *Journal of Geoscience, Engineering, Environment, and Technology*, *6*(2), 81-85.

27) Survey, K. G. (2012). Hydraulic Fracturing of Oil and Gas wells in Kansas.
28) Valkó, P. and M. J. Economides (1995). Hydraulic fracture mechanics, Wiley Chichester.
29) Yang, F. (2014). Performance comparison of transverse and longitudinal fractured horizontal wells over varied reservoir permeability, Missouri University of Science and Technology.
30) Yao, S. (2013). Modeling of Multi-Stage Fractured Horizontal Wells, The University of Regina (Canada).
31) Zhang, J. J. (2019). *Applied petroleum geomechanics* (Vol. 1). Houston, TX, USA: Gulf Professional Publishing

Appendix

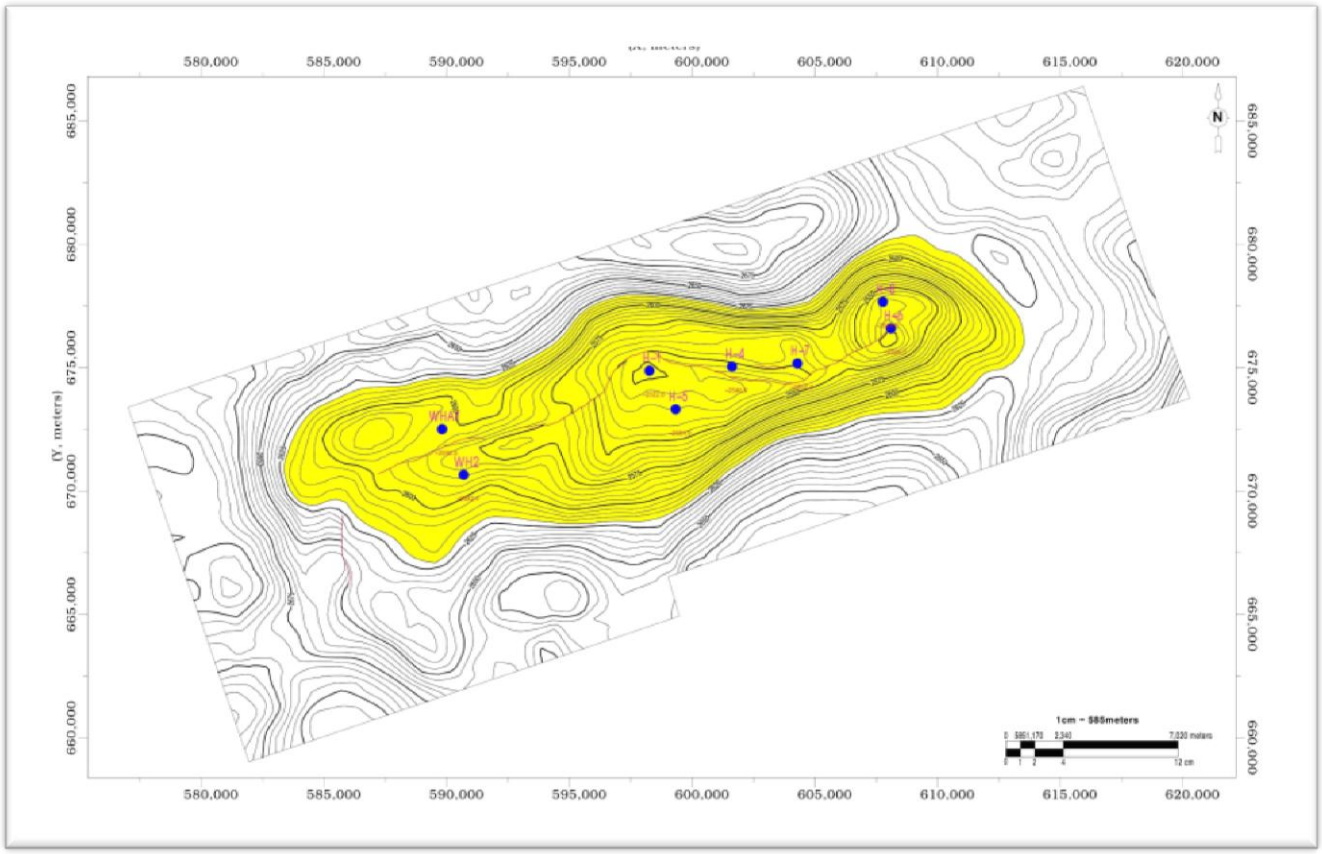

AP1. **Top structure of Adigrat formation in Hilala gas field (POLY-GCL Ethiopia, 2021)**

33 Hydraulic fracturing proppants in the catalog

Proppant	Bulk volume, lbm/ft^3	Mean Diametr, in	Specific Gravity
10/14 BorPROP	114.24324	0.057874047	3.09
10/14 ForeRCP	101.13336	0.072283504	2.93
10/14 ForePROP	104.87904	0.067795312	2.85
12/18 XE112	111.12184	0.055905542	3.2
12/18 BorPROP	116.74036	0.051732311	3.04
12/18 ForePROP	109.87328	0.048661444	2.93
12/18 ForeRCP	106.75188	0.053700816	2.89
16/20 Treg	96.13912	0.037401595	2.64
16/20 Ceramax	98.01196	0.041732306	2.66
16/20 ForePROP	108.00044	0.037755926	2.83
16/30 ForePROP	108.00044	0.036259862	2.83
16/20 BorPROP	114.86752	0.037755926	3.02
16/30 BorPROP	114.86752	0.029606315	3.09
20/40 BorPROP	112.3704	0.026063006	3.02
8/14 CarboP	124.856	0.06692917	3.38
12/18 CarboP	117.36464	0.050826799	3.3
16/20 C-Lite	102.007352	0.037362225	2.72
16/20 CarboP	118.6132	0.03917325	3.3
16/20 CarboP	111.995832	0.048464593	3.2
12/20 SinLit	112.99468	0.044763804	3.25
16/30 SinLit	119.86176	0.034803168	3.2
16/30 Chi C-Lite	93.642	0.034251987	2.74
20/40 C-Lite	101.75764	0.028464582	2.72
20/40 SinLite	123.60744	0.034803168	3.02
8/16 TX Brown	99.8848	0.066008378	2.65
12/20 TX Brown	99.8848	0.049661042	2.65
16/30 TX Brown	99.8848	0.036607218	2.65
20/40 TX Brown	96.13912	0.025308314	2.65
30/70 TX Brown	95.51484	0.010604175	2.65
12/18 CarboHSP bauxite	131	0.050826799	3.61
16/30 CarboHSP bauxite	131	0.037637816	3.61
20/40 CarboHSP bauxite	131	0.02744096	3.61
30/60 CarboHSP bauxite	131	0.016929143	3.61

Hydraulic Fracturing Proppant (Guk et al., 2014)

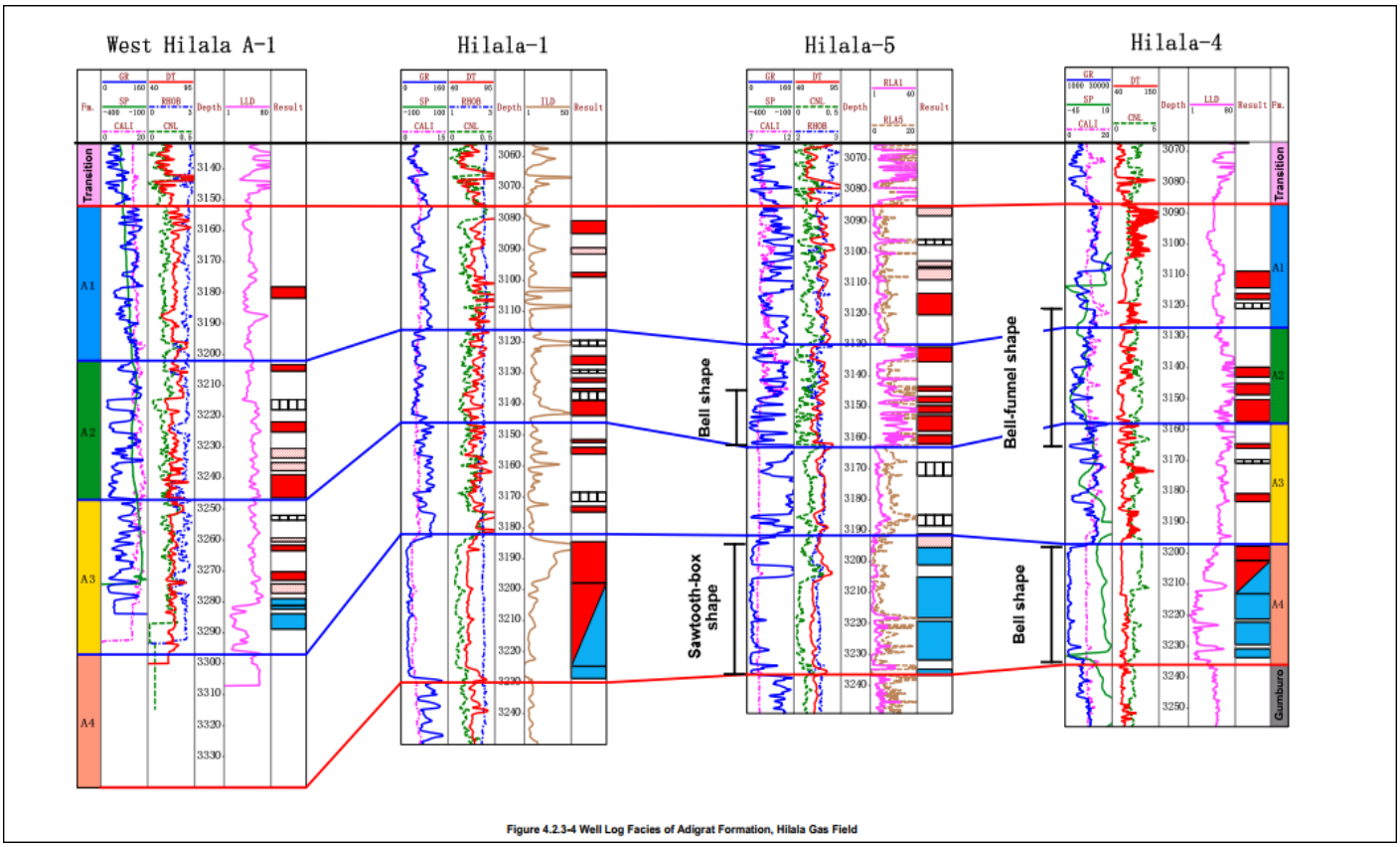

Figure 4.2.3-4 Well Log Facies of Adigrat Formation, Hilala Gas Field

Well Log Facies of Adigrat Formation in Hilala Gas Field (POLY-GCL, 2017)

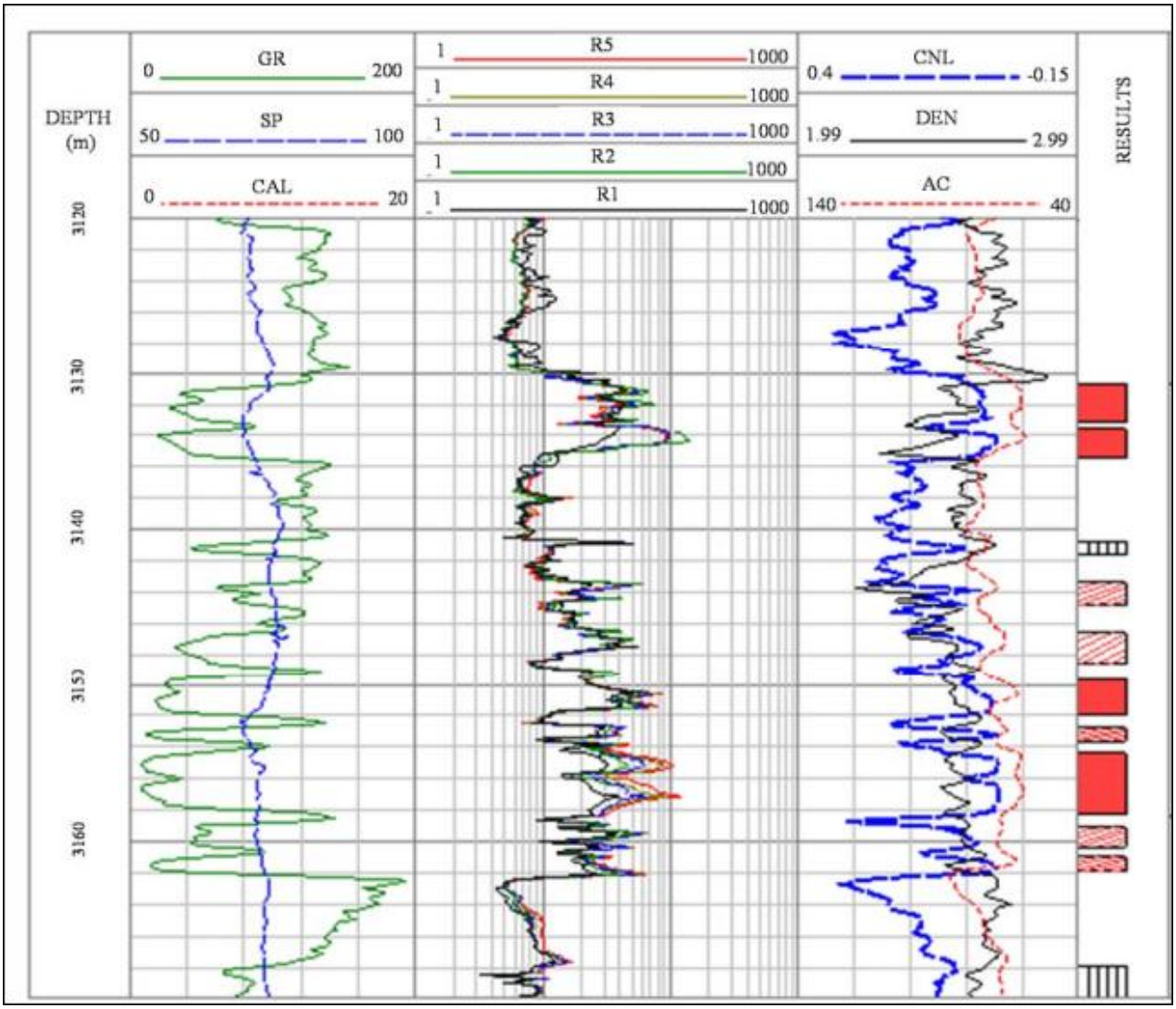

Typical Logging Curve of Adigrat sandstone- Hilala Gas Field (POLY-GCL,2017)

b. Adigrat formation

The formation lithology consists of mudstone, silt-fine sandstone and a small amount of gritstone, gypsum rocks, and pelitic sandstone, and the features of various ithology and logging response are shown as follows:

Sandstone: the resistivity is between 1 Ω·m and 100 Ω·m, which is generally more than 10 Ω·m, and the natural gamma-ray value is low, i.e. about 13 API. The density is about 2.5 g/cm^3, the interval transit time is generally about 62 μs/ft, and the neutron value is about 0.03.

Pelitic sandstone: the resistivity is between 3 Ω·m and 30 Ω·m, which is generally more than 10 Ω·m, and the natural gamma-ray value is medium, i.e. about 50 API. The density is about 2.55 g/cm^3, the interval transit time is generally about 70 μs/ft, and the neutron value is about 0.13.

Mudstone: the resistivity is between 3 Ω·m and 10 Ω·m, which is generally less than 10 Ω·m, and the natural gamma-ray value is high, which is generally more than 80 API. The density is about 2.60 g/cm^3, the interval transit time is generally about 80 μs/ft, and the neutron value is about 0.20.

Sonic and Density Log results of Adigrat formation in Hilala Gas Field(POLY-GCL, 2017)